Electric Technology U.S.S.R.

ЭЛЕКТРИЧЕСТВО

Volume 1, 1961

Selected papers from
Elektrichestvo Nos. 1, 2 and 3, 1961

blished by

PERGAMON PRESS NEW YORK LONDON OXFORD PARIS LOS ANGELES

for Pergamon Institute, Washington and Oxfo

ELECTRIC TECHNOLOGY, U.S.S.R.

PERGAMON INSTITUTE

A DIVISION OF PERGAMON INTERNATIONAL CORPORATION, OPERATED IN THE PUBLIC SERVICE FOR THE FURTHERANCE AND DISSEMINATION OF SCIENTIFIC KNOWLEDGE

President of the Scientific Advisory Council:
Sir Robert Robinson, O.M., F.R.S.

Executive Director: Captain I. R. Maxwell, M.C.

122 *East 55th Street New York* 22, *N.Y.* (*Telephone No. Plaza* 39651).
Headington Hill Hall, OXFORD. (*Telephone No. Oxford* 64881)

Pergamon Institute can occasionally use additional translators for science and engineering material to assist with this programme of translation from Russian and other Slavonic languages.

Scientists and engineers who have a knowledge of Russian, and who are willing to assist with this work, should apply to the Administrative Secretary of the Institute. They should write to New York or Oxford for rates of payment and other details.

Four volumes per annum. Approximately 700 pages per annum.
Annual Subscription Rate £20 ($56).
Single volumes may be purchased for £6 ($14).

Orders should be sent to the distributors at either of the following addresses

Headington Hill Hall, Oxford
122 East 55th Street, New York 22, N.Y.

PUBLISHED BY

PERGAMON PRESS LTD.

NEW YORK · LONDON · OXFORD · PARIS · LOS ANGELES

July 1961

ELECTRIC TECHNOLOGY U.S.S.R.

VOLUMES 1—4, 1961

Selected papers from Elektrichestvo, Nos. 1—12, 1961

PERGAMON PRESS LTD.

OXFORD . LONDON . NEW YORK . PARIS

PERGAMON PRESS LTD.
Headington Hill Hall, Oxford.
4 and 5 Fitzroy Square, London, W.1.

PERGAMON PRESS INC.
122 East 55th Street, New York 22, N.Y.

GAUTHIER-VILLARS
55, Quai des Grands-Augustin, Paris VIe.

PERGAMON PRESS G.m.b.H.
Kaiserstrasse 75, Frankfurt-am-Main.

PERGAMON INSTITUTE

A DIVISION OF PERGAMON INTERNATIONAL CORPORATION, OPERATED IN THE PUBLIC SERVICE FOR THE FURTHERANCE AND DISSEMINATION OF SCIENTIFIC KNOWLEDGE.

Elektrichestvo

Editor-in-Chief : N. G. DROZDOV

EDITORIAL BOARD

AUTHOR INDEX, VOLUMES 1-4, 1961

SUBJECT INDEX, VOLUMES 1-4, 1961

REDUCING THE LOSSES IN THE MAGNETIC CIRCUIT OF A LARGE FERRORESONANT VOLTAGE STABILIZER*

E".K. SUKAZOV

(Leningrad)

(Received 6 July 1960)

Ferroresonant voltage stabilizers have a comparatively low efficiency. The efficiency of 1 to 10 kVA stabilizers designed as in Fig. 1 is between 0.78 and 0.85 [1]. Not only are the losses themselves considerable, but they also irregularly distributed between the saturated (1) and unsaturated (2) parts of the magnetic circuit. A large part of the losses is concentrated in the core (2) which gives rise to additional difficulties in heat dissipation and also complicates the design of stabilizers over kVA.

Fig. 2 shows a typical magnetic circuit of high power ferroresonant stabilizers. The windings are in the form of cylindrical coils of identical inside diameter for technological reasons.

The core (2) must be saturated over the range of variation in the primary voltage U_1 if their performance of the stabilizers is to be satisfactory. For large ferroresonant stabilizers effective induction B_s in core 2 is usually 1.35 Vb/m^2 "in the state of the second reference point" (i.e. resonance of the currents on no load) [2]. Since B_s is linked with maximum

$$B_m = \frac{\pi}{2k_{sh}} B_s$$

and since an equal-sided trapezium with a shape factor of $k_{sh} = 1.06$ can

* *Elektrichestvo*, No. 1, 39-41, 1961.

be substituted with sufficient accuracy for the output voltage curve, maximum induction is therefore 2.0 Vb/m^2. Core 1 is 1.7 to 2 times larger in cross section than core 2.

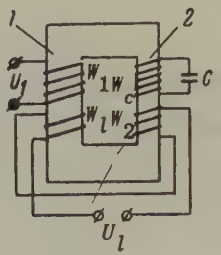

Fig. 1.

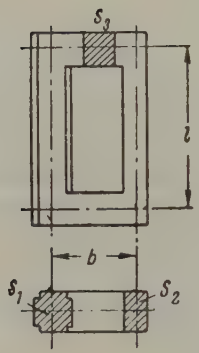

Fig. 2.

Under conditions of current resonance on no load the ratio of the losses in the saturated part to total losses in the magnetic circuit is

$$\beta_1 = \frac{S_2 l d p_1 (B_{m(2)})^2 \cdot 100\%}{S_2 l d p_1 (B_{m(2)})^2 + S_1 (l + 2b) d p_1 \left(B_{m(2)} \frac{S_2}{S_1}\right)^2} = \quad (1$$

$$= \frac{100\%}{1 + \frac{S_2}{S_1}\left(1 + 2\frac{b}{l}\right)},$$

where d is the specific gravity of transformer steel,

p_1 the specific losses in the transformer steel at maximum induction;

$B_{m(2)}$ the maximum induction in the saturated core.

But the ratio of the weight of the saturated core to the gross weight of the magnetic circuit provided $S_3 = S_1$ is

$$\beta_2 = \frac{S_2 ld \cdot 100\%}{S_2 ld + S_1 (l + 2b) d} = \\ = \frac{100\%}{1 + \frac{S_1}{S_2}\left(1 + 2\frac{b}{l}\right)}. \quad (2)$$

Suppose we substitute in equations 1 and 2 the above ratio of S_1 to S_2 and the recommended ratio of b to l for the magnetic circuit [l = = (1.5 to 2.0) b] [1,3,4]. We then find that 45 per cent of the total loss in the magnetic circuit is concentrated in the saturated core which is only about 20 per cent by weight of the magnetic circuit.

If we can vary the operating induction in the unsaturated part of the magnetic circuit within definite limits without adversely affecting stability, the losses can then be reduced in the saturated part by reducing the specific losses of the metal.

Another way of reducing losses in the saturated core of large ferroresonant stabilizers is to increase the cross-section of the saturated core without altering the rest of the stabilizer elements. To keep the same standard of stabilization as before, the material used for the saturated core must have different properties from that used for the unsaturated part of the magnetic circuit. In his book on ferroresonant stabilizers Lur'e [2] has produced a curve showing the relationship between the magnetism of the saturated core and the stabilization and basic dimensions of the stabilizer. This characteristic represents the effective intensity H_s of the magnetic field as a function of the effective induction B_s:

$$H_s = aB_s^{m+1}. \quad (3)$$

An increase in the cross section of the saturated core by a factor k ($k \leqslant \frac{s_1}{s_2}$) leads to a proportional decrease in core induction (for current resonance conditions on no load). To maintain the same general regularing characteristic [2] of the stabilizer, the value of the coefficient in equation (3) for the material of the saturated core should be

$$a' = ak^6, \quad (4)$$

where a is the corresponding coefficient of the material used for the

unsaturated part of the magnetic circuit.

To define the magnetic properties of the metals by means of Lur'e's primary magnetic characteristics, the induction of the material used for the saturated core should be k-times lower than that of the material used for the unsaturated part of the magnetic circuit. If the specific losses corresponding to the maximum hysteresis cycle can be reduced to a greater extent than the saturation induction, total losses in the saturated core can then also be reduced.

The material used for the saturated core should therefore satisfy the following requirements:

$$\left.\begin{aligned} B_{sat} > B'_{sat};\quad B'_{sat} \geq \frac{B_{sat}}{k};\\ \frac{p'}{p} < \frac{B'_{sat}}{B_{sat}}, \end{aligned}\right\} \tag{5}$$

where B'_{sat} and p' are respectively the saturation induction and specific losses corresponding to the maximum hysteresis cycle for the magnetic material of the saturated core; and

B_{sat} and p are the same quantities, but for the material used for unsaturated part of the magnetic circuit (transformer steel).

The losses due to hysteresis are about 85 per cent of the total losses in 0.5 to 0.35 mm gauge transformer steel on a.c. at 50 c/s with a form factor close to that of a sinusoid [5]. The specific losses can therefore only be reduced appreciably if the hysteresis losses are reduced. The hysteresis losses during one cycle can be estimated by Anderson, Lanse and Gumlikh's emphirical formula [6]:

$$p_h = \alpha B_m H_c, \tag{6}$$

where p_h represents the hysteresis losses during one cycle per unit volume of the material;

H_c the coercive force corresponding to the hysteresis cycle with the desired maximum induction, and

$$\alpha = 4\pi(0{,}225 + 0{,}89 \times 10^{-2} B_m + 0{,}86 \times 10^{-1} B_m^2).$$

The coercive force remains unchanged if the saturation induction of

ferromagnetic metal is reduced by alloying it with an element with which it forms a solid solution [5]. But in some cases H_c can be increased or decreased by extraneous phenomena. Using formula to estimate the loss due to hysteresis in the maximum cycles for certain materials with successively diminishing saturation induction we see that losses are reduced to a greater extent, the more the saturation induction is decreased. The reduction in losses is a maximum at the lower limit of saturation induction (k = 1.7 to 2).

A study has been made of various elements which form solid solutions with iron and can reduce saturation induction as required. Nickel and aluminium are of particular interest. Permalloy satisfies condition (5), but nickel is in such short supply that permalloy cannot be used for the magnetic circuits of large ferroresonant stabilizers.

In Fe-Al alloys there is a uniform reduction in saturation induction with increasing Al - content up to approximately 14.5 per cent Al.

At this point saturation induction is at a minimum.

Tests on two magnetic circuits have shown that losses then decrease in the saturated core. The dimensions of the magnetic circuits were as follows:

Magnetic circuits	l, mm	b, mm	S_1, cm^2	S_3, cm^2	S_2, cm^2
1	150	100	16.23	12.8	9.6
2	150	100	16.23	12.8	16.23

The saturated section of magnetic circuit 2 was made of sheet Fe-Al alloy 0.35 mm thick. Magnetic circuit 1 and the unsaturated part of 2 was made of E 42 grade transformer steel of the same gauge. Both magnetic circuits were tested in the ferroresonant stabilizer circuit on no load. Tests conditions were such that the induction was the same in the sections S_1 and S_3 over the entire range of variation in the primary voltage of both magnetic circuits.

The tests results showed that with the same stabilization factor the losses in the saturated section of magnetic circuit 2 over the entire range of stabilization were almost a quarter of the losses in the saturated section of magnetic circuit 1. The losses were also more uniformly distributed in magnetic circuit 2 than in 1. Winding losses were the same for both stabilizers.

In conclusion the author wishes to thank V.S. Mes'kin and M.I. Voichinskii for their assistance in this work.

Translated by O.M. Blunn

REFERENCES

1. D.G. Vlasov; *Vest. Elektroprom.*, No. 7, (1953).
2. A.G. Lur'e; *The theory of ferrorezonant voltage stabilizers, (Teoriia ferrorezonansnykh stabilizatorov napriazheniia).* Gosenergoizdat, (1958).
3. V.B. Gurvich; *Vest. sviazi*, No. 10, (1951).
4. D.I. Bogdanov and G.K. Evdokimov; *Ferroresonant stabilizers, (Ferrorezonansnye stabilizatory).* Gosenergoizdat, (1958).
5. V.S. Mes'kin; *Ferromagnetic alloys, (Ferromagnitnye splavy).* ONTI, (1937).
6. I.I. Kifer and V.S. Pantiushin; *The testing of ferromagnetic materials, (Ispytanie ferromagnitnykh materialov).* Gosenergoizdat, (1955).

THE EFFECT OF DEMAGNETIZATION ON THE PERMEABILITY OF MATERIALS USED FOR MAGNETIC CIRCUITS*

O.N. AL' TGAUZEN, N.A. SEMENOVA and A.N. STEPANOVA

(Received 2 October 1959)

The initial and maximum magnetic permeability and the permeability in a given field are the fundamental characteristics of materials used for the magnetic circuits of transformers, apparatus and instruments etc. These characteristics are usually defined by the ballistic method. On magnetization, there are certain properties of soft magnetic materials which lead to irreproducible results in the measurement of magnetic permeability,

A study has been made of the effect of demagnetization on magnetic permeability and the variation of magnetic permeability with time for certain soft magnetic materials.

The following Fe-Ni alloys were investigated: 50N, 50NP and 65NP grades with a 50 and 65% Ni – content; 79NM with a 79% Ni-content alloyed with molybdenum; and 80NKhS grade with an 80% Ni-content alloyed with chromium and silicon [1-3]. We also investigated E42 and E43 grade hot-rolled electrical steel with a 4% Si-content and E330 grade grain-oriented cold-rolled 3% silicon steel (GOST 802-58) and an IU.16 grade Fe-Al alloy with a 16% Al-content. The testpieces were stacks of stamped rings 6 to 10 mm high with inside and outside diameters of 20 and 30, or 40 and 50 mm.

For grain-oriented alloys, the rings were formed from 10 mm strip in such a way that the direction of rolling was along the strip. The average diameter of these rings was 5 to 20 mm.

---

* *Elektrichestvo*, No. 1, 51-55, 1961.

To obtain the necessary magnetic properties and remove the cold hardening due to the rolling and stamping of the rings of bending of the strip, the testpieces were heat-treated in vacuo at 1100° for 2 to 4 hr. The residual pressure in annealing was up to 1 to 2 x 10^{-2} mm Hg.

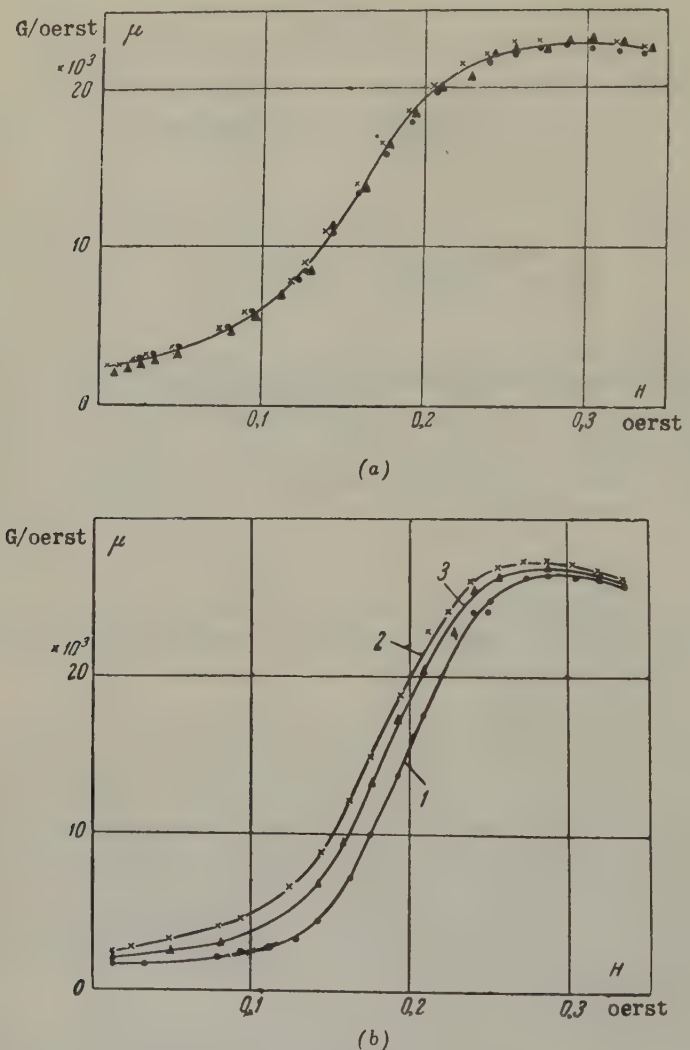

Fig. 1. Magnetic permeability as a function of field intensity for 50N grade Fe-Ni alloy:
a – thickness 1 mm; *b* – thickness 0.1 mm; *1* – after heat treatment; *2* – immediately after demagnetization; *3* – after 168 hr.

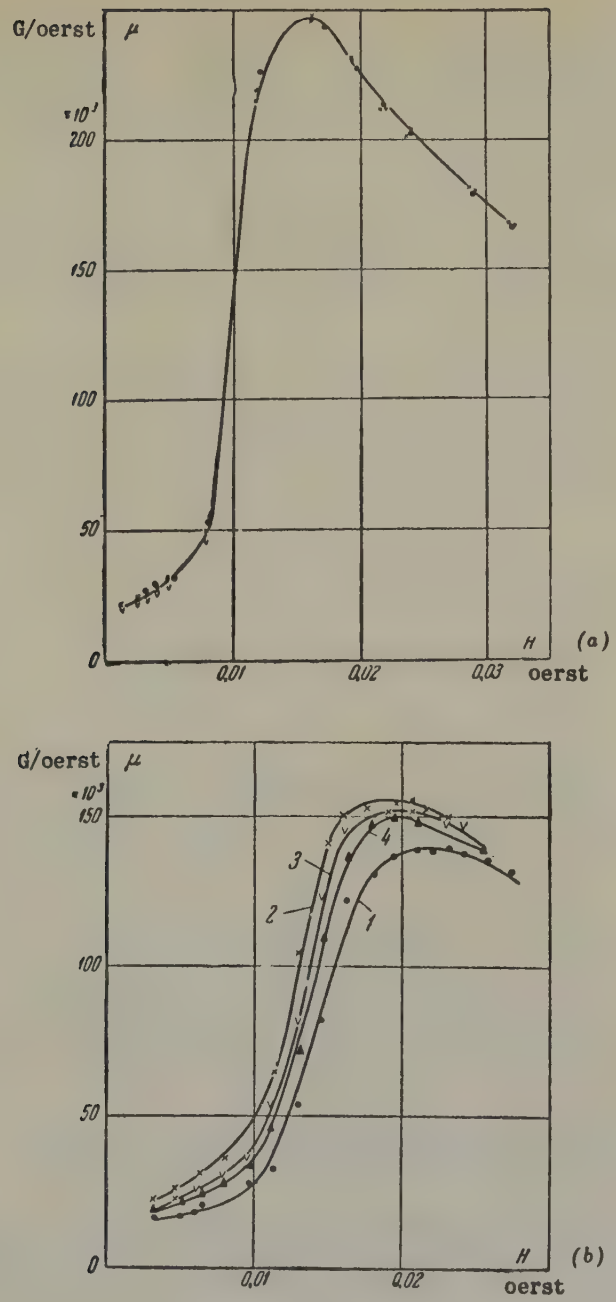

Fig. 2. Magnetic permeability as a function of field intensity for 79NM grade Fe-Ni-Mo alloy:
a – thickness 1 mm; *b* – thickness 0.2 mm; *1* – after heat treatment; *2* – immediately after demagnetization; *3* – after 24 hr; *4* – after 168 hr.

For hot-rolled steel delivered ex-works after high temperature annealing, the ring stampings were tempered at 750° to eliminate cold hardening. For 65 NP grade Fe-Ni alloy thermo-magnetic treatment was applied at 700° in a field of 15 oersted to obtain optimum properties after high temperature annealing [1-4].

To obtain reproducible results, the magnetic properties were measured after demagnetization of the specimens by alternating current of 50 c/s which diminished to zero.

In order to discover the effect of demagnetization on the magnetic properties, the latter were measured immediately after heat treatment of the specimens which had never before been under the influence of a magnetic field and again after demagnetization of the same specimens by an alternating field. The measurements were taken on d.c. by the ballistic method [5].

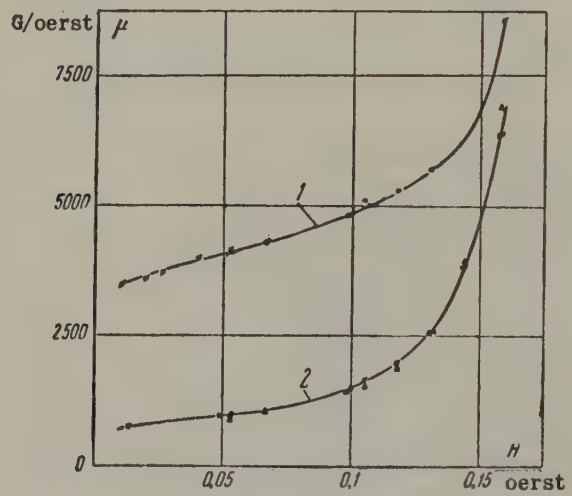

Fig. 3. Magnetic permeability as a function of field intensity for 50NP grade Fe-Ni alloy (thickness 0.05 mm):
1 – after heat treatment; 2 – immediately after demagnetization.

The variation in magnetic properties with time was also measured on these specimens. Different periods of time were allowed to elapse after demagnetization. These measurements were also taken by the ballistic method.

Demagnetization by an a.c. field was repeated after each measurement. The period of time was counted from the moment the demagnetization ceased.

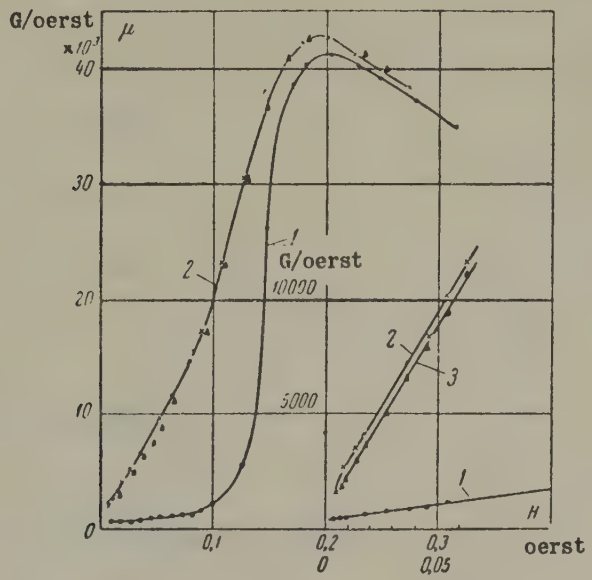

Fig. 4. Magnetic permeability as a function of field intensity for 3% silicon steel (gauge 0.2 mm): *1* – after heat treatment; *2* – immediately after demagnetization; *3* – 24 hr after demagnetization.

Figs. 1 and 2 show the as-measured magnetic permeability of various thicknesses of 50N and 79NM grade Ni-Fe and Ni-Mo-Fe alloys (similar curves were obtained for the 80NKhS grade Fe-Ni-Ch-Si alloy). Fig. 3 illustrates the 50NP grade Fe-Ni alloy and Fig. 4 the electrical steel. The magnetic properties of these alloys are given in Table 1.

The effect of demagnetization

As can be seen from Figs. 1, 2 and 4, the curve for permeability after heat treatment is below that obtained after demagnetization. Demagnetization usually gives rise to the most marked increase in magnetic permeability in the intermediate regions of permeability. Initial and maximum permeability is practically constant. For 50N (Fe-Ni), 80NKhS (Fe-Ni-Ch-Si), 79NM (Fe-Ni-Mo) and 65NP (Fe-Ni) alloys there is a more marked change in permeability with increasing thickness of the material. There is practically no change in permeability at a thickness of 1.0 mm.

TABLE 1

The magnetic properties of test alloys after heat treatment and demagnetization

Grade of alloy	Thickness, mm	Magnetic permeability G/oerst		B_8^*, G	B_r^{**}, G	H_c^{***}, oerst	Magnetic permeability after demagnetization by a.c. field of 50 c/s (magnetic permeability after heat treatment without demagnetization taken as 100%)		
		Initial μ_0	Maximum μ_{max}	Magnetization in a field of 8 oerst			$0'$, %	μ_{max}', %	Maximum change along curve, %
E42	0.5	500	7 800	—	—	—	110—120	—	—
E43	0.35	600	13 800	—	—	—	—	—	—
E330	0.5	450	—	15 500 (H=24oerst)	—	0.5	—	—	—
E330	0.35	800	45 000	14 000 (H=0.6oerst)	—	0.10	200	—	340
E330	0,2	780	42 000	17 000	13 500	0,14	220	105	1 200
50N	1	2 500	23 000	14 100	9 100	0.16	100	100	100
	0.5	2 900	32 300	14 100	10 900	0.17	110	100	110
	0.35	2 600	35 500	14 250	11 100	0.16	110	100	120
	0.2	2 000	33 500	14 500	11 700	0.21	100	100	115
	0.10	2 300	27 500	14 200	11 200	0.22	130	105	240
80NKhS	1	40 000	154 000	6 650	—	0.0135	105	105	115
	0.5	33 000	140 000	7 100	—	0.0147	110	110	130
	0.35	28 000	113 000	6 650	—	0.016	105	105	140
	0.20	30 000	80 000	7 050	—	0.02	125	110	125
	0.1	16 000	55 000	6 500	—	0.036	110	105	140

79NM	1	21 500	248 500	8 000	6 700	0.013	100	100	100
	0.5	21 500	274 000	8 100	5 800	0.013	120	100	165
	0.35	24 000	275 000	8 050	5 750	0.0133	120	105	250
	0.2	—	155 000	8 050	4 500	0.017	125	110	200
	0.1	28 000	135 500	8 050	5 100	0.025	120	110	165
IU16	0.35	—	67 000	5 650	3 500	0.022	130 (H=0.005oerst)	100	130
	0.10	2 400	50 000	5 250	2 600	0.03	120	110	140
65NP	0.35	1 300	412 000	13 300	B_r/B_s=0,98	0.036	200	160	—
50NP	0.05	700	62 000	14 800	B_r/B_s=0,915	0.185	15	100	Lowest value 15

* B_8 – induction in field of 8 oerst.

** B_r – residual induction.

*** H_c – coercive force.

Unlike the other Fe-Ni alloys, the curve for permeability after heat treatment is the higher in the case of 50NP grade Fe-Ni alloy (Fig. 3), and a considerable reduction in magnetic permeability occurs in the region of weak fields on demagnetization.

There was no change in the other magnetic characteristics of any of the alloys ("saturation induction", residual induction, coercive force in the maximum hysteresis cycle).

Table 1 shows the magnetic properties of these alloys, the changes in their initial and maximum permeability on demagnetization and the maximum change in their permeability for the whole curve. Table 1 also shows the changes in permeability in respect of 65NP grade Fe-Ni alloy (here the last technological operation was heat treatment with the superimposition of a magnetic field). Unlike the other alloys, there was a considerable increase in permeability on demagnetization, due chiefly to the fact that the alloy was magnetized after thermo-magnetic treatment and the measurement of permeability began from the point of residual induction.

We suppose that the effect of demagnetization on the magnetic permeability of alloys is a magnetic re-orientation ("texturing") in the material in the direction of the demagnetizing field during the process of demagnetization. High magnetic properties are produced in the 50NP grade Fe-Ni alloy during the process of heat treatment by grain orientation ("crystalographic texture") in the direction in which the strip was rolled. It is also possible that a magnetic re-orientation takes place here in the direction of rolling, whereas demagnetization by alternating current changes it and leads to a reduction in permeabili-

The decrease in permeability with time

The decrease in permeability with time has been the object of many investigations [6-12], but the majority have mainly studied the decrease which takes place in short periods of time between the end of magnetization and the beginning of the measurement. We will now give the results we obtained after periods of time lasting from 15 min to dozens of hours. Figs. 1, 2 and 5 refer to 50N grade Fe-Ni alloy and 79NM grade Fe-Ni-Mo alloy and Figs. 4, 6 and 7 to electrical steel.

It can be seen from the curves for Fe-Ni alloys that magnetic permeability usually decreases with increasing periods of time between the end of demagnetization and the start of the measurement. An increase sometimes occurs during periods of 15 to 30 min. The decrease in mag-

netic permeability is most marked at the beginning of the curve (Fig. 5). It can last dozens of hours. Every curve measured after a long period of time tends to approximate to the curve as measured after heat treatment without demagnetization. The effect of demagnetization and the drop in magnetic permeability are more pronounced, the thicker the material under investigation. No decrease with time was observed in specimens in which no demagnetization effect was observed.

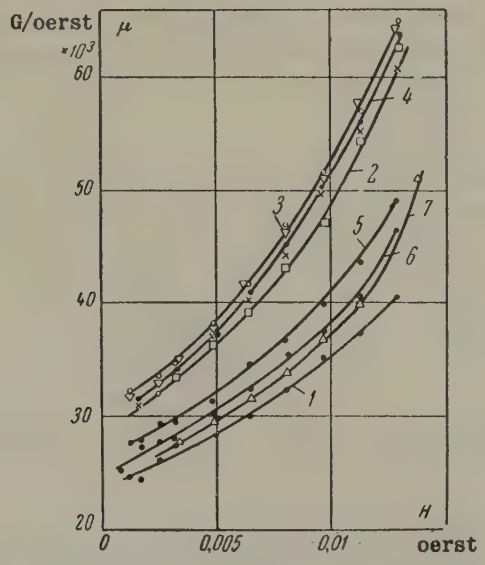

Fig. 5. The magnetic permeability of 79NM grade Fe-Ni-Mo alloy in weak fields (0.01 mm thick):
1 - after heat treatment; *2* - immediately after demagnetization; *3* - after 15 and 30 min; *4* - after 2 hr; *5* - after 24 hr; *6* - after 168 hr; *7* - after 336 hr.

In the case of electrical steel no series of tests was made on specimens of the same heat (melt) but of different gauge. No conclusions can therefore be drawn about the relationship between properties and thickness. Specimens of E-42 and E-43 grade hot-rolled steel of 0.5 mm and 0.35 mm gauge respectively were tested and a decrease with time was observed. The longer the period of time, the greater the decrease (Fig. 6).

Fig. 4 shows curves for cold-rolled 3% silicon steel of 0.2 mm gauge. Despite the considerable increase in permeability on demagnetization, the decrease with time was extremely small even after 48 hr. For E330 grade 0.5 mm gauge steel there was a notable decrease even after 15 min

(Fig. 7); the decrease in permeability continued as the waiting period was increased*. On some steel testpieces the noticeable drop in permeability which began 10 to 15 min after the end of demagnetization and continued for several hrs, can fluctuate during long periods of time. "Delays" also occurred in the start of the decrease with time (during short periods of time the magnetic permeability increased compared with that measured immediately after demagnetization), and the drop in permeability only occurred 2 hr later. At a later date it is necessary to investigate the conditions favouring the various manifestations of the decrease in permeability with time in cold-rolled electrical steel and, above all, the composition of the alloy, the production procedure and the heat treatment.

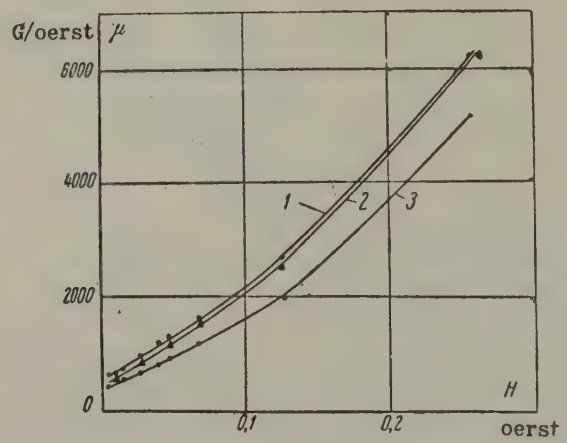

Fig. 6. The magnetic permeability of E43 grade hot-rolled electrical steel (0.35 mm gauge):
1 - immediately after demagnetization; 2 - after 2 hr;
3 - after 24 hr.

Our research into the effect on magnetic permeability of demagnetization and the decrease in permeability with time suggests that the increase in the permeability of 50N, 79NM and 80NKhS grade soft magnetic alloys (Fe-Ni, Fe-Ni-Mo and Fe-Ni-Ch-Si alloys) and the E42 and E43 grade hot-rolled steels on demagnetization is apparently due to the magnetic re-orientation, and that the decrease in permeability with time is due to its reversal. The physics of this phenomenon is not clear and a special investigation is required [6-12]. In grain-oriented material such as 50NP grade Fe-Ni alloy and cold-rolled 3% silicon steel, the cause of changes in magnetic permeability is apparently more complicated. It may be supposed that the grain orientation during heat treatment is accompanied by magnetic orientation and that demagnetization changes it

back and this may lead to an increase or a decrease in permeability. Such changes in permeability may only be partially reversible.

The observable variation in permeability as a function of the first demagnetization after heat treatment and the period of time between the end of demagnetization and the start of the test requires a standard method of determining the magnetic properties of soft magnetic alloys.

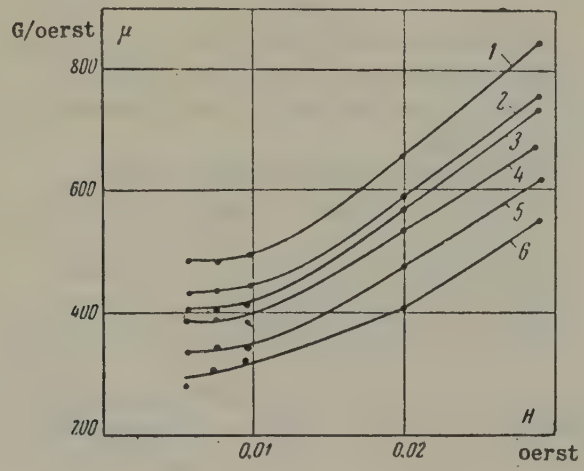

Fig. 7. The magnetic permeability of E330 grade cold-rolled electrical steel (0.5 mm gauge):
1 – immediately after demagnetization; 2 – after 15 min; *3* – after 30 min; 4 – after 1 hr; 5 – after 2 hr; 6 – after 24 hr.

Attention should be paid to the variation in permeability with the period after demagnetization when using these alloys as it can be a source of instability in the operation of electrical gear and a source of additional noise.

Translated by O.M. Blunn

REFERENCES

1. N.P. Gromov, A.I. Il'ichev and N.M. Kasatkin; *Precision alloys, (Pretsizionnye splavy).* Sborn. trud. TsNIIChM.
2. V.Ia. Skotnikov and K.D. Mart'ianova; *Precision alloys, (Pretsizionnye splavy).* Sborn. trud., TsNIIChM, Metallurgizdat, No.15, (1956).
3. V.Ia. Skotnikov and K.D. Mart'ianova; *Precision alloys (Pretsizionnye*

splavy). Sborn. trud., TsNIIChM, Metallurgizdat, No. 23, (1960).
4. O.N. Al'tgauzen, Sh.I. Zusman and A.N. Stepanova; *Metalloved. i term. obrabotka*, No. 11, (1958).
5. I.I. Kifer and V.S. Pantiushin; *The testing of ferromagnetic materials, (Ispytanie ferromagnitnykh materialov)*. Gosenergoizdat, (1955).
6. S.V. Vonsovskii and Ia.S. Shur; *Ferromagnetism, (Ferromagnetizm)*. Gostekhizdat, (1948).
7. R. Bozort; *Ferromagnetism, (Ferromagnetizm)*. *Iz. inost. lit.*, (1956).
8. Iu.S. Vail'; *Iz. Akad. Nauk SSSR, ser. fiz.*, 21, No.9, 1281, (1957).
9. V.V. Druzhinin; *Biull. tekh. inf.*, VIZ, 42, (1957).
10. R.V. Telesnin; *Scientific records of the MGU, (Uchenye zapiski MGU)*. Fiz. 6, No. 162, (1952).
11. F. Schreiber; *Z. ang. Phys.*, 9, No.4, 203, (1957).
12. E.S. Annalik and J. Singer; *J. Appl. Phys.*, 29, No. 3, 412, (1958).

THE ELIMINATION OF ARCING IN HIGH FREQUENCY A.C. CIRCUITS*

V.S. KRAVCHENKO and SUN IUI-CHI

(Mining Institute of the Academy of Sciences USSR)

(Received 20 June 1960)

The research which has so far been undertaken into the phenomena of electrical discharges in high frequency a.c. circuits [1-5] has still to provide a satisfactory answer to the problem of making such circuits free from arcing. It has been shown that arcing is more pronounced when opening capacitive-inductive circuits or circuits with a very low inductance on high frequency a.c. than on d.c. The reason is the shortened length of the discharges when quenched during the passage of current through zero.

Gavril'chenko has now discovered that the ignition currents will only increase up to a definite frequency [2]. A further increase in frequency leads to a decrease in ignition current. Thus, for example, in one series of experiments an increase in frequency up to 20 kc/s led to a fourfold increase in the value of the arcing current on a.c. as compared with d.c. In another series of experiments Gavril'chenko found that a further increase in supply frequency up to 150 kc/s reduced this current by a factor of three.

It is well known that a considerable increase in frequency leads to the failure of the electrodes to cool on the passage of current through zero and the conditions in the sparkgap continue favourable for a discharge. Thus conditions again arise at still higher frequencies which are instrumental in maintaining the electrical arc and increasing the energy developed there. This paper is a continuation of the research

* *Elektrichestvo*, No.1, 77-80, 1961.

referred to above in which a study was made of the conditions under which inductive and inductive-capactive a.c. circuits can be made proof against arcing at frequencies of 5 to 20 kc/s in hydrogen-air atmospheres of the most explosive composition (hydrogen content 20% of air by volume).

It is now considered that the arcing capacity of the discharges which occur when low-power electrical circuits are opened mainly depends on the magnitude of the energy A which enters into the discharge. For inductive-capacitive and inductive d.c. circuits (Fig. 1) the value of A is approximately [6,7]:

$$A \approx \frac{LI^2}{2} + \frac{UI}{6}\tau_m, \qquad (1)$$

where L is the inductance of the circuit;

I the current;

U the voltage of the current source; and

τ_m the maximum duration of the discharge.

Explosion of the medium takes place if $A \geqslant A_{min}$, where A_{min} is the minimum value of the energy sufficient to initiate an arc (limit of ignition).

Equation 1 shows that the arcing capacity of the discharges which occur when the specified circuits are opened is fully defined by the inductance, current and voltage. It is therefore customary to estimate the degree of freedom from arcing by plotting the discharge current as a function of the circuit inductance and applied voltage using the results of tests in explosion chambers with the same probability of explosion (e.g. $P = 10^{-3}$ or $P = 10^{-5}$).

For inductive-capacitive circuits (Fig. 2) in which the discharge of the capacitance takes place on the breakdown of the sparkgap, the explosion is determined by the amount of energy in the arc on the discharge of the capacitance [6]:

$$A = \frac{CU_{Cm}^2}{2}. \qquad (2)$$

where U_{Cm} is the maximum possible voltage on the discharged capacitance which determines the amount of energy stored there.

The level of ignition to a large extent depends on the arc quenching

properties of the electrodes. It has been established that the arc-extinguishing effect of the electrodes diminishes the further they are apart. Therefore, the level of ignition is lowered abruptly if the gap is increased [9]. They cease to have any quenching effect when 2 mm apart and the level of ignition is then a minimum (this is also its "absolute limit", equal to 0.019 mJ for hydrogen-air and 0.28 mJ for methane-air).

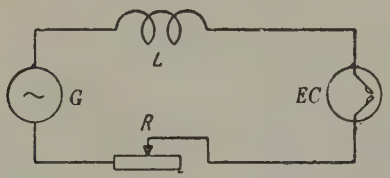

Fig. 1. Inductive circuit.
G – h.f. generator; *EC* – explosion chamber with a conventional spark-producing device.

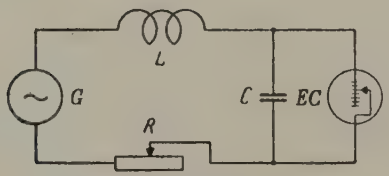

Fig. 2. Inductive-capacitive circuit.
G – h.f. generator; *EC* – explosion chamber with a "make-break"-type spark-producing device.

In accordance with equation (2) we have plotted experimental curves which take the actual conditions of arc formation into account and define the freedom from arcing of capacitive circuits. They represent the variation in maximum capacitor voltage with the magnitude of the capacitance. They are based on the results of tests in explosion chambers with the same probability of explosion [8].

These were the principles we followed in order to estimate the arcing capacity of discharges when opening a.c. circuits.

Fig. 3 shows experimentally-determined curves for estimating the extent to which d.c. and a.c. inductive circuits are proof against arcing as a function of inductance (a) and frequency (b). The effect of generator self-inductance was eliminated by shunting the inductance of

the input transformer by a "non-reactive resistance" (capacitive reactance) the magnitude of which we fixed by trial and error. The discharges were produced by parting a steel wire 0.2 mm in diameter from a steel bar 0.8 mm in diameter. The probability of explosion was $P = 10^{-3}$. The d.c. supply voltage from an accumulator was 170 V. The maximum voltage of the a.c. source was 177 V.

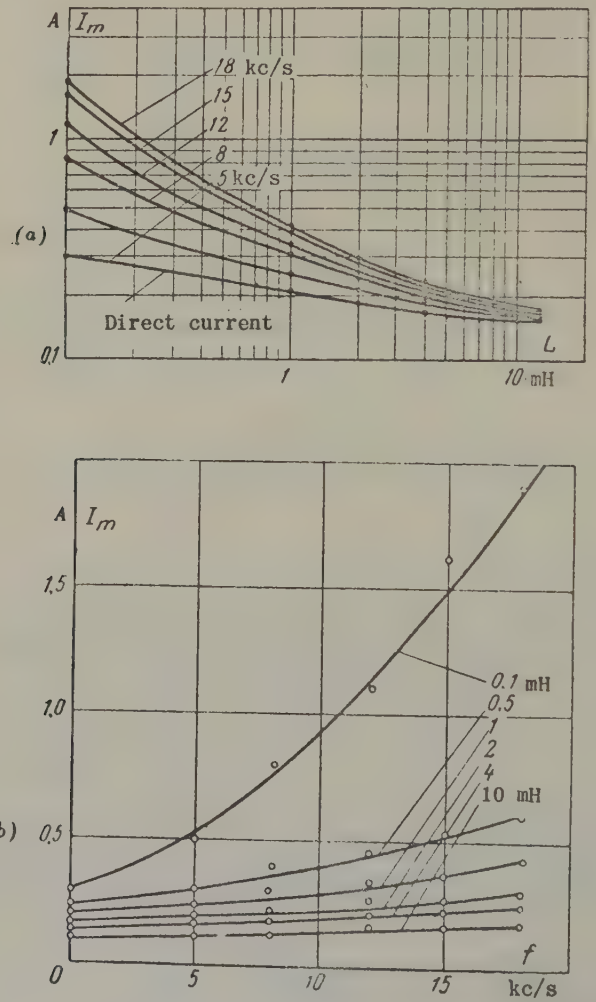

Fig. 3. Minimum ignition currents ($P = 10^{-3}$) in an inductive circuit.

The test results show that arcing currents increase in inductive circuits with increases in supply frequency up to 20 kc/s. Compared

with direct current, this increase is four times greater in a.c. circuits with a small inductance (< 0.5 mH) than in d.c. circuits, but it is barely noticeable in a.c. circuits if the inductance is greater than 1 mH. In all cases under investigation (inductances from 0.1 to 10 mH) discharges were always more dangerous (i.e. explosions occurred at lower currents) when opening d.c. circuits than when opening high frequency a.c. circuits. The difference between d.c. and a.c. arcing currents become less and less as the inductance was increased from 0.5 to 10 mH.

Fig. 4 shows the curves obtained to estimate the freedom from arcing of d.c. and a.c. inductive-capacitive circuits. The discharges were produced in a similar hydrogen-air medium by a sparking device which provided intermittent arcing (which is more dangerous in capacitive circuits) by the movement of a sharp steel wire 0.2 mm in diameter over the surface of a notched steel plate. The probability of explosion was $P = 5 \times 10^{-2}$.

We used the following formula to determine the amplitude of the capacitance alternating voltage after opening (or before making) the circuit:

$$U_{Cm} = \frac{I\sqrt{2}}{\omega C}, \qquad (3)$$

where I is the effective current with open contacts, and $\omega = 2\pi f$ the angular frequency.

The maximum calculated surges on the capacitance were between 1.2 and 1.5 U_{Cm} (1.35 U_{Cm} on average) at different moments of time during the opening of the circuit.

The tests showed that the degree of proof against arcing in inductive-capacitive circuits under the given arcing conditions depends entirely on the "steady state" voltage on the capacitance at the ignition limit for the various values of capacitance and it is this characteristic which we found at frequencies of 5 to 15 kc/s and inductance of 1 to 20 mH under resonant and non-resonant conditions. The minimum ignition energy was roughly constant and equal to 0.24 ± 0.03 mJ (i.e. the average deviation was only $\pm$ 12 per cent) for circuit capacitance between 0.01 and 1 F, inductance between 1 and 20 mH, maximum voltage on the capacitance between 22 and 253 V, trip current between 0.07 and 0.42 A and at frequencies between 5 and 15 kc/s.

The minimum ignition energy was greater than the level of ignition. The explanation is the considerably flame-quenching effect of the con-

tacts, typical of ordinary conditions of interruption. Thus, in high frequency inductive-capacitive circuits the arcing capacity of the discharges in the range under investigation mainly depended on their energy. The arcing capacity was independent of frequency changes and circuit factors.

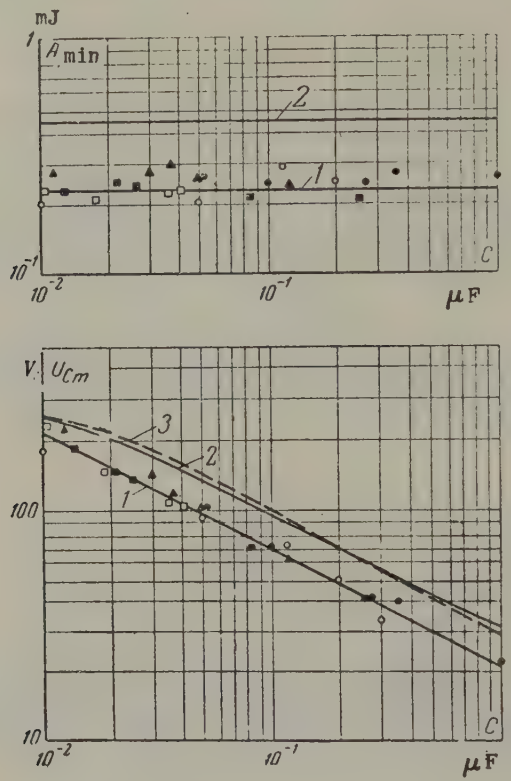

Fig. 4. Minimum ignition energy and maximum capacitor voltages ($P = 5 \times 10^{-2}$) as a function of capacitance at various frequencies and different values of circuit inductance:
1 – amplitudinal values of the steady state voltages on the capacitance and the corresponding energies; 2 – maximum values of the overvoltages on the capacitance and the corresponding energies; 3 – ignition voltages on discharge of the capacitor [8]. ▲ 15 kc/s, ■ 10 kc/s, ● 5 kc/s with resonance; □ 10 kc/s, ○ 5 kc/s without resonance.

We will now consider the effect of frequency changes on the ignition

currents for various values of circuit capacitance and inductance. It follows from equations 2 and 3 that the minimum ignition current ($A = A_{min}$) in an inductive-capacitive circuit is:

$$I_{min} = \omega \sqrt{CA_{min}}, \quad (4)$$

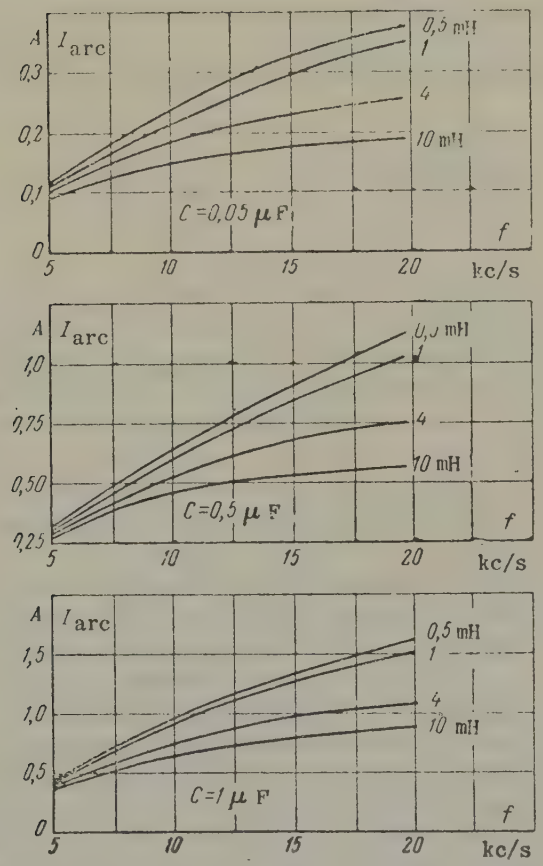

Fig. 5. The effective minimum ignition currents as measured in inductive-capacitive circuits before "opening" of the capacitance as a function of the current frequency at various values of the inductance and capacitance.

The minimum ignition current is therefore greater, the higher the frequency and capacitance and it is independent of other circuit factors.

These circuit factors can be determined from the condition of the equality of the current in an inductive-capacitive circuit to the maximum ignition current. Thus, for example, given the inductance, the explosion of the medium takes place if the resistance of the circuit does not exceed:

$$R=\sqrt{\frac{U^2}{\omega^2 C A_{\min}}-\left(\omega L-\frac{1}{\omega C}\right)^2}, \tag{5}$$

where U is the effective voltage of the h.f. current source.

The minimum ignition current in a circuit with a closed capacitance is:

$$I_{arc}=\frac{U}{\sqrt{R+\omega^2 L^2}}=\frac{U}{\sqrt{\frac{1}{\omega^2 C}\left(\frac{U^2}{A_{\min}}-\frac{1}{C}\right)+2\frac{L}{C}}}. \tag{6}$$

Fig. 5 shows the ignition current as a function of frequency for various values of circuit inductance and capacitance. It can be seen that an increase in frequency up to 20 kc/s always entails an increase in I_{ig} within the given limits of inductance and capacitance. Large currents correspond to large capacitances and small inductances.

In connexion with the constancy of the minimum ignition energy at different voltages, capacitances, inductances and frequencies, it is of interest to mention that a considerable part of the energy entering into the discharge when an inductive circuit is opened is energy which has been stored in the inductance. With increasing inductance this component of the energy approximates to the stated limit 0.24 mJ equalling 0.22 mJ for L = 10 mH at frequencies between 5 and 18 kc/s (P = = 10^{-3}). However, with decreasing inductance, the stated energy component drops abruptly and only amounts to about one tenth of the minimum ignition energy for an inductance of 0.5 mH under the same conditions. In this latter case the rest of the energy comes from the current source. As previously pointed out [5], the energy component in question is greatly dependent on frequency. Hence the effect of frequency on the ignition current is most marked in circuits with small inductance.

Conclusions

1. This analysis of the phenomena of the discharges which occur when opening high frequency circuits has confirmed that the minimum ignition energy of these discharges is constant within the investigated limits.

A mathematical expression has been derived for the arcing conditions in inductive-capacitive circuits.

2. The calculations and test results show the effect of frequency on minimum ignition currents in inductive and inductive-capacitive circuits for various values of circuit inductance and capacitance.

3. Our new experimental data concerning minimum ignition currents and voltages in inductive and inductive-capacitive high frequency circuits with and without resonance at various values of circuit inductance and capacitance can be used in the development to make a qualitative estimate of the extent to which electrical circuits are proof against arcing at frequencies up to 20 kc/s.

Translated by O.M. Blunn

REFERENCES

1. N.I. Brozknik and K.A. Skrynikov; *Zhur. tekh. fiz.*, 4, (1934).
2. L.I. Gavril'chenko; *The freedom of explosive mixtures from arcing in the use of h.f. currents, (Iskrobezopasnost' vzryvnykh semesei pri primenenii tokov vysokoi chastoty).*
3. A.V. Itin; *Izvest, Dnepro. gorn. inst.*, XXIII, (1958).
4. P.F. Kovalev; *Principles underlying sparkproof electrical mining equipment, (Printsipy vzryvobezopasnosti rudnichnogo elektrooboru dovaniia).* Ugletekhizdat, (1951).
5. V.S. Kravchenko; *Fundamentals of the safe use of electricity in underground workings, (Osnovy bezopasnogo primeneniia elektrichestva v podzemnykh vyrobotkakh).* Sborn. "Sov. gorn. nauk", Ugletekhizdat, (1957).
6. B.A. Petrenko; *Scientific research on the winning of coal and ore deposits, (Nauchnye issledovaniia po razrabotke ugol'nykh i rudnykh mestorozhdenii).* Gosgortekhizdat, (1959).
7. B.A. Petrenko; *The elimination of arcing in electrical equipment, (Vzryvobezopasnoe elektrooborudovanie).* TsBTI Elektroprom., (1959).
8. M.B. Blanc, P.G. Guest, G. Elbe and B. Lewis; *J. chem. phys.*, 15, No. 11, (1947).

A ZERO SEQUENCE POWER RELAY WITH CURRENT POLARIZATION*

V.I. GRINSHTEIN

(Cheboksary)

(Received 17 March 1960)

This new relay is a two-way power relay. It is for use in systems of earth fault protection and also in those cases when there is no corresponding voltage transformer. The relay has two windings. One winding carries the zero sequence current of the equipment to be protected and the other winding the polarizing current which can be obtained from current transformers. The relay can also be used for transverse differential protection.

Use is made of P7-type polarized relays as the "executive" devices in the relay in question.

The circuit of the new relay is shown in Fig. 1. It operates on the following principle.

The primary windings of the input transformers *Tr* 1 and *Tr* 2 are divided into two sections. The series and parallel connexion of these sections is used to change the sensitivity of the relay.

The secondary windings of the transformer are also sectionalized and connected in pairs so that the geometric sum of the two transformers is obtained at the output of one pair of secondary windings:

$$\dot{E}_1 + \dot{E}_2 = \dot{U}_2, \tag{1}$$

---

* *Elektrichestvo*, 1, 81-82, 1960.

and their geometric difference at the output of the other pair:

$$\dot{E}_1 - \dot{E}_2 = \dot{U}_1. \qquad (2)$$

The sum and difference of the voltages in question are fed to the windings of two interposing relay via rectifier bridges composed of junction-type germanium diodes.

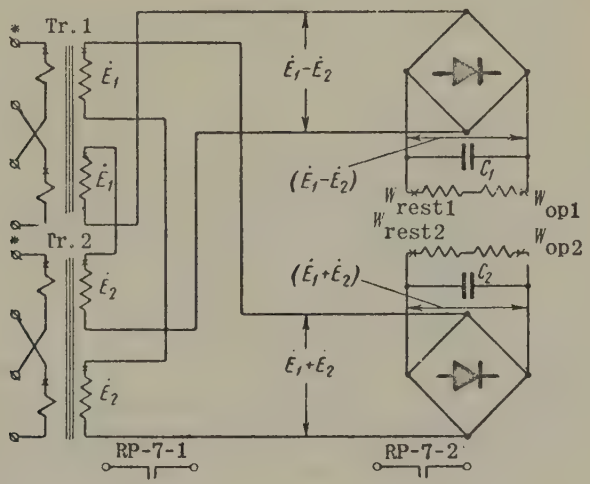

Fig. 1. Relay circuit.

The windings of the interposing relays are in two parts (the one part operating and the other restraining). The windings contain the same number of turns. The restraint winding of the first relay and the operating winding of the second relay are connected to voltage U_1, and the operating winding of the first relay and the restraint winding of the second to the voltage U_2.

The angle of maximum sensitivity $\phi_{m.s}$ is 0 and 180° for the same primary currents in the transformers. When $\phi_{m.s} = 0$

$$\dot{E}_1 - \dot{E}_2 = 0; \qquad (3)$$

$$\dot{E}_1 + \dot{E}_2 = \dot{U}_2 = 2E_1. \qquad (4)$$

Under these conditions maximum current flows in the operating winding of the first relay and in the restraint winding of the second relay, which leads to the operation of the first interposing relay and the restraint of the second.

The reverse takes place if $\phi_{m.s} = 180^{\circ}$.

If $\phi = \pm 90^{\circ}$, then $\dot{U}_1 = \dot{U}_2$ and the operating and restraining moments of the relays are different and the interposing relays do not function.

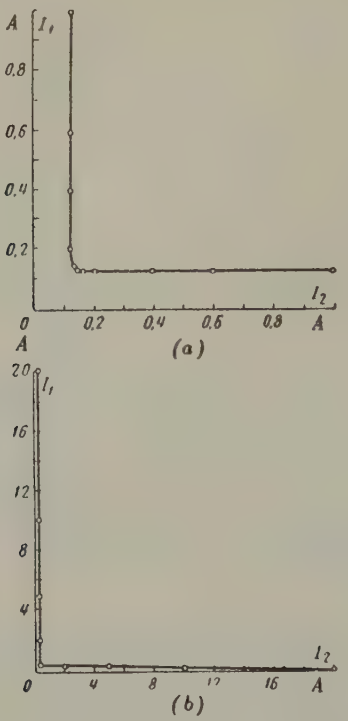

Fig. 2. I_1 as a function of I_2 at an angle $\phi_{m.s}$ of maximum sensitivity equal to 0° (a) and 180° (b).

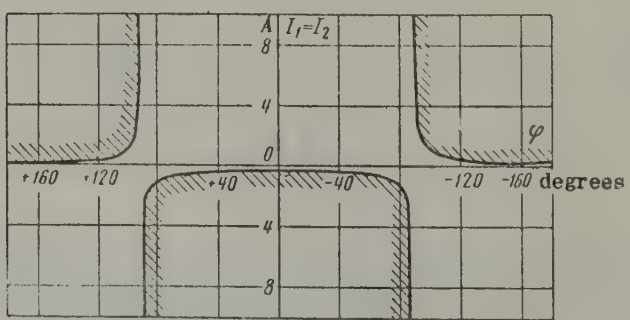

Fig. 3. Angular characteristics of the relay.

This method can therefore be used to make two-way power relays.

The operating current of the relay in question is 0182 A and the power consumption 4.5 volt-amps on each winding. The angle of maximum sensitivity is sufficiently stable over a wide range of current variation.

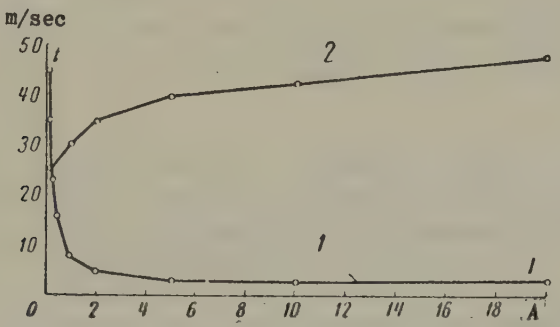

Fig. 4. Time characteristics of the relay: 1 – the time to close the normally open contact on an instantaneous increase in current; 2 – the time to open the normally open contacts on an instantaneous decrease in current from a given value to zero.

Compared with existing induction-type power relays, this new relay has smaller dimensions, lower power consumption, greater sensitivity, faster operating speed and there are no rotating parts.

Translated by O.M. Blunn

ABSTRACTS FROM PAPERS PUBLISHED IN ELEKTRICHESTVO No.1, 1961

Design Formulae

Calculations in circuits with elements of non-linear inertia. O.M. Bogatyrev, (pp. 69-76).

A study is made of circuits with one, two and three different non-linear inert elements under steady state sinusoidal conditions. An analytical method is developed in place of the graphical method previously used. An example is given.

Magnetism

An appraisal of methods of calculating magnetic circuits with air gaps for instruments and apparatus. Z.T. Tikhomirova, (pp. 42-48).

A comparative critical analysis is made of four Soviet methods of designing the magnetic circuits of electrical apparatus on the basis of experimentally-determined data. The Sotskov graphical-analytical method is the simplest but it is only suitable for preliminary calculations. Numerical integration, graphical integration and the "isocline" method are considered. (An isocline is defined as the locus of points at which the tangents to the integral curves have the same slope).

Measuring losses in ferro-magnetic materials magnetized simultaneously by fields of different frequencies. N.M. Rudnyi, et al., (pp. 48-51).

An original method is proposed for measuring losses for the most general case of combined magnetization when the frequencies of the

individual field components are "non-multiple" and none are zero. The wattmeter measuring device is described with particular reference to a special phase-shifting voltmeter. The error is ± 5 per cent.

Power systems

The efficiency of inter-system transmission lines for supplying a local distributed load. Lo Bai-chan, (pp. 1-8).

Power systems have been developed in the U.S.S.R. and China on a regional basis owing to the vastness of these countries. The author considers the optimum conditions for inter-system links with or without uniform load distribution throughout the various regions.

The design of reinforced-aluminium conductors for transmission lines. O.G. Veksel'man, (pp. 9-15).

After reviewing Western experience with reinforced aluminium conductors, the author states the case for reducing the unnecessarily high safety factor on similar Russian constructions. The value of dampers is stressed.

Relays and Protection

Special features of relay protection on lines supplying traction substations. D.I. Veprik et al., (pp. 15-22).

The proposal to electrify about 20 thousand km of railway lines on single phase a.c. at 50 c/s under the current 7-year plan requires that the supply conditions of the substations should be arranged to meet the needs of relay protection and automatic equipment. Transverse differential directional protection, three-stage directional zero sequence current protection, automatic reclosure and 'reserve disconnexion' systems are considered.

Rotating Machines

The parameters, steady state characteristics and stability of synchronous generators with electronic self-excitation.

V.F. Chesachenko, (pp. 22-29).

A study is made of the static and dynamic stability of an unsaturated synchronous non-salient pole generator supplying infinite bus-bars through a reactance. The author studies the adjustment of the anode-grid regulation, the nominal firing angle and the transformation ratio of the anode transformer.

The motor drive of the winches for the fore cables of a dredge. B.Sh. Burgin, (pp. 30-34).

An analysis is made of cable forces and speeds in a new d.c. motor-generator system for which definite advantages are claimed over a.c. variable speed motors.

The design of current regulators for the electronic excitation systems of rolling mill motors. N.P. Kunitskii, (pp. 34-39).

A method is proposed for calculating the current winding unit in a system of ionic excitation for reversible rolling mill motors developed in the U.S.S.R. The current winding is connected via a rectifier to a voltage proportional to the difference between the voltage drop in the compensation and compole windings and a reference voltage.

Automation of the motor drive for a continuous reduction tube-rolling mill. S.S. Roizen et al., (pp. 82-85).

Excessive heating of the motors occurred on a Russian 20-stand tube rolling mill. Some of the motors were overloaded and other passed into generator conditions. It was decided to provide all the motors with regulators to maintain their speed constant to within 0.5 per cent. An account is given of how this problem was tackled by using the frequency of an a.c. tacho-generator as the speed reference together with a special converter.

Switchgear

Determining the power factor of a test circuit by means of a wattmeter vibrator. I.B. Bolotin, (pp. 66-69).

A new improved device called a "wattmeter vibrator" has been developed to measure the power factor of circuits for testing the

rupturing capacity of switchgear.

Transformers

Current transformers with an air gap in their steel core. I.M. Sirota, (pp. 56-61).

Large m.m.f. arise in current transformers used in relay protection under certain conditions. Residual magnetization has been eliminated by making the magnetic circuits of the transformers with a small gap. A study is made of the relationships governing the size of this gap. A gap equal to $\frac{1}{500}$th of the centre magnetic limb is recommended for one type of steel.

Transients in current transformers. E.M. Pevzner, (pp. 61-66).

Since relay protection operates while the current transformer is still under transient conditions, the author proposes a new practical method of calculating the transient performance of the transformer. This can be estimated to within 15 to 20 per cent. Residual induction and a number of other factors is taken into account. The peak magnetization current can be fixed in time.

THE RE-SYNCHRONIZATION OF THE GENERATOR BY THE TURBINE SPEED-GOVERNOR*

M.P. CHESNOV

Power Institute of the Academy of Sciences U.S.S.R.

(Received 12 November 1960)

When the dynamic stability of a generator in a large power system is disturbed, it is possible for it to brought back into step without the interference of the service personnel [1]. Research at the Moscow Power Institute** on a dynamic simulator has shown that the motion of the generator rotor under transient out-of-step conditions is mainly determined by the speed-governor of the turbine. It is therefore of interest to study how the turbine speed-governor affects re-synchronization.

It is well known that the passage of the instantaneous slip through zero is a necessary condition for the re-synchronization of a generator. This condition can be represented in the form [2]:

$$[s_{av}(t)]_{min} \leqslant \sqrt{\frac{2M_{12}}{J}}. \qquad (1)$$

The variation in average slip with time $s_{av}(t)$ under asynchronous conditions can be defined by the joint solution of the linear equations of the individual parts of the speed governor [3] and the linearized equation of motion of the rotor. The periodic components of the electromagnetic moment of the generator can be ignored since they have

---

*Elektrichestvo, 2, 24-28, 1961.

**The research was undertaken by the author jointly with Iu.M. Gorskii.

practically no effect on turbine torque owing to the inertia of the speed control system (this is particularly the case with hydro-electric turbines) [2, 5]. The equation of motion of the rotor can be linearized by representing the asynchronous torque curve as a series of short straight lines. Ignoring the impedance of the supply, the equation of rotor motion simplifies to

$$J\frac{ds_{av}}{dt}+(a_n+k_n s_{av})=M_t, \tag{2}$$

where $a_n + k_n s_{av}$ is the equation of the n-th section of the piecewise-linear asynchronous torque curve of the generator.

Omitting the intermediate calculations, the differential equations with respect to s_{av} in their final form are:

(a) Throttle partly open ($|\sigma|<1$)

$$\begin{aligned} &JT_iT_s\frac{d^3s_{av}}{dt^3}+[T_iT_sk_n+J(T_s+\beta T_i)]\frac{d^2s_{av}}{dt^2}+\\ &+\left[(T_s+\beta T_i)k_n+iJ+\frac{T_iM_{t.nom}}{\mu_{x.x}\delta_{nu}}\right]\frac{ds_{av}}{dt}+\\ &+\left[ik_n+\frac{M_{t.nom}}{\mu_{x.x}\delta_{nu}}\right]s_{av}=i(M_{t0}-a_n). \end{aligned} \tag{3}$$

(b) Throttle completely open ($|\sigma|=1$)

$$J\frac{ds_{av}}{dt}+k_ns_{av}=M_{t.c.o}-a_n\pm M_{t.nom}\frac{t}{\mu_{x.x}T_s}. \tag{4}$$

(c) For control gear of turbine completely "off":

$$J\frac{ds_{av}}{dt}+k_ns_{av}=M_{t.r}-a_n. \tag{5}$$

Unlike the previous case [2]*, the flexible feedback of the speed regulator now has to be included in forming these equations. However, equations (4) and (5) are independent of the type of speed regulator. They are identical to the corresponding equations used in the previous paper [2].

---

* The article referred to has already been translated and appears in Electric Technology U.S.S.R. vol. 6, 1960. The speed regulator then had rigid feedback.

We can find the average slip as a function of time by differentiating equations (3) to (5). On passing from the $(n-1)$-th straight section of the asynchronous torque curve to the n-th section, the tangent of the angle of inclination k_n of this section to the X-axis can differ from k_{n-1} both in magnitude and in sign. The coefficients which depend on k_n in the foregoing differential equations and the roots of the characteristic equations can also vary in magnitude and sign. Consequently, the solutions of equations (3) to (5) can change on moving from one linear section of the asynchronous torque curve to another.

We will now consider the most typical case when all the coefficients in (3) are positive and the general solution of (3) is:

$$s_{av}(t) = Ae^{-\alpha_1 t} + e^{-\alpha t}(B\sin\gamma t + C\cos\gamma t) + s_{av.st}, \tag{6}$$

where $s_{av.st}$ is the particular solution of equation (3), numerically equal to the slip at the point where the static characteristic of the speed regulator intersects that of the asynchronous generator torque;

$$B = \frac{(\alpha^2 - \alpha_1^2 - \gamma^2)[d + \alpha_1(s_{av0} - s_{av.st})] - (\alpha_1 - \alpha)[f - \alpha_1^2(s_{av0} - s_{av.st})]}{\gamma(\alpha^2 - \alpha_1^2 - \gamma^2) + 2\alpha(\alpha_1 - \alpha)};$$

$$d = \frac{M_{t0} - a_n - k_n s_{av0}}{J};$$

$$f = \frac{\sigma_0 M_{t.nom}}{JT_s\mu_{n.1}} - \frac{k_n}{J^2}(M_{to} - a_n - k_n s_{av0});$$

$$C = -\frac{[d + \alpha_1(s_{av0} - s_{av.st})]2\alpha + f - \alpha_1^2(s_{av0} - s_{av.st})}{(\alpha_1 - \alpha)^2 + \gamma^2};$$

$$A = s_{av0} - s_{av.st} - C.$$

The variation in turbine torque with time can be found by equations (2) and (6):

$$M_t(t) = J[e^{-\alpha t}(C_1\cos\gamma t - B_1\sin\gamma t) - \alpha_1 Ae^{-\alpha_1 t}] + a_n + k_n s_{av}, \tag{7}$$

where

$$B_1 = \alpha B + \gamma C;$$

$$C_1 = \gamma B - \alpha C.$$

It follows from (6) and (7) that the free components of the slip $s_{av}(t)$ are damped during the passage of time and, consequently, the turbine torque $M_t(t)$ is in this case also damped. But it should be borne in mind that even if only one of the roots of the characteristic equation is positive on certain of the linear sections of the asynchronous torque curve, then these components have a tendency to increase indefinitely with time. Physically, this implies that the excess torque affecting the rotor is still further increased when the slip changes through the transient torque section in question.

Under transient asynchronous conditions, especially when the slip is considerable, part of the speed control process takes place when the governor valves are completely open and it is then represented by equation 4. The general solution of this equation is:

$$s_{av}(t) = De^{p_1 t} \pm Nt + L, \qquad (8)$$

where p_1 is the root of the characteristic equation;

$$L = \frac{\mu_{x.x} k_n T_s (M_{t.c.o.v} - a_n) \mp J M_{t.nom}}{\mu_{x.x} T_s k_n^2};$$

$$N = \frac{M_{t.nom}}{T_s k_n \mu_{n.l}};$$

$$D = s_{av.c.o.v} - L.$$

In this case the change in the turbine torque can be found from equations (2) and (8):

$$M_t(t) = J(p_1 D e^{p_1 t} \pm N) + a_n + k_n s_{av}. \qquad (9)$$

If the turbine control gear is completely "off" for a certain period of time under transient conditions, the motion of the rotor is then determined by equation (5) of this section. Its general solution can be written in the form:

$$s_{av}(t) = Ge^{p_2 t} + E, \qquad (10)$$

where p_2 is the root of the characteristic equation;

$$E = \frac{M_{t.r} - a_n}{k_n};$$

$$G = s_{av.t.g.\overline{c}} E.$$

In analysing the transient process, the extent to which the throttle is open σ can be found from the equations of the various components of the speed regulator [3,4].

The effect of the speed regulator on the process of re-synchronization can be traced by analysing the dynamic characteristics of the speed regulator $M_t = f(s_{av})$. These give a complete picture of the generating set under transient conditions. Such curves are easy to plot if the functions $s_{av}(t)$ and $M_t(t)$ are known.

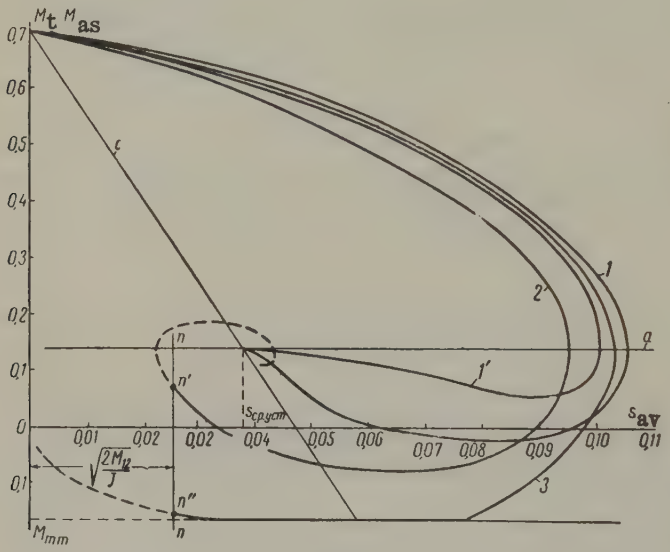

Fig. 1.

$1 - \beta = 5$ and $T_i = 8$ sec; $2 - \beta = 5$ and $T_i = 3$ sec; $3 - \beta = 0$ and $T_i = 8$ sec; $i = 2.35$; $\mu_{n.l} = 0.85$; $J = 15.1$ sec; $1'$ – experimental curve; 1 – corresponding calculated curve.

Figs. 1 and 2 show M_t as a function of s_{av} as well as the static characteristics (c, c' and c'') of the speed regulator and the asynchronous torque curves (a, a' and a'') of the generator. These are assumed to be linear for the sake of simplicity. This is a justi-

assumption since the asynchronous torque curve is usually a maximum when the slip is very small and the section of the curve lying to the left of this maximum can be ignored.

Out-of-step operation thus takes place on the section of the asynchronous torque curve lying to the right of the maximum. This section can usually be linearized over a considerable range of slip values for turbo and hydro-electric generators having damper windings. However, this is not a necessary simplification, and it is only made so as to reduce the amount of calculation.

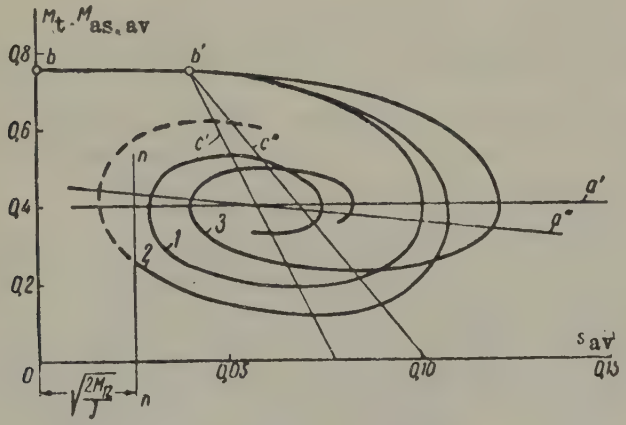

Fig. 2.

1 – $M_{as.av} = 0.5$ and $\delta_{st} = 0.05$; 2 – $M_{as.av} = 0.46 - s_{av}$ and $\delta_{st} = 0.05$; 3 – $M_{as.av} = 0.4$ and $\delta_{st} = 0.08$; $T_s = 7$ sec; $T_i =$; $\beta = 1$; $\mu_{n.1} = 0.75$ and $J = 12.5$ sec.

It will be seen from Figs. 1 and 2 that the rotor shaft is affected under out-of-step conditions by an excess torque $M_{ex} = M_t - M_{as.av}$ which accelerates the rotor. Owing to its inherent inertia, the speed regulator cannot react to the increased slip instantaneously and therefore the turbine torque M_t will not vary along the static characteristic of the speed regulator, but along its dynamic characteristic $M_t = f(s_{av})$. The acceleration of the rotor will persist so long as $M_{ex} < 0$.

The average slip is a maximum when the torques on the rotor shaft are in equilibrium ($M_{ex} = 0$) and then deceleration of the rotor commences since the excess torque has become negative. The rotor will be retarded as long as $M_{ex} < 0$. The average slip is a minimum during this decceleration when the torques on the rotor shaft are in equilibrium

again and if there is a corresponding adjustment of the speed regulator, a positive excess moment can re-appear which re-accelerates the rotor again and so forth (see curve 3 in Fig. 1).

The maximum and minimum average values of the slip always correspond under transient asynchronous conditions to the points at which the $M_t = f(s_{av})$ curve intersects the asynchronous torque curve where the excess moment affecting the rotor changes sign.

It will be seen from Figs. 1 and 2 that in the course of time the $M_t = f(s_{av})$ curves approach the point where the static characteristics of the speed regulator intersect the asynchronous torque curves. This point corresponds to the steady asynchronous state of the generator. The shape of the $M_t = f(s_{av})$ curves as they approach this point mainly depends on the characteristics of the turbine speed regulator.

Re-synchronization of the generator under asynchronous conditions is only possible if condition 1 is satisfied. Otherwise the generator will remain out-of-step unless external conditions alter.

Fig. 1 illustrates the effect of the value of the time constant T_i of the isodrome* and the value of the feedback coefficient β on the operation of the generator during asynchronous conditions. The experimental curve 1' corresponding to the calculated curve 1 was obtained from an oscillogram taken on a dynamic simulator at the Moscow Power Institute**. Comparison of these two curves shows that there is satisfactory agreement with the dynamic characteristic of the turbine speed regulator.

An analysis of the $M_t = f(s_{av})$ curves in Fig. 1 shows that their shape on approaching the point where the static characteristics of the speed regulator and the asynchronous torque curves intersect is very much dependent on the value of T_i and β. Thus, curves 2 and 3 make a considerable detour to the left before approaching this point, whereas curve 1 approaches it more or less smoothly from the right. If T_i and β are increased, the maximum and minimum mean slip values during out-of step conditions also increase and consequently condition 1 is not necessarily fulfilled at certain of these values, i.e. re-synchronization of the generator is impossible (see curve 1 for example).

Lines n-n have been drawn parallel to the Y-axis in Figs. 1 and 2 at a point $s_{av} = \sqrt{\frac{2M_{12}}{J}}$ along the X-axis (see condition 1). If, in

* Isodrome – a hyperbolical position – determining system or curve, (Translator).

** A hydro-electric generator with a damper winding was simulated.

calculating the mean slip, the $M_t = f(s_{av})$ curve is tangential to this line or intersects it at a certain instant (Fig. 1 curves 2 and 3 point n' and n''), then condition 1 is fulfilled and from this moment on, overswings of the rotor set in after successful re-synchronization which gradually face away under the influence of damping factors so that the set returns to its original state provided the electrical system is still the same. After the overswings of the rotor have started, the mean slip is zero and therefore part of the $M_t = f(s_{av})$ curve lying beyond the point where it intersects the n-n line (marked by a dotted line in the diagrams) can only be found mathematically on the assumption that condition 1 is not fulfilled.

It will be seen from Fig. 1 that condition 1 is not fulfilled if $T_i = 8$ sec and $\beta = 5$, (curve 1) and consequently re-synchronization of the generator is impossible. If $T_i = 3$ sec or $\beta = 0$ (curves 2 and 3), condition 1 is then fulfilled and re-synchronization is therefore possible.

Fig. 2 shows curves 1 and 3 for various degrees of statism δ_{st} of the speed regulator ("statism" is defined as the percentage deviation of the controlled quantity at rated load from its value on open circuit, Translator). It can be seen from these curves that an increase in statism leads to a deterioration in the conditions for re-synchronization since the maximum mean slip is increased during transient asynchronous conditions and this can generally result in condition 1 not being fulfilled, Therefore, the less the statism, the more favourable the conditions for re-synchronization. Curves 1 and 3 in Fig. 2 do not intersect the n-n line and consequently condition 1 is not fulfilled, i.e. re-synchronization is impossible.

However, this diagram also illustrates the effect of asynchronous generator torque on the course of asynchronous operation. For simplicity, we confine ourselves to two straight line characteristics a' and a'' at different angles to the X-axis but having a common point of intersection with the static characteristic of the speed regulator. We can therefore trace the effect of the slope (steepness) of the asynchronous torque curve on the dynamic characteristic of the speed regulator. We can always approximate the real asynchronous torque characteristic by several linear sections if it is not a straight line and include its effect on the motion of the rotor in this way.

It can be seen from curves 1 and 2 in Fig. 2 that the conditions for re-synchronization of the generator are improved by steeper asynchronous torque curves since the minimum mean slip is then reduced. Thus, for example, curve 2 which corresponds to a steeper asynchronous torque

characteristic than curve 1, intersects the n-n line, whereas curve 1 does not even touch it. Re-synchronization is therefore possible in the first case, but impossible in the second, since condition 1 is only fulfilled in the former.

It is necessary to consider the effect of the valve limiter on the possibility of re-synchronization. The valve limiter determines the maximum load on the turbine for any position of the static characteristic of the speed regulator.

The speed regulator does not alter the turbine torque within the zone b-b' (Fig. 2) where the valve limiter is effective, and the slip remains less than the value at point b'. This shifts the dynamic characteristic of the speed regulator to the right, in which case conditions are naturally less favourable for re-synchronization since the minimum mean slip value increases by an amount approximately defined by the zone within which the valve-limiter is effective and condition 1 may not be fulfilled as a result.

Finally, without graphically illustrating the point, it can be shown that an increase in the time constant T_s of the servo motor, or a decrease in the mechanical time constant J of the machine, can reduce the maximum mean slip under asynchronous transient conditions, and that this favours conditions for re-synchronization of the generator.

If operating conditions are such that re-synchronization cannot be ensured by appropriate design of the speed regulator, special measures have to be taken [3, 5].

Symbols*

M_{12} – amplitude of the synchronous generator torque;

$M_{as.av}$ – average asynchronous torque of the generator;

$M_{t.nom}$ and M_{t0} – rated and initial turbine torque;

M_t – turbine torque;

$M_{t.r}$ – braking (restraint) torque of turbine with fully closed turbine control gear;

$M_{t.c.o.v.}$ – turbine torque at the moment when the throttle is completely open;

* Angles and time are expressed in electrical radians and other quantities in relative units.

s_{av} – average slip (positive if the speed of the rotor is above its synchronous speed);

$s_{av.\ c.o.v.}$ – average slip at the moment when the throttle is completely open;

$s_{av.\ c.g.c.}$ – average slip at the moment when the turbine control gear is fully closed;

δ – the angle between the generalized vector of the stator voltage and the transverse axis of the rotor;

$\mu_{n.l}$ – opening of the turbine control gear on no load;

σ – extent to which the throttle is open;

β – feedback coefficient;

i – the ratio of the extent of the non-uniformity of the pendulum which is left, to that still to be used;

δ_{st} – "statism" of the turbine speed regulator ("statism" is defined as the percentage deviation of the controlled quantity at rated load from its value on no load, Translator);

δ_{nu} – the non-uniformity of the pendulum to be used;

T_s – time constant of the servo motor;

T_i – time constant of the "isodrome" (hyperbolical position – determining system or curve, Translator);

J – mechanical time constant of the machine;

t – time.

Translated by V. Alford

REFERENCES

1. I.M. Markovich and S.A. Sovalov; *Elektrichestvo*, 4, (1955).
2. M.P. Chesnov; *Elektrichestvo*, No. 6, (1960); Translation printed in Electric Technology U.S.S.R., vol, 6, (1960).
3. V.A. Venikov; *Elektromechanical transients in electrical systems, (Elektromekhanicheskie perekhodnye protsessy v elektricheskikh sistemakh)*, Gosenergoizdat, (1958).
4. Iu. E. Garkavi and M.S. Smirnov; *The control of hydro-electric turbines, (Regulirovanie gidroturbin)*. Mashgiz, (1954).
5. L.G. Mamikoniants, M.G. Portnoi and A.A. Khachwturov; *Asynchronous automatic reclosure of transmission lines with two-way supply, (Nesinkhronnoe APV linii elektroperedachi s dvustoronnym pitaniem)*. Inf. mat. VNIIE', No. 37, (1959).

A CONTINUOUS CONTROL SYSTEM FOR THE MAIN DRIVE OF A REVERSIBLE ROLLING MILL*

V.I. ARKHANGEL'SKII

TsPKB Glavproektmontazhavtomatika

(Received 1 August 1960)

Contactless control systems have had to be designed in order to create optimum transient conditions in the main drives of reversible rolling mills and to improve their reliability.

Several types of contactless control system have been developed at the TsKPB for M.A.R. and amplidyne-type generator-motor drives [1,2].

In this paper a study is made of a new control system for the main drive of a reversible blooming mill (Figs. 1 and 4) which is now in use at a Soviet iron and steel works**.

Control of the armature current of the motor under regenerative braking conditions

When controlling the roll motor up to fundamental speed, i.e. no weakening of the excitation field, the armature current is low during braking and reversing and no special measures are therefore necessary to limit it. Automatic devices are only needed for limiting the armature current when reversing and braking the motor at higher speeds when the field has been weakened.

---

* *Elektrichestvo*, 2, 33-39, 1961.

** A.A. Pivovarov, T.Ia. Vashchenko, G.M. Maliutin and V.A. Lebedev took part in the development and tests of the system proposed by the author.

The explanation is that two processes take place when the command to slow down is received, namely, strengthening of the motor field and reduction in the generator voltage. These two processes acting simultaneously cause an abrupt change in the transient current in the armature of the motor. The regeneration current is usually limited by delaying the reduction in the generator voltage until the motor field has been strengthened.

These two processes are kept separate in relay-contactor control systems by degenerative (negative) feedback of the armature current at the input to the dynamoelectric amplifier (amplidyne) used for the excitation of the generators [3,4]. This was the principle used in the continuous systems described in previous works [1,2].

The disadvantage of using a current regulator to separate these two processes is the notable delay in its operation owing to the considerable magnetic inertia of the voltage control system of the generators. The command-signal to slow down cannot be blocked at the input to the amplidyne of the generators and the first change in the regeneration current is relatively large.

The second real disadvantage of regenerative current regulators is as a rule the oscillations which occur in the motor armature current.

In the circuit in Fig. 1, a saturable reactor (choke) *SR* is connected in the a.c. circuit feeding the push-pull magnetic amplifier *MG* for the excitation of the generators. If the field of the roll motor is weak, the reactor (choke) reduces the possible forcing of the generator amplidyne several times over so that during regenerative braking the reduction in motor speed from maximum to fundamental speed is almost exclusively due to field strengthening. The generator voltage remains practically constant. In this way the armature current can be strictly controlled.

When the field has been strengthened, the reactor restores a high degree of forcing which controls the voltage of the generators and ensures the required reversing speed at speeds up to the fundamental speed.

The steady state voltage of the generator is unaffected by the magnetization of the reactor (whether saturated or not).

Use is made of the following windings to control the reactor *SR* (Fig. 1b):

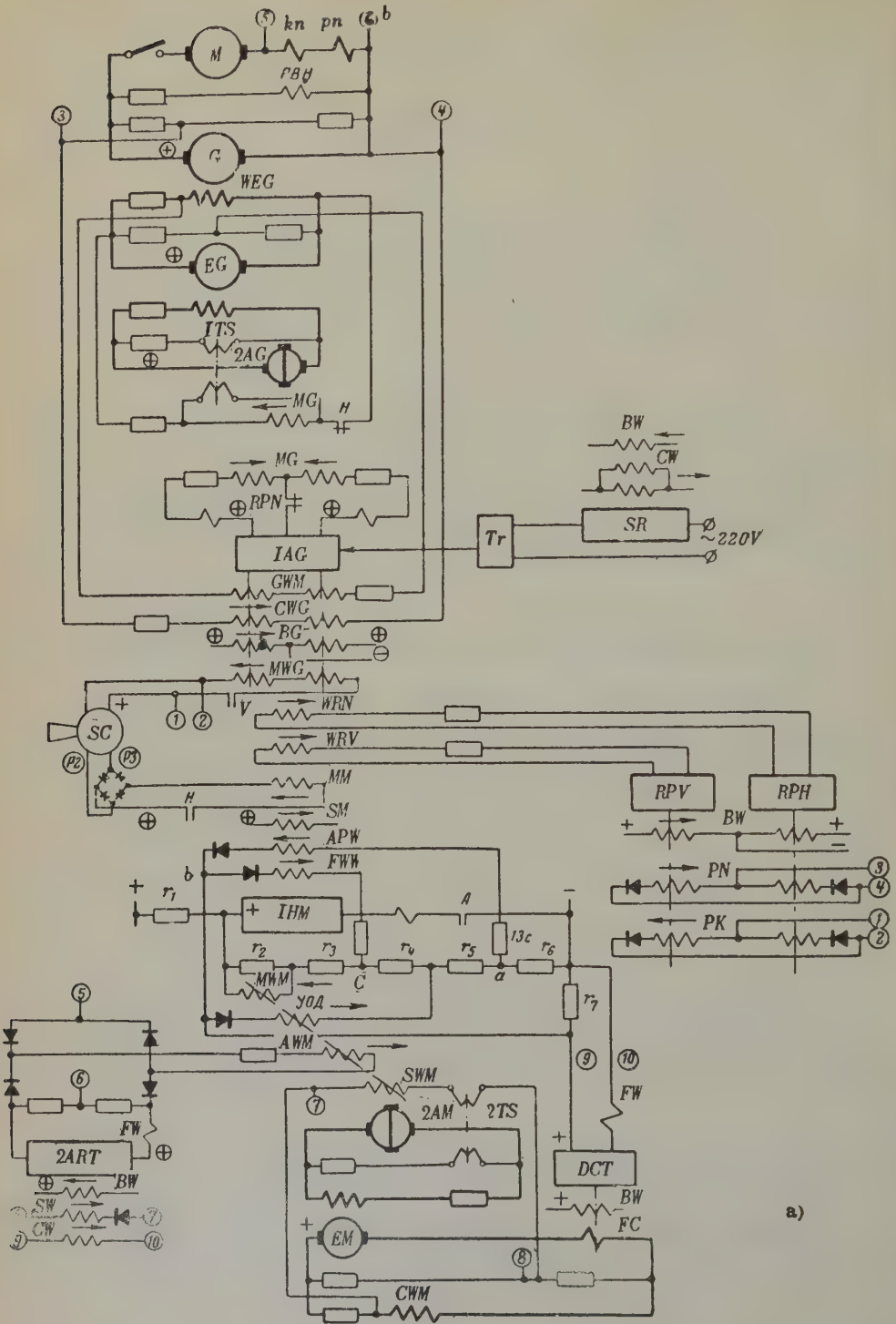
M
kn
pn
b
rBg
G
WEG
EG
ITS
2AG
MG
H
RPN
IAG
Tr
SR
~220V
BW
CW
GWM
CWG
BG
MWG
WRN
WRV
SC
V
MM
SM
APW
FWW
IHM
r1
r2
r3
r4
r5
r6
r7
MWM
УОД
AWM
SWM
2AM
2TS
2ART
FW
BW
SW
CW
DCT
FC
EM
CWM
RPV
RPH
PN
PK
a)

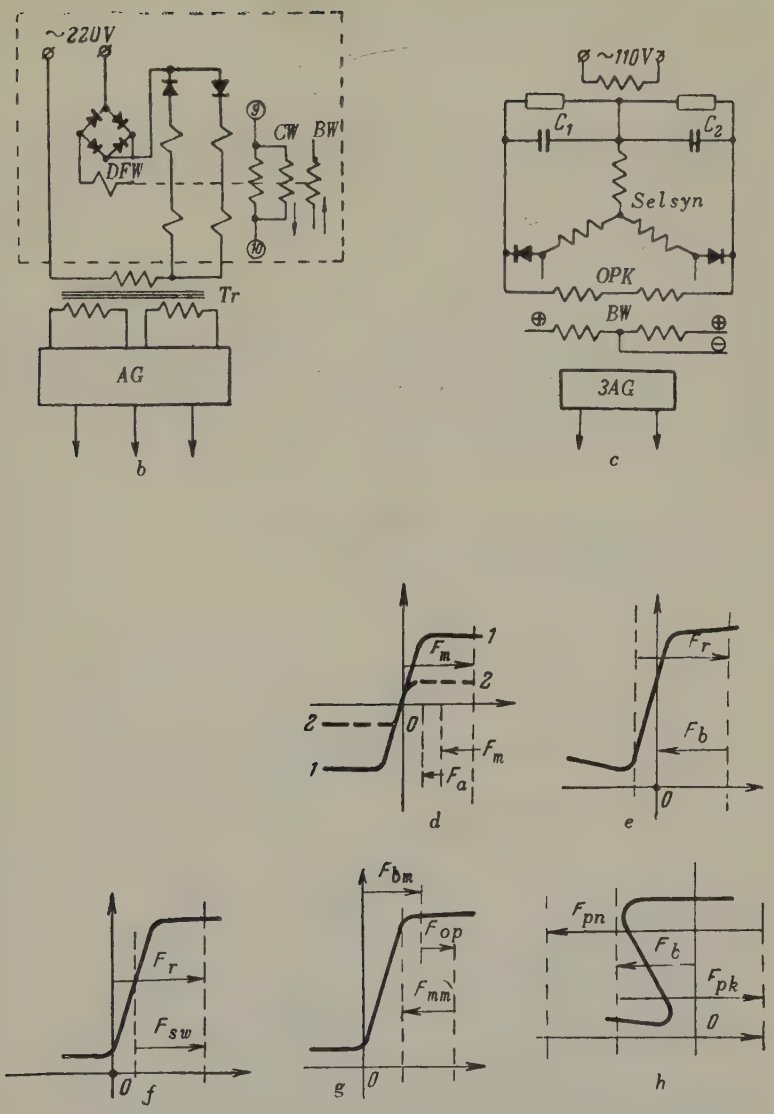

Fig. 1. *a* - continuous control system for the main drive of a reversible rolling mill; *b* - arrangement of the reactor windings; *c* - circuit of the continuous controller; *d* - characteristic of the amplifier *AG*; *e* - reactor characteristic; *f* - characteristic of the amplifier 2 *ART*; *g* - characteristic of the amplifier 1*AM*; *h* - characteristics of the contactless relays *RPV* and *RPN*.

1. A series degenerative (negative) feedback winding *DFW* for the load current of the reactor. This winding is connected via a full-wave rectifier;

2. bias winding *BW*;

3. control winding *CW* which is connected to the excitation current transformer *DCT*. Its m.m.f. is proportional to the motor excitation current.

The characteristic of the reactor is shown in Fig. 2.

The reactor is fully saturated at the rated excitation current of the motor so that the magnetic amplifier *AG* receives the maximum alternating voltage. Conversely, the rezctor is not saturated when the field of the motor has been fully weakened and the alternating voltage supplied to the amplifier *AG* is much lower.

Curve 1 for the amplifier *AG* in Fig. 3 refers to the total motor flux and curve 2 to the weakened flux.

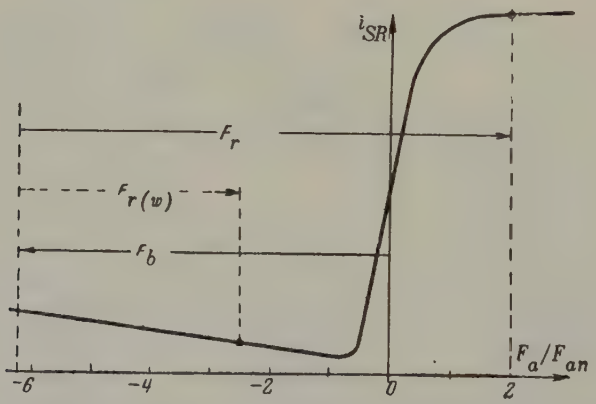

Fig. 2. Characteristic of the reactor *SR*.
$F_{r(n)}$ and $F_{r(w)}$ - m.m.f.'s of the reactor proportional to the excitation current of the roll motor for nominal and weakened motor fields;
F_b - bias m.m.f.

On acceleration of the motor to a higher speed than the fundamental speed, there is no restriction on the excitation by the reactor *SR* during the increase in generator voltage up to 80 to 85 per cent of rated forcing. When the field of the motor begins to weaken, there is

a gradual de-saturation of the reactor and the forcing of the excitation of the generator is restricted. However, this is a normal transient condition. The degree of saturation of the reactor has no effect on any further acceleration owing to the weakening of the motor field.

The command-controller *CC* ("sequence" control) issues two simultaneous commands when the motor begins to slow down from maximum speed. One is to strengthen the motor field and the other to reduce the voltage of the generators. The strengthening of the field takes place at once, but the reduction in the voltage of the generators is a gradual process since the amplifier *AG* is operating on curve 2 in Fig. 3 which excludes forced excitation of the generator. There is therefore only a slight change in the armature current. After the field of the motor has increased to 70-80 per cent of its rated value, the amplifier *AG* begins to operate on curve 1 in Fig. 3 and forcing of the generator excitation is restored.

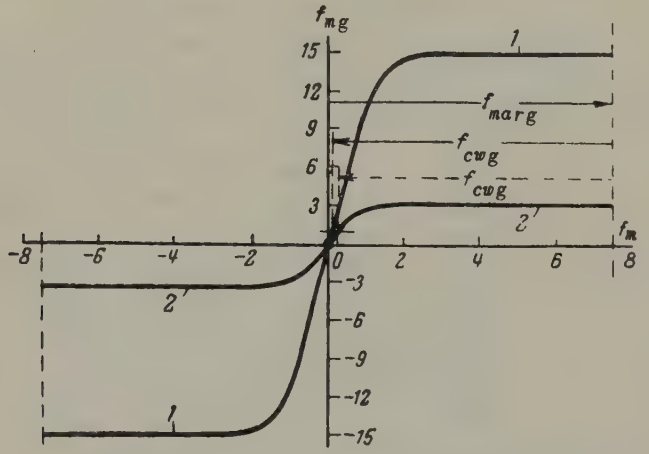

Fig. 3. Test curve for reactor-amplifier (1*AG*) unit.
1 – reactor saturated; 2 – reactor not saturated.

We will now consider the relationship between the degree of reduction in the rate of variation of the generator voltage and the magnitude of the master m.m.f. of the amplifier 2*AG*.

As an approximation, suppose that the magnetization curves of the exciter *EG*, generator *G* and amplidyne *DEA* are linear and that the electromagnetic time constant of the amplidyne is constant. We then get (Fig. 4):

$$U_{ag} = k_{ag} F_{dg}; \tag{1}$$

$$U_{eg} = k_{eg} i_{eg}; \tag{2}$$

$$U_g = k_g i_g; \tag{3}$$

$$U_{ag} = r_{eg} i_{eg} (1 + T_{eg} p); \tag{4}$$

$$U_{eg} = r_g i_g (1 + T_g p); \tag{5}$$

$$F_{dg} = F_{mas.g} - F_{mg}, \tag{6}$$

where U_{ag}, U_{eg} and U_g are the voltages of the amplidyne *DEA*, the exciter *EG* and the generator *G*;

k_{ag}, k_{eg} and k_g coefficients defined from the linear sections of the magnetization characteristics;

F_{dg} - the resultant m.m.f. of the generator amplidyne;

i_{eg} and i_g - excitation current of the exciter *EG* and the generator *G*;

r_{eg} and r_g - the resistance of the excitation circuits of the exciter *EG* and generator *G* including the "additional" resistances;

T_{eg} and T_g - electromagnetic time constants of the excitation circuits of the exciter and generator;

F_{mg} - the m.m.f. of the flexible negative (degenerative) feedback created by the winding *MG* of the amplidyne.

The joint solutions of equations (1) to (6) gives:

$$U_g = \frac{k_{ag} k_{eg} k_g}{r_{eg} r_g} \frac{F_{dg}}{(1 + T_{eg} p)(1 + T_g p)}. \tag{7}$$

The current in the circuit of the winding *MG* is approximately proportional to the derivative of the voltage of the exciter *EG*. We can put:

$$F_{mg} = k_{mg} p U_{eg}, \tag{8}$$

where k_{mg} is the feedback coefficient of the winding *MG* which is connected to the statically-balanced dynamic bridge.

By virtue of 8, the resulting m.m.f. of the amplidyne is

$$F_{dg} = F_{mas.g} - \frac{k_{mg}}{k_g} r_g p\ (1 + T_g p)\ U_g. \tag{6a}$$

The joint solution of equations 6(a) and (7) gives:

$$U_g\ (1 + T_{eg.eg}p)\ (1 + T_g p) = k_{g.eg} F_m, \tag{9}$$

where

$$\left.\begin{aligned} k_{g.eg} &= \frac{k_{ag} k_{eg} k_g}{r_{eg} r_g}; \\ T_{eg.eg} &= T_{eg} + \frac{k_{ag} k_{eg} k_{mg}}{r_{eg} r_g} = T_{eg} + T_{mg}, \end{aligned}\right\} \tag{10}$$

and $T_{eg.eq}$ is the equivalent time constant of the generator exciter consisting of the natural time constant T_{eg} and the component T_{mg}. (The subscript mg presumably refers to the MG winding. Translator).

The solution of equation (9) is

$$U_g = A_1 e^{\alpha_1 t} + A_2 e^{\alpha_2 t} + k_{g.eq} F_m, \tag{11}$$

where

$$\alpha_{1,2} = \frac{1}{2}\ \frac{T_{eg.eq} - T_g}{T_{eg.eq} T_g} \pm \sqrt{\frac{1}{4}\left(\frac{T_{eg.eq} - T_g}{T_{eg.eq} T_g}\right)^2 - \frac{1}{T_{eg.eq} T_g}}; \tag{12}$$

and A_1 and A_2 are integration constants.

At the start of reversing $t = 0$, we have:

$$\left.\begin{aligned} F_m &= -F_{mw}; \\ U_g &= U_{gs}; \\ \frac{dU_g}{dt} &= 0, \end{aligned}\right\} \tag{13}$$

where F_{mw} is the reduced value of the m.m.f. of the master windings of the amplidyne on account of the reactor *SR* (Fig. 3);

U_{gs} – the steady state voltage of the generator *G*.

We can define the integration constants in equation (11) from (13). We get:

$$U_g = \frac{U_{gs}+k_{g.eq}F_{mw}}{\alpha_2-\alpha_1}(\alpha_2 e^{\alpha_1 t}-\alpha_1 e^{\alpha_2 t}) - k_{g.eq}F_{mw}. \qquad (14)$$

Suppose we put

$$u_g = \frac{U_g}{U_{gr}},\quad f_{mw} = \frac{F_{mw}}{F_{mr}} \text{ and } U_{gr} = k_{g.eg}F_{mr},$$

We can then re-write equation (14) in relative units

$$u_g = \frac{1}{\alpha_2-\alpha_1}(\alpha_2 e^{\alpha_1 t}-\alpha_1 e^{\alpha_2 t}) - f_{mw}\left[1-\frac{1}{\alpha_2-\alpha_1}(\alpha_2 e^{\alpha_1 t}-\alpha_1 e^{\alpha_2 t})\right], \qquad (14a)$$

where f_m is the degree of forcing of the generator excitation reduced as a result of the reactor *SR*;

F_{mr} – the m.m.f. of the amplidyne under rated excitation of the generator;

U_{gr} – the rated voltage of the generator (it is presupposed that the steady state voltage of the generator U_{gs} is equal to the rated value prior to reversing).

The radicand in (12) is often negative for large drives. In this case we can write:

$$\alpha_{1,2} = -\alpha \pm j\gamma, \qquad (15)$$

where

$$\alpha = \frac{T_{eg.eq}+T_g}{T_{eg.eq}T_g};$$

$$\gamma = \sqrt{-\frac{1}{4}\left(\frac{T_{eg.eq}+T_g}{T_{eg.eq}T_g}\right)^2+\frac{1}{T_{eg.eq}T_g}},$$

and the solution of equation (11) is

$$u_g = e^{-\alpha t}\left(\cos\gamma t + \frac{\alpha}{\gamma}\sin\gamma t\right) - \\ - f_{mw}\left[1 - e^{-\alpha t}\left(\cos\gamma t + \frac{\alpha}{\gamma}\sin\gamma t\right)\right]. \quad (16)$$

Both equations (16) and (14a) consist of two terms. The first is solely defined by the characteristics of the excitation control system of the generator. The second describes the rate of change in the generator voltage due to the reduced m.m.f. f_{mw} of the amplidyne. The value of the second term is directly proportional to f_{mw}, the forcing of the excitation.

Since the rate of change in the generator voltage is defined by the first derivative of this quantity, we can write for equations (14a) and (16):

(a) non-periodic transient processes

$$\frac{du_g}{dt} = (1 + f_{mw})\frac{\alpha_2\alpha_1}{\alpha_2 - \alpha_1}(e^{\alpha_1 t} - e^{\alpha_2 t}); \quad (17)$$

(b) periodic processes:

$$\frac{du_g}{dt} = (1 + f_{mw})\left(1 + \frac{\alpha^2}{\gamma^2}\right)\gamma e^{-\alpha t}\sin\gamma t. \quad (18)$$

The circuit in Fig. 4, in respect of which the relations have between considered which define the rate of change in the generator boltage as a function of the degree of amplidyne forcing of the excitation f_{mw}, differs from the voltage regulator as in Fig. 1 in that the winding *MG* of the amplifier 2*AG* is connected to the stabilizing transformer *ITS*. On test both regulators (given the right flexible feedback coefficient F_{mg}) produced practically identical results. The two types are therefore equally good.

For the regulator with the stabilizing transformer, oscillations occur in the system if the circuit is opened, whilst positive (regenerative) feedback may arise at the input to the amplidyne if the circuit with the dynamic bridge is opened. The latter can give rise to an excessive increase in the generator voltage.

For a 500 h.p. reversing motor (750 V 50/100 rev/min) for a rail and structural mill with a continuous control system, we have: (a) amplification factor $k_{ag} = 6.0$; $k_{eg} = 45$; $k_g = 8$; $k_{mg} = 0.3$; $k_{g.eq} = 87$;

(b) time constants T_{eg} = 0.5 sec; T_g = 1.1 sec; $T_{eg.eq}$ = 3.1 sec;

(c) resistances r_{eg} = 31 ohm; r_g = 0.8 ohm.

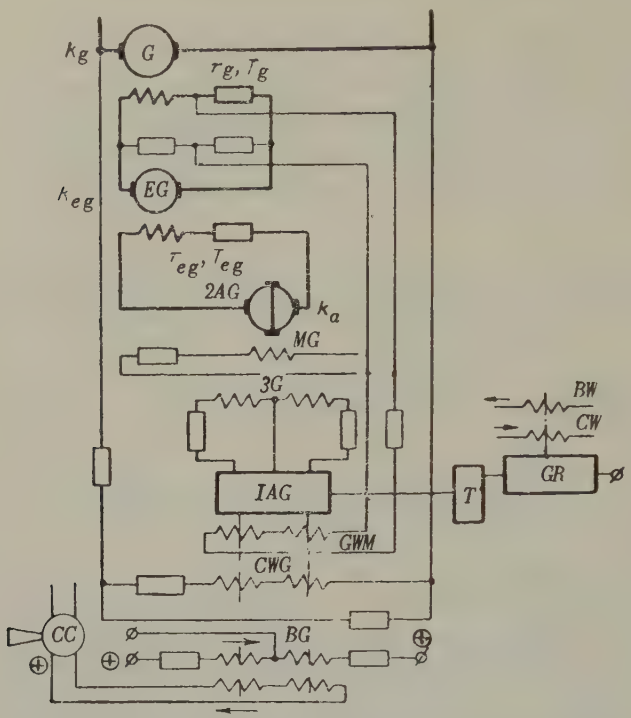

Fig. 4. Control system for the generator voltage.

The transient variation in the generator voltage on reversing is described by equation (16). Substituting numerical values for the coefficients, we get:

$$u_g = e^{-0,51t}(\cos 0,17t + 3\sin 0,17t) - \\ - f_{mw}[1 - e^{-0,51t}(\cos 0,17t + 3\sin 0,17t)]. \qquad (16a)$$

Equation (18) for the first derivative of the generator voltage takes the form:

$$\frac{du_g}{dt} = 1,7\,(1 + f_{mw})\,e^{-0,51t}\sin 0,17t. \qquad (18a)$$

The master m.m.f. of the amplidyne during full excitation forcing when the reactor is saturated equals $f_{m.max}$ = 15; when the reactor is

unsaturated, it is reduced to $f_{mw} = 3$.

The magnetizing force (control power) of the amplidyne at the steady rated generator voltage equals $F_{m.nom} = 9.0$ VA.

Substituting these figures in (18a), we can determine the extent of the decrease in the rate of change of the generator voltage at high motor speeds at the start of reversing due to the reactor *SR*. The degree k_f of the decrease in forcing is

$$k_f = \frac{f_{mm}}{f_{mw}} = \frac{15}{3} = 5;$$

and the degree k_d of the reduction in the value of the derivative according to (18a) equals

$$k_d = \frac{1 + f_{mm}}{1 + f_{mw}} = \frac{16}{4} = 4.$$

Fig. 5 shows the magnetization curve of the amplidyne. This illustrates the effect of reducing the forcing of the generator excitations when the master m.m.f. of the amplidyne falls. It will also be seen from Fig. 5 that our conclusions cannot be significantly affected by ignoring the saturation of the magnetic circuits.

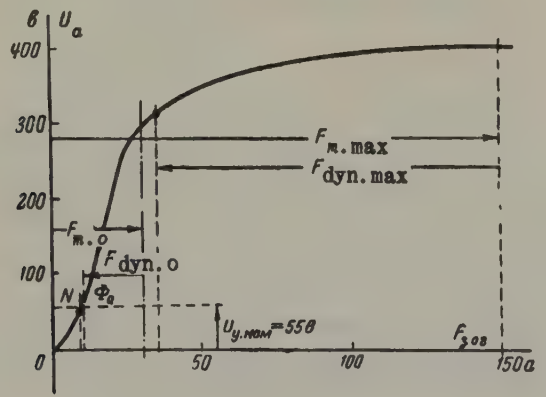

Fig. 5. The resulting characteristic 1*AG*-2*AG*. $F_{m.max}$ and $F_{dyn.max}$ – m.m.f.'s of the master and dynamic windings of the amplifier 2*AG* with the reactor saturated; $F_{m.o}$ and $F_{dyn.o}$ – the same, but with the reactor unsaturated.

Two m.m.f.'s are active at the input to the amplidyne, namely, the master m.m.f. F_m and the "dynamic" m.m.f. F_{dyn} which is subtracted from F_m. Since the difference between these two m.m.f. is much less than either component, it follows that the degree of reduction in F_{dyn} cannot be very much different from the degree of reduction in F_m. The magnitude of F_{dyn}, which is proportional to the rate of increase in the voltage of the exciter EG, defines the forcing of the generator excitation.

Incidentally, the equivalent time constant $T_{eg.eq}$ of the excitation of the generator exciter is six times greater than the electromagnetic time constant of the exciter excitation circuit (T_{eg} = 0.5 sec and $T_{eg.eq}$ = 3.1 sec).

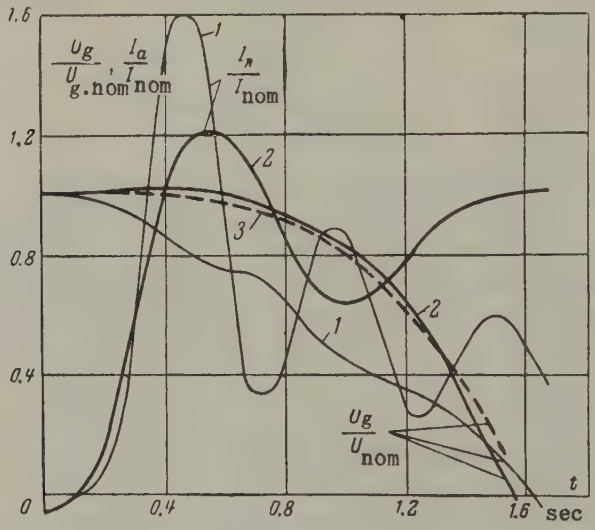

Fig. 6. Curves for the transient phenomena which take place on reversing a 5000 h.p. motor of 750V, 5400A, 50/100 rev/min and i_{en} = 340 A.

1 – contact control system; 2 – continuous control system; 3 – calculated curve for the voltage in the continuous control system; U_g – generator voltage; I_a armature current of motor.

According to expression (10), the magnitude of $T_{eg.eq}$ increases with increasing flexible feedback of the amplidyne. Its m.m.f. F_{dyn} is defined by the coefficient $k_{m,g}$. Consequently, it is not always wise to try and reduce the electromagnetic time constant T_{eg} of the exciter to a very small quantity. The second term T_{mg} in expression (10) can easily be adjusted, whereas this is not the case with T_{eg}. The system

can thus be adjusted to the desired dynamic conditions.

Fig. 6 illustrates the advantage of a regulator for the regenerative current of the motor in which the parametric principle is used without direct control over the armature current. For purposes of comparison, curves are given for the armature current and generator voltage when the motor is slowed down whilst reversing under contactor and contactless control. All the curves have been plotted from oscillograms of the transient phenomena taking place in a 5000 h.p. motor on no load. Considerable changes occur with a regenerative current regulator which lead to sparking on the motor and generator commutators, mechanical shocks in the rolling mill, a reduction in the mean torque of the motor and so on.

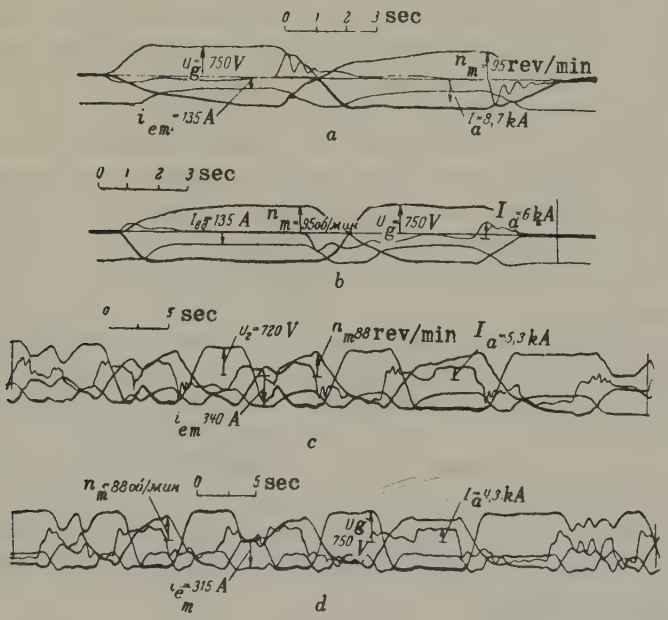

Fig. 7. Oscillograms of the transient phenomena on accelerating, reversing and braking an unloaded motor (*a*, *b*) and oscillograms of the rolling cycles (*c*, *d*). *a* and *c* – contact control systems; *b* and *d* – continuous control systems.

The oscillograms in Fig. 7(a) and (b) show the transient conditions during acceleration, reversing and braking of the motor (when the shaft is unloaded). The changeover to contactless control considerably shortens transient conditions. The rolling cycle of one billet was accordingly reduced by 10 to 12 per cent on average.

Control of the motor excitation current

Optimum conditions for dynamic control of the motor field can be created by a special arrangement of the control windings in the magnetic amplifier 1*AM* and the amplidyne 2*AM*. The amplidyne 2*AM* uses a master winding *MWM*, a control winding *CWM*, a current winding *AWM* and a stabilization winding *SWM* (Fig. 1a).

The master winding *MWD* is connected to the d.c. 220V network via a resistor r_1 and part of the load current of the amplifier 1*AM* also flows through it. A reference voltage is produced across the resistors r_5 and r_6. These are a part of the load of the amplifier 1*AM*. The reference voltage is produced at the input to the amplifier 1*AM* by the command-controller. The master m.m.f. created by the *MWM* winding depends on the extent to which the field is weakened; it is smaller when the field is weak than when excitation is complete.

The branches *ab* and *bc* are intended to create optimum dynamic conditions for the drive. Under steady state conditions no current is carried in them since $u_a < u_b$ and $u_b < u_c$. The current in the circuit of the control winding *CWM* depends solely on the difference between the voltage drops across the resistors r_7 and r_5–r_6. The diode 1*D* only allows current to flow in the *CWM* winding if $U_{r7} > U_{r5,\ r6}$. The voltage drop U_{r7} is proportional to the excitation current of the motor. The d.c. transformer *DCT* is connected in the excitation circuit of the motor.

The reference voltage produced by the amplifier 1*AM* determines the magnitude of the excitation current of the motor. The master winding of this amplifier is supplied via a rectifier from the selsyn command-controller. The m.m.f. of this winding is proportional to the angle of deflection of the selsyn.

The control windings of the amplifier 1*AM* are connected in the branches *ab* and *bc* in order to create dynamic conditions, i.e. the winding *FWW* restricts the forcing when the field is weakened and the winding *APW* limits the initial forcing when the field of the motor is strengthened.

At the start of the field weakening the voltage drop across the resistors r_4–r_6 is sharply reduced and the potential at point *c* becomes less than that at point *b*; a current is then produced in the *FWW* winding and the positive m.m.f. of this winding slightly increases the output voltage of 1*AM*. This reduces the change in m.m.f. of the differential winding *CWM* and limits the reduction in the m.m.f. of the *MWM*

winding of the amplifier 2*AM*. The voltage drop across the resistor r_7 becomes less with decreasing motor excitation current and the current in the *FWW* winding disappears.

Under strong field conditions there is first a sudden increase in the voltage drop across the resistor r_6 and a current arises in the *APW* winding of the amplifier 1*AM*. The negative m.m.f. of this winding limits the increase in the output voltage of the amplifier 1*AM* and this in its turn limits the increase in the master m.m.f. (*MWM* winding) of the amplifier 2*AM*. Then the effect of the bc circuit is weakened and the field forcing increases with increasing motor excitation current.

In order to separate the states of control over the voltage of the generators and the field of the motor, the amplifier 1*AM* is provided with windings *WRV* and *WRN* which are supplied by the field relays *RPV* and *RPN*. The m.m.f.'s of these windings prevent the weakening of the field until the voltage of the generators reaches about 85 per cent of its rated value during acceleration. Fig. 1(g) illustrates the relationship between the m.m.f.'s of the control windings in the amplifier 1*AM*. If there are no m.m.f.'s F_{mm} and F_{op}, the amplifier 1*AM* is completely opened by the m.m.f. F_{bm} of the bias winding and the reference voltage (the output of the amplifier) is at a maximum corresponding to the rated excitation current of the motor [1].

Unlike previous systems [1,2], the proposed system of control for the motor field (Fig. 1a) provides a wider range of control over the excitation current of the motor and makes it easier to adjust for the desired conditions of dynamic control.

Conclusions

1. The continuous control system in Fig. 1(a) has real advantages over relay-contactor systems. They are:

(a) more rational conditions are created for controlling the drive which improves the efficiency of the electrical equipment and increases the productivity of the rolling mill;

(b) the control system is more reliable and easier to maintain;

(c) favourable conditions are created for applying automation to the rolling process.

2. The use of this control system on a reversible rolling mill

reduced the rolling cycle by 10 to 12 per cent.

Translated by V. Alford

REFERENCES

1. V.I. Arkhangel'skii; *Elektroprom. i priborstr.*, No.11, TsINTI Elektroprom., (1960).
2. V.I. Arkhangel'skii; *Contactless control systems for the drives of reversiable rolling mills, (Beskontaknye skhemy upravleniia elektroprivodami reversivnykh prokatnykh stanov).* Gosenergoizdat, (1960).
3. A.B. Cheliustkin and E.A. Rozenman; *Automatic control of rolling mills, (Avtomaticheshoe upravlenie prokatnymi stranami).* Metallurgizdat, (1955).

CAPACITIVE TRANSMISSION OF SURGE VOLTAGES IN TRANSFORMERS HAVING A BUSHING AT THE MID-POINT OF THE HIGH VOLTAGE WINDING*

S.D. LIZUNOV

Moscow Electrical Works

(Received 4 May 1960)

Introduction

In high voltage transformers having the line terminal at the mid-point of the high voltage winding, the induced potentials in the low-voltage winding due to surges reach considerable magnitude and in some cases (in 400-500 kV transformers) special measures must be taken to eliminate this undesirable phenomenon.

Not only may large potentials on the low voltage winding be dangerous to the earth insulation of this winding, but variations in this potential also affect the insulation between the low and high voltage windings and considerably increase the gradients** in the high tension (HT) winding. These conditions particularly affect three-winding transformers and auto-transformers when the LT winding is arranged between the high- and mid-voltage windings.

Thus, in conventional 220 kV transformers with the low tension (LT) winding in the centre, the potential induced in the middle of this

---

* *Elektrichestvo*, 2, 62-67, 1961.

** By gradients is meant the voltages on small sections of the longitudinal (centre turn) insulation.

winding by an impulse of 1.5/40 μ sec is about 30 sec per cent of that at the line end of the HT winding. This voltage has a considerable effect on the gradients and "lineals" (voltages about the line end) of the HT winding. It increases the gradients by a factor of 1.3 to 1.4 and the lineals still more owing to the oscillatory component at the natural frequency of the LT winding (Fig. 1).

The impulse method [1,3] of determining the gradients ignores the effect of the LT winding. The potentials on the LT windings can be much larger with chopped waves. But their effect on the gradients of the HT winding is somewhat weaker owing to the short duration of the main peak in the HT gradient.

There are usually no dangerous voltages on the LT windings when the line potential is introduced at the end of the HT winding since it is earthed at both ends by the large capacitance of the network.

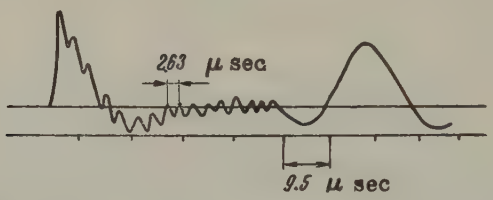

Fig. 1. Oscillogram of voltage transfer No.6 relative to the line in the HT winding of a 220 kV transformer of 40,000 kVA. The LT winding is placed between the high- and mid-voltage windings. The ends of the LT winding are earthed.

We assume throughout that the two ends of the LT winding are earthed as in impulse tests.

Capacitive transmission of the potential from the HT winding to the LT winding.

The initial induction of voltage on the LT winding by a surge with a vertical wavefront. In calculating the capacitive induction in transformers having a line terminal at the mid-point of the HT winding, we can confine ourselves to one branch and the corresponding half of the LT winding of each core; the fictitious discontinuity of the middle of the LT winding is assumed to be insulated.

We will now consider a method of estimating the capacitively-induced

voltages on the low and mid-voltage windings (i.e. the secondary windings) given a non-uniform HT winding.

The interturn capacitance of a secondary winding can greatly affect the magnitude and distribution of the voltage induced in this winding. But the effect of this capacitance on the distribution of the voltage on the primary winding is usually very small and can be neglected. There is then no difficulty in estimating the capacitive distribution of the voltage on the primary winding regardless of the interturn capacitance of the low- and mid-voltage windings for any degree of non-uniformity in this winding. The secondary windings are usually made uniform.

Given the approximate distribution of the voltage on the primary winding, even though it is non-uniform (only non-uniform interturn capacitances are in mind), by expressing it analytically we can then find an expression for the distribution of the capacitively-induced voltage on uniform secondary winding. This can be done by solving an inhomogeneous differential equation of a lower order than the homogeneous equation for the case when the primary winding is uniform but the distribution of the voltage over it unknown [3, 4].

The original distribution of the potential on the primary winding $U_{1\ \mathrm{init}}(x)$ is assumed to be given (Fig. 2). (Here x is the relative axial distance from the line end of the HT winding or from the middle of the LT winding; half the height of the winding is taken as unity).

To form the differential equation 1, we have to assume that the voltage $U_{1\ \mathrm{unit}}(x)$ is produced by an infinite power source all over the winding and that it remains unchanged on connexion of the capacitive circuit:

$$\frac{d^2 U_{2\mathrm{init}}(x)}{dx^2} - \frac{c_{12}+c_{02}}{c_{l2}} U_{2\mathrm{init}}(x) = -\frac{c_{12}}{c_{l2}} U_{1\mathrm{init}}(x). \tag{1}$$

where all the capacitances are referred to a unit of axial length. The subscript 1 refers to the primary winding, 2 – to the secondary (LT) winding, l to the interturn capacitances and 0 to the earth capacitances. The point $x = 0$ corresponds to the line end of the HT winding and the mid-point of the LT winding arranged opposite to it.

It is presupposed that the voltage in the primary winding can be defined as follows:

$$U_{1\mathrm{init}}(x) = Ae^{-\nu x} + Be^{-\eta x} \tag{2}$$

and that the windings can be regarded as infinite. Then the voltage for the potential on the secondary winding, if the boundary conditions are satisfied, is

$$U_{2\text{init}}(x) = \frac{c_{12}}{c_{12}+c_{02}}\left[A\frac{\lambda^2}{\lambda^2-\nu^2}\left(e^{-\nu x}-\frac{\nu}{\lambda}e^{-\lambda x}\right)+\right.$$
$$\left.+B\frac{\lambda^2}{\lambda^2-\eta^2}\left(e^{-\eta x}-\frac{\eta}{\lambda}e^{-\lambda x}\right)\right], \qquad (3)$$

where

$$\lambda = \sqrt{\frac{c_{12}+c_{02}}{c_{12}}}.$$

The voltage at the mid-point of the LT winding (if $x = 0$) is

$$U_{B\text{init}} = U_{2\text{init}}(0) = \frac{c_{12}}{c_{12}+c_{02}}\left(A\frac{\lambda}{\lambda+\nu}+B\frac{\lambda}{\lambda+\eta}\right). \qquad (4)$$

If $U_{1\ \text{init}}(x) = e^{-\nu x}$, formulae (3) and (4) are simplified.

Formulae can also be obtained similarly for a three-winding transformer. To estimate the voltage induced on an LT winding placed between the high- and mid-voltage windings we can use the formulae for a two-winding transformer since in this case the interturn capacitance of the mid-voltage winding will have very little effect on the distribution of the voltage on the LT winding. The earth capacitances of the LT winding can only be estimated if the earth capacitances of the mid-voltage winding are considered.

Impulses with a finite wavefront or chopped waves. For standard impulses (1.5/40 μ sec and chopped waves) it is necessary to include the inductance if the voltage in the LT winding is to be calculated correctly.

The voltage at the mid-point of the LT winding can be calculated by a simple equivalent network which need only be valid for the point in question (point *B* in Fig. 3). The period of fundamental oscillations of the LT winding is found from the formula

$$T = 2\pi\sqrt{L(c_1+c_2)} = 2\pi\sqrt{\frac{1}{4}L_2(c_{12}+c_{20})\,h}, \qquad (5)$$

where h is the total height of the winding.

The inductance L_2 can be estimated as follows. Suppose that the LT

winding occupies a mid-way position between the high voltage and mid-voltage windings. We can then find L_2 as the leakage inductance between half of the LT winding and the adjacent windings on the assumption that the whole leakage flux travels in channels between the windings and that there is none at all in the copper.

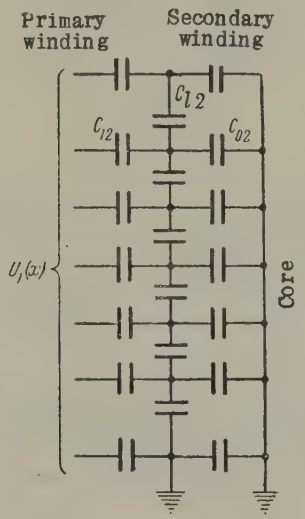

Fig. 2. Equivalent capacitive network of a two-winding transformer with a given distribution of the voltage on the primary winding.

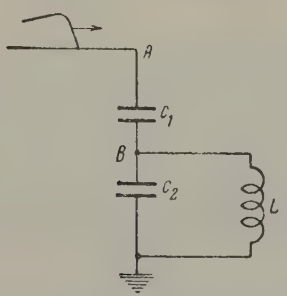

Fig. 3. Equivalent network for determining the shape of the voltage oscillations in the middle of the LT winding.

If the LT winding is at the core, L_2 is still found in the same way, but the surface of the core is regarded as a conducting screen since the

flux is excluded from the steel by the eddy currents. The residual effect of the core can be included by multiplying the value of L_2 by a factor of about 2.5. The period T is usually 3 to 6 μ sec for LT windings.

If an infintely long surge with a vertical wavefront (a "square" wave) is incident at point A, the unit amplitude of the potential at point B can be expressed by the formula*

$$U_{Bl}(t) = \underset{B(\text{init})}{U} \cos\left(2\pi \frac{t}{T}\right). \tag{6}$$

We assume that an impulse with a finite wavefront is of infinite length (this assumption has practically no effect on the magnitude of the voltage induced in the LT winding):

$$U_A(t) = 1 - e^{-mt}. \tag{7}$$

An expression can be found for the voltage induced by such a surge at the mid-point of the LT winding from formulae (6) and (7) by means of the Duhamel integral [3]. After simplifications we get:

$$U_B(t) = \underset{B(\text{init})}{U} \sin\varphi \left[\sin(\omega t + \varphi) - \sin\varphi e^{-mt}\right], \tag{8}$$

where

$$\sin\varphi = \frac{1}{\sqrt{1 + \left(\frac{\omega}{m}\right)^2}} = \frac{1}{\sqrt{1 + 5{,}2\left(\frac{s}{T}\right)^2}};$$

$U_{B(\text{init})}$ is defined by formula (4);

$\omega = \frac{2\pi}{T}$ - the "circular" (angular) frequency of the natural oscillations of the LT winding;

$s = \frac{2{,}75}{m}$ - a conventional wavefront expressed by equation (7) [2].

The incidence of the non-periodic component of formula (8) is defined by the wavefront of the effective surge. It is quite accurate to assume that expression (8) is at a maximum at the same moment as the sinusoidal term in square brackets. Hence the formula for the maximum voltage at the mid-point of the LT winding is

---

* Formulae (6), (8), (9) and (11) were derived by E.S. Frid.

$$U_{B\text{M}} = U_{B(\text{init})} \sin\varphi (1 + \delta), \tag{9}$$

where

$$\delta = \sin\varphi e^{-\tan\varphi \left(\frac{3}{2}\pi + \varphi\right)}.$$

It follows from formula (9) that the voltage in the LT winding is smaller, the larger the ratio $\frac{S}{T}$.

With a chopped wave the induced potentials are much larger, since the inverse wave (component 2 in Fig. 4), which chiefly determines the induction with a chopped wave, is much steeper and is $1 + k_0$ times greater in amplitude than at the "chop" which is taken as 100 per cent (k_0 is the relative transition of the voltages through zero at chopping).

In addition, the potentials induced from the two components (Fig. 4) may be identical in sign at the moment the total potential is a maximum and they can be added (Fig. 5). The potential induced with the chopped wave increases as the coefficient of transition through zero increases.

Component 2 of the chopped wave (Fig. 4) can be expressed by the following formula if damping of the oscillations is excluded:

$$U_A(t) = -\frac{1 + k_0}{2}\{1 - \cos[\omega_{cp}(t - \tau_{cp})]\}, \tag{10}$$

where $\omega_{av} = \frac{2\pi}{T_{av}}$ is the angular frequency of the oscillations of the potential at point A after the "chop";

τ_{av} – the pre-discharge time (Fig. 4).

Using formulae (7), (8) and (10) and the Duhamel integral, the absolute maximum potential at point B is defined after simplification by the expression

$$U_{B\text{M}} = U_{B(\text{init})}\left[\frac{1 + k_0}{2(1 - \beta^2)}(1 + \cos\beta\pi) - \right.$$
$$\left. - \sin\varphi \cdot \sin(\omega\tau_{cp} + \beta\pi + \varphi)\right], \tag{11}$$

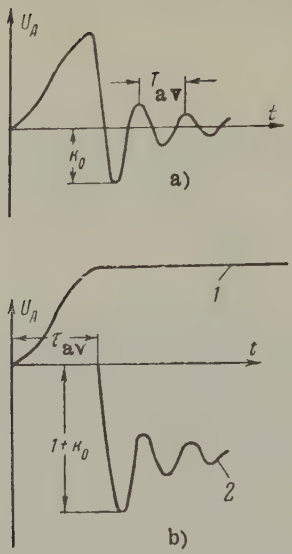

Fig. 4. The chopped waveform and its components;
a – chopped waveform;
b – expansion into its two components.
1 – un-chopped component;
2 – inverse component;

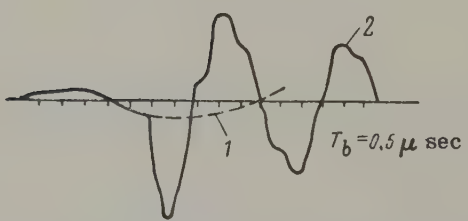

Fig. 5. Oscillogram of the potential induced in the middle of the LT winding of a 220 kV 40,000 kVA transformer due to a chopped surge. The dotted line shows the potential induced by an unchopped surge.

where

$$\beta = \frac{\omega}{\omega_{av}} = \frac{T_{av}}{T},$$

$$\sin\varphi = \frac{1}{\sqrt{1 + 5{,}2(\tau_{av}/T)^2}}.$$

Typical voltages induced in the middle of the winding of various transformers are given in the Table.

Transformer	Voltage class of mid-voltage winding, kV	Position of LT winding	Potential at the mid-point of the LT winding as a percentage			
			Total wave 1.5/40 sec		Chopped wave	
			Test	Call	Test	Call
40,000 kVA, 220kV (3-w (3-winding)	110		24	29	69	73
60,000 kVA, 400 kV (2-winding model) ..	–	–	11	15.6	33	39.6

N.B. The calculated values are angular because damping was ignored.

The capacitive effect of voltage oscillations in the LT winding on the gradients in the HT winding

Nature of the effect. The LT winding usually has a mainly capacitive effect on the gradients in the HT winding. We ignore those cases where the effect is inductive.

Corresponding to the capacitive distribution of the voltage on the HT winding (Fig. 6) the first moment after the incidence of a surge with a vertical wavefront, there is a capacitively-induced voltage distribution of the same sign on the LT winding, i.e. $U_{2\ init}(x)$. After a period of time equal to a half-wave of the natural frequency of the LT winding, this voltage changes sign on passing through zero and capacitively induces an additional voltage in the HT winding which is

opposite in sign to that of the surge.

Since the natural frequencies of the winding are widely different, it follows that we can more or less regard these oscillations as independent of each other. The change in the voltage of the LT winding relative to that at the first moment (assuming synchronous change at all points), can be expressed in the form:

$$\Delta U_2(x, t) = U_2(x, t) - U_{2\text{init}}(x)(1 - \cos \omega t), \tag{12}$$

where $\Delta U_2(x, t)$ is the change in the voltage of the LT winding affecting the HT winding;

$U_{2\ \text{init}}(x)$ the initial value of the voltage induced in the LT winding;

$U_2(x, t)$ - the voltage of the LT winding.

When studying the gradients in the HT winding it is therefore necessary to consider two actions, namely, the actual surge at the line end of the HT winding (the waveform is assumed to be square), and the wave via the capacitance on the LT winding side in the form of (12).

The criterion for estimating the gradients is the curve for the initial voltage distribution [1,2]. For an actual surge, this initial distribution can be obtained in the usual way. It can be roughly calculated analytically for the second component given uniform windings (for a square waveform via the capacitance on the LT winding side). The line end of the HT winding must be regarded as earthed owing to the great capacitance of the line.

The voltage distribution is illustrated in Fig. 6(a) for both components.

The expression for the initial voltage distribution for calculating the induced gradients. The induction in the HT winding is calculated in a similar way to that illustrated in Fig. 2, except that the voltage $U_{2\ \text{init}}$ is now regarded as given. The differential equation is exactly the same as equation (1), it being only necessary to substitute the subscript 2 for 1.

For the sake of simplicity it is assumed that the initial voltage distribution along the LT winding is linear:

$$U_{2\text{init}}(x) = U_{B(\text{init})}(1 - x). \tag{13}$$

Operating experience with 220kV transformers has shown that expression (13) is very near the actual voltage distribution along the LT winding; the initial voltage induced in the HT winding is then

$$U_{1\text{init}}(x) = \frac{c_{12}}{c_{12} + c_{01}} U_{B(\text{init})}(1 - x - e^{-\alpha x}), \tag{14}$$

where

$$\alpha = \sqrt{\frac{c_{12} + c_{01}}{c_{11}}}. \tag{15}$$

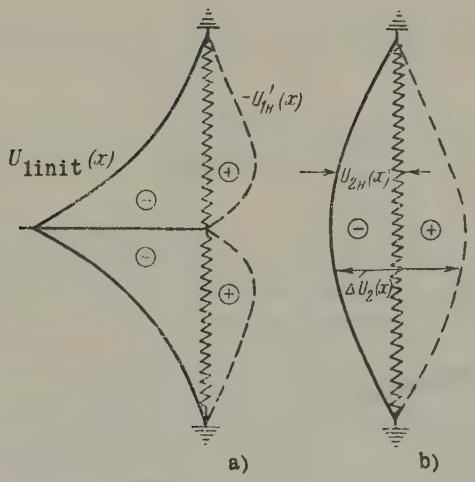

Fig. 6. The capacitive effect on the LT winding; a – initial distribution along the HT winding – two components; b – distribution along the LT winding.

Only the exponential term – $e^{-\alpha x}$ in the expression in brackets has any real importance in inducing gradients. Hence, from the point of view of calculating these gradients, the sudden application to the LT winding of a voltage which is defined at each point by expression (13), is equivalent to the square waveform of opposite polarity to that of the voltage in the LT winding at the line end of the HT winding and having an amplitude $\frac{c_{12}}{c_{12} + c_{01}} U_{B(\text{init})}$.

To calculate the induced gradients (given a synchronous change in the voltage all over the LT winding) we can replace the voltage $U_B(t)$ in the LT winding by the surge at the line end of the HT winding with the waveform

$$U'_A(t) = -\frac{c_{12}}{c_{12}+c_{01}} U_B(t). \tag{16}$$

The induced gradients with a surge having a finite wavefront. From the point of view of the effect of the oscillations in the LT winding on the gradients in the HT winding, the change in the voltage of the LT winding due to the presence of these oscillations (by analogy with formula (12) for a surge of square waveform and in accordance with (7) and (8) must be

$$\begin{aligned}\Delta U_2(x, t) &= U_2(x, t)_k - U_2(x, t)_a = \\ &= -U_{2\text{init}}(x)\{(1-e^{-mt}) - \\ &- [\sin\varphi \cdot \sin(\omega t + \varphi) - \sin^2\varphi \cdot e^{-mt}]\},\end{aligned} \tag{17}$$

where $\Delta U_2(x, t)$ is the change in the LT voltage affecting the HT winding;

$U_2(x, t)_a$ – the capacitively-induced voltage in the LT winding in the absence of oscillations;

$U_2(x, t)_k$ – the actual voltage in the LT winding.

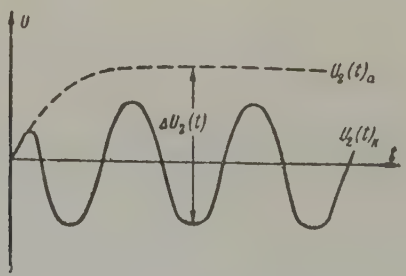

Fig. 7. The voltage of the LT winding due to a surge with a finite wavefront.

Fig. 7 shows the voltages $U_2(x, t)_k$ and $U_2(x, t)_a$ as a function of time at any point of the secondary winding.

In accordance with formula (16), the equivalent effect of a surge of

square waveform at the line end of the HT winding corresponding to the change in the voltage in the LT winding from formula (17), is found by the expression

$$U'_A(t) = \frac{c_{12}}{c_{12}+c_{01}} U_{B(\text{init})} (1 - e^{-mt}) - \\ - [\sin\varphi \cdot \sin(\omega t + \varphi) - \sin^2\varphi \cdot e^{-mt}]\}. \tag{18}$$

Formula (18) changes into formula (19) for surges of square waveform as $m \to \infty$:

$$U'_A(t) = \frac{c_{12}}{c_{12}+c_{01}} U_{B(\text{init})} [1 - \cos\omega t]. \tag{19}$$

If the frequency drops to zero, the conditional equivalent effects (18) and (19) also tend to zero and, consequently, so do the induced gradients.

Suppose we consider the components of the gradient induced in the HT winding by each term in expression (18).

The gradient of induction g'_1 from the term $\frac{c_{12}}{c_{12}+c_{01}} \times U_{B(\text{init})}$ $(1 - e^{-mt})$ in expression (18) can be estimated by the formulae for surges having a finite wavefront as proposed previously by Frid [2].

An expression for the gradient from the term $N \sin(\omega t + \phi)$ can easily be found from the formula for the gradient of a surge with a square waveform by the Duhamel integral. For example, for the second interval, i.e. if $X < Vt < (X+D)$:

$$g'_2(X, t) = -N\left\{\frac{1}{1+\nu^2}\cos\varphi[\nu + \tan\varphi] e^{-A(X+D)} \times \right. \\ \times \sinh AVt - \frac{1}{1+\nu^2}\cos\varphi[\nu \sinh AX + \tan\varphi \cdot \cosh AX] \times \\ \times e^{-AVt} + \frac{\nu^2}{1+\nu^2}[e^{-AX}(1 - e^{-AD})] \times \\ \left. \times \sin(\omega t + \varphi) + \frac{1}{1+\nu^2}\sin\left[\omega\left(t - \frac{X}{V}\right) + \varphi\right]\right\}. \tag{20}$$

where in reference to the HT winding:

V is the velocity of propagation along the conductor (about 150 m/μsec for windings in oil and 210 m/μsec for windings in air);

D – the length of the conductor section in question;

$X = xL_w$ – the distance along the conductor from the beginning of the winding;

L_w – the total length of the winding conductor;

x – the distance from the beginning of the winding;

w – the number of turns per unit of axial length;

l_w – the average length of a turn;

$A = \alpha / l_w w$ – the capacitive parameter;

$\nu = \omega / AV$ – the relative frequency of the LT winding;

$N = \frac{c_{12}}{c_{12} + c_{01}} U_{B\ (init)} \sin \phi$ – the conventional amplitude.

It is easy to show that all the terms with the exception of that with the coefficient $\frac{\nu}{1+\nu^2}$ can be safely ignored for the usual 3-6 μ sec periods of natural oscillation in the LT winding. Expression (20) then takes the form:

$$g_2'(X, t) = -N \frac{\nu^2}{1+\nu^2} [e^{-AX}(1 - e^{-AD})] \times \sin(\omega t + \varphi). \qquad (21)$$

We would still arrive at the same expression if we were to consider the third interval, i.e. the case $Vt > (X + D)$.

The less steep the wavefront of the surge, the smaller the conventional amplitude of the gradient N, since the multiplier $\sin \phi$ is less.

In view of the short period of oscillations we can always assume that the positive half-wave of a sine curve is disposed near the maximum of the main gradient. It is therefore advisable to put $\sin(\omega t + \phi) = 1$ in formula 21.

The component of the gradient g''_2 from the term $N \sin^2 \phi\, e^{-mt}$ is also easy to find. The gradient g''_2 is close in magnitude but opposite in sign to the sum of the non-periodic components of the gradient from formula (20) which we ignored; by subtracting g''_2 from that sum we get a negligible quantity which can be ignored completely (it is just the same for the third interval). Thus, the component of the gradient g''_2 can be excluded.

Formula (14) for the initial voltage distribution contains the linear component $(1-x)$ which up to now has been ignored in deriving gradient

formulae. It can easily be shown that this component varies synchronously with the effective voltage during the course of time. It is a relatively small quantity in any section of the winding, but it is easy to calculate and no difficulties arise by including it. This gradient component is opposite in sign to the main gradient of the HT winding:

$$g_2'''(X,t) = N\frac{D}{L_w}\sin(\omega t+\varphi). \tag{22}$$

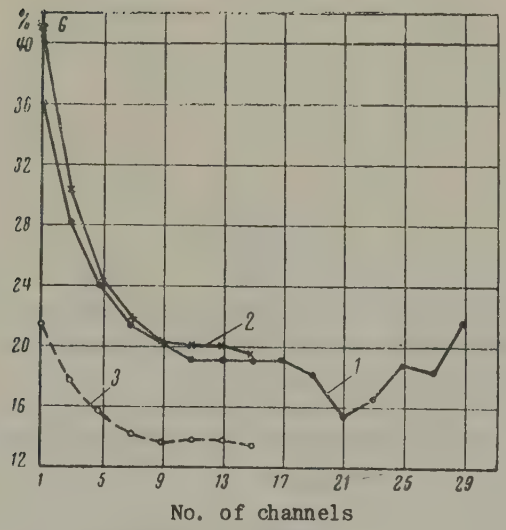

Fig. 8. Gradients of impulses of 1.5/40 μsec in a 220 kV 20,000 kVA test transformer:
1 – test data; 2 – calculated with LT effect included; 3 – calculated without LT effect included [2].

The general formula for calculating the second part of the induced gradient (corresponding to the terms in square brackets in (18)) simplifies to

$$g_2(X,t_M) = g_2'(X,t_M) + g_2'''(X,t_M) =$$

$$= \frac{c_{12}}{c_{12}+c_{01}}U_{B(\text{init})}\sin\varphi \times$$

$$\times\left\{\frac{\nu^2}{1+\nu^2}\left[e^{-AX}(1-e^{-AD})\right]-\frac{D}{L_w}\right\}. \tag{23}$$

The first component of the induced gradient due to the term $(1 - e^{-\alpha t})$ in formula (18) could have been included when calculating the main peak of the gradient. It is necessary to start from the curve for the initial voltage distribution over the HT winding calculated on the assumption of a continuous conducting and earthed screen instead of the LT winding (the capacitive parameter α is defined by formula (15)).

Fig. 8 shows typical curves for the maximum gradients of an impulse in winding of an experimental 220 kV transformer with the LT winding between the 220 kV and 110 kV windings and short insulation distances (increased effect of the LT winding). The maximum voltage at the mid-point of the LT winding as calculated by formula 9 was 33.5 per cent.

It will be seen from Fig. 8 that the maximum gradients from Frid's formulae are slightly below actual, whereas those calculated by the proposed method with the effect of the LT winding included agree satisfactorily.

Conclusions

1. Considerable potentials are capacitively-induced in the LT windings of transformers having the line voltage terminal at the mid-point of the HT winding when surges occur on the HT side.

2. The resulting oscillations of the potential in the LT winding increase the gradients in the HT winding by reverse capacitive induction.

3. The proposed method of estimating the stated effects is simple and sufficiently accurate for practical purposes.

Translated by O.M. Blunn

REFERENCES

1. E.S. Frid; *Surge gradients in transformer windings, (Impul'snye gradienty v obmotkakh transformatorov).* Diss. MEI, (1949).
2. E.S. Frid; *Elektrichestvo,* No.9, (1959).
3. L.V. B'iulei; *Surges in transmission lines and transformers, (Volnovye protsessy v liniiakh peredachi i transformatorov).* ONTI, (1938).
4. P.A. Abetti; Trans. AIEE, III, vol. 73, 1407, (1954).

COLD-ROLLED NON-ORIENTED ELECTRICAL STEEL*

A.A. NEFEDOV and P.I. BORZOVA

Central Ferrous Metals Research Institute

(Received 4 July 1960)

The cold-rolled electrical steel at present produced in the U.S.S.R. is somewhat inferior in quality to that produced abroad. The explanation is that Soviet iron and steel works do not have the necessary equipment. This deficiency is shortly to be overcome by the opening of new electrical steel plants at the Novo-Lipetsk Iron and Steel Works. This works will produce top grade steel in roll and sheet form and in different gauges, widths and lengths with an insulation coating giving high space-factor. The delivery of steel in roll form will enable electrical engineering works to save steel by rationalizing the arrangement of stampings.

The Novo-Lipetsk Iron and Steel Works is also to produce a new kind of cold-rolled transformer steel developed by the Central Ferrous Metals Research Institute with a relatively non-oriented grain structure. There will be two grades, namely, a low-alloy steel with a 1.3 to 1.7% Si-content and a high-alloy steel with a 2.9 to 3.3% Si-content. Unlike conventional grain-oriented steel, these particular grades have fewer ferrite grains with the cube faces oriented along the direction of rolling. The result is that the electrical and magnetic properties of these steels are practically the same along the direction of cold-rolling as they are across it, i.e. the steel approximates to hot-rolled steel.

Trial batches of this steel have already been produced by the same process that will be used in Lipetsk. The properties of the steel have

---

* *Elektrichestvo*, 2, 85-87, 1961.

been investigated in weak, medium and strong fields. The properties of cold-rolled non-oriented 1.34% silicon steel and 3.29% silicon steel (gauge 0.5 mm) are given in the Table.

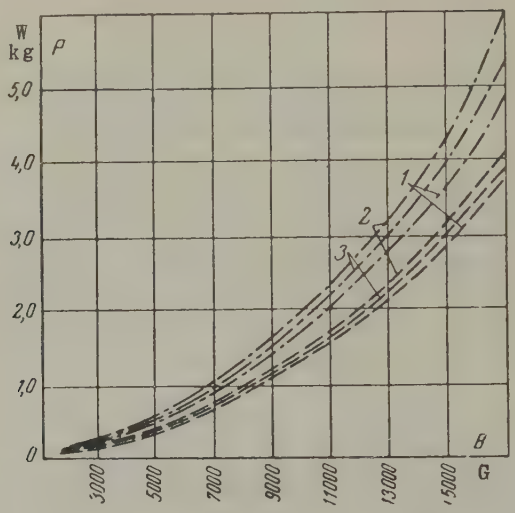

Fig. 1. Specific losses in cold-rolled non-oriented steel (gauge 0.5 mm):
– .–. –. –. –. low-alloy steel; -------- high-alloy steel;
Direction of specimens: 1 – lengthwise; 2 – transverse; 3 – middle (45°?).

The specific losses P_2-P_{17} and magnetic induction B_{25}-B_{100} of the steel were determined on a one-kilogram Epstein test apparatus by the absolute method. Coercive force was measured at a strength of 125 oersted. The testpieces were plates 0.5 x 30 x 250 mm in size with no special annealing to remove work hardening after cutting; when testing, the plates were "overlapped" end to end.

Magnetic induction $B_{0.002}$-B_{10} was measured on the same apparatus by the same testpieces but double overlapped. The testpieces were heat-treated at 750° before the tests to remove work hardening after cutting. More detailed information is given in Figs. 1 to 6.

From tests the magnetic induction $B_{0.002}$-$B_{0.01}$ is greatest in the high-alloy steel. It is the other way round in strong fields. As was to be expected, specific losses P_2-P_{17} were lowest in the high-alloy steel.

Properties of cold-rolled non-oriented silicon steel (gauge 0.5 mm)

Grade	Direction of specimens	Specific losses, w/kg			Magnetic permeability, G/oerst		Magnetic induction, G					Coercive free,	
		$p10/_{50}$	$p15/_{50}$	$p17/_{50}$	0.002	max	$B_{0.1}$	$B_{1.0}$	B_{10}	B_{25}	B_{50}	B_{100}	
Low-alloy (1.34% Si)	Lengthwise	1.70	3.61	4.84	450	12,030	320	10,970	16,120	16,680	17,800	19,290	0.35
	Cross	1.96	4.28	5.83	380	9,290	225	9,880	14,990	15,410	16,750	18,400	0.42
	45^{o}	1.83	3.94	4.34	–	–	–	–	–	16,040	17,270	18,840	–
High-alloy (3.29% Si)	Lengthwise	1.30	2.80	3.67	510	10,575	310	9,970	15,280	15,930	17,150	18,540	0.30
	Cross	1.41	3.18	3.42	427	9,010	220	9,110	14,360	14,850	16,200	17,850	0.34
	45^{o}	1.36	2.99	3.80	–	–	–	–	–	15,390	16,670	18,190	–

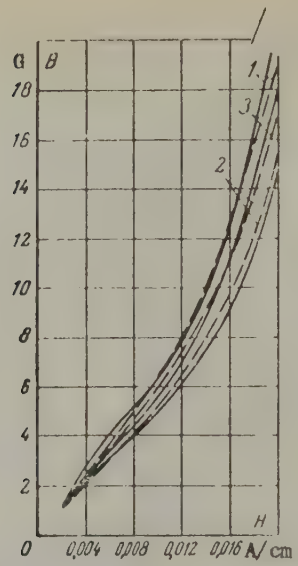

Fig. 2. Magnetic induction of cold-rolled non-oriented steel in weak field (gauge 0.5 mm). ——— low-alloy steel; – – – – high-alloy steel. Direction of specimens: 1 – lengthwise; 2 – transverse; 3 – middle (45°).

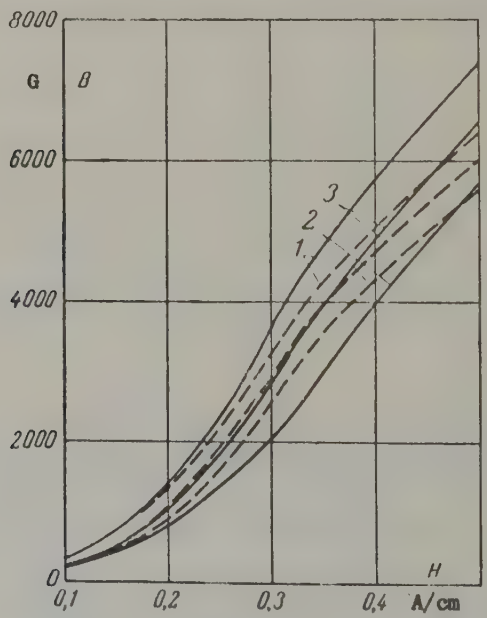

Fig. 3. Magnetic induction of cold-rolled non-oriented steel in medium fields (gauge 0.5 mm). ——— low-alloy steel; – – – – high-alloy steel. Direction of specimens: 1 – lengthwise; 2 – transverse; 3 – middle (45°).

Comparison of the properties of cold-rolled non-oriented steel with those of hot-rolled steel of the same chemical composition shows that the non-oriented cold-rolled steel is superior. It has lower specific losses and higher magnetic induction.

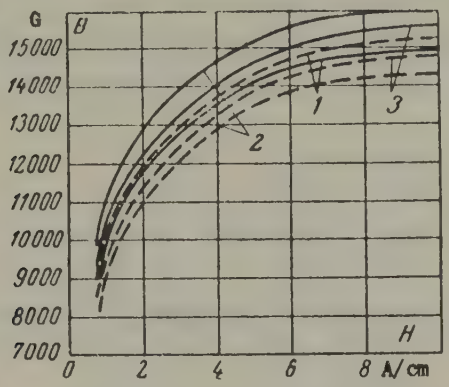

Fig. 4. Magnetic induction of cold-rolled non-oriented steel in medium fields (gauge 0.5 mm).
——— low-alloy steel; – – – – high-alloy steel.
Direction of specimens: 1 – lengthwise;
2 – transverse; 3 – middle (45°).

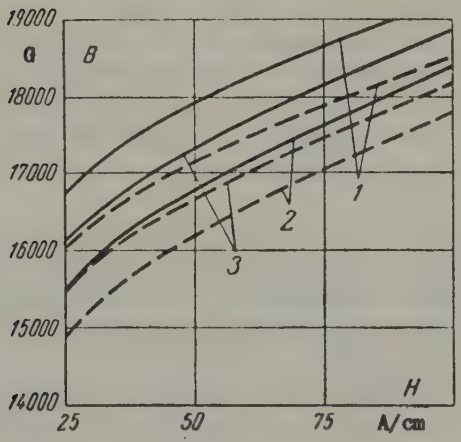

Fig. 5. Magnetic induction of cold-rolled non-oriented steel in strong fields (gauge 0.5 mm).
——— low-alloy steel; – – – – high-alloy steel.
Direction of specimens: 1 – lengthwise;
2 – transverse; 3 – middle (45°).

Satisfactory results were obtained in tests on cold-rolled non-oriented steel in electrical machines.

Samples of the steel have been produced in the Novosibirsk Iron and Steel Works under much worse conditions than at Lipetsk. This steel was tested at the "Dynamo" works. Losses were reduced 10 per cent by replacing grade E11 and E12 hot-rolled steel by cold-rolled low-alloy steel.

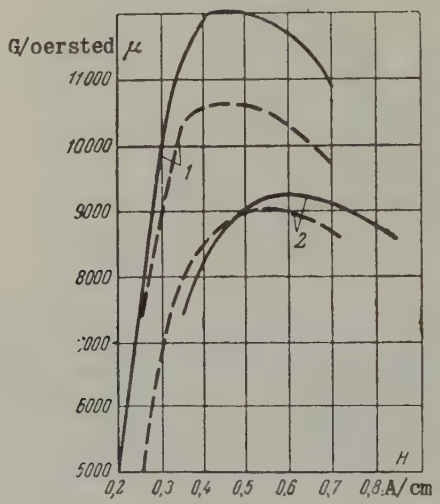

Fig. 6. Magnetic permeability of cold-rolled non-oriented steel (0.5 mm gauge).
——— low-alloy steel; - - - - high-alloy steel.
Direction of specimens: 1 - lengthwise; 2 - transverse.

Better results were obtained at the "Uralelektroapparat" works where cold-rolled high-alloy steel was substituted for grade E11 and E12 hot-rolled steel. Losses were reduced by a factor of 1.4 to 1.7 on prototype machines. Still better results are expected from the steel to be produced at Novo-Lipetsk.

Translated by O.M. Blunn

ABSTRACTS FROM PAPERS PUBLISHED IN ELEKTRICHESTVO No. 2 1961

Bushings

The Design of Oil-filled Bushings. L.I. Fedorov, (pp. 68-73).

Methods are proposed for designing bushings used for high voltage conductors, particularly from the point of view of heat dissipation and insulation.

Control Engineering

A Reversible Electronic Drive with Polarity Switch in the Power Circuit. B.R. Gendel'man, (pp. 17-24).

In 1959 the author patented a control system for the "ionic" drive of the rollgangs on a blooming mill. The system comprised one or two sets of mercury arc rectifiers and a polarity switch in the main circuit. Provision was then made for controlled starting, reversing and braking, but the author has now elaborated the system further and in this article he gives a description of a new but similar system which provides for all conditions of stepped control of the motor.

The Parameters of Non-linear Elements (with a parabolic voltampere Characteristic) connected in Pulsed-Current Circuits. B.M. Shliaposhnikov, (pp. 79-81).

Equations are produced to define the operating conditions of non-linear elements as used in modern remote control, measuring and computing devices.

Discharges across Contacts

Electrical Breakdown of Micro-Gaps in Gaseous Media. A.I. Frolov, (pp. 73-76).

A study is made of the electrical breakdown of small gaps measured in microns and tens of microns in particular reference to phenomena on Ni, Ag, Fe, Al, Cu and Pt-Ir contacts. A novel test is used.

Domestic Appliances

Concerning Domestic Power Consumption. B.L. Shifrinson, (pp. 76-78).

An account is given of the plans to increase the production of electric cookers for domestic use.

Electric Furnaces

The Calculation of Operational Short Circuit Currents in Three-phase Arc Furnaces. N.A. Markov et al., (pp. 28-33).

A practical method is proposed for calculating the asymmetrical short circuits which occur during the operation of electric arc furnaces in order to avoid the false operation of the relay protection and automatic regulators of the furnace.

Electrical and Magnetic Fields

Application of a Corollary of Green's Formula for calculating Electrical and Magnetic Fields. V.S. Khvostov et al., (pp. 14-17).

Owing to the difficulties involved in drawing the original equipotential lines in the Richter method, the author proposes a simple method of determining the potential at certain points within a region if the values of the potential are known at the boundary. An example is given.

Power systems

Consolidation of the U.S.S.R. Power pool System in Europe and Siberia.

It is recognized that industrial output will still largely be concentrated in the European part of the U.S.S.R. in the forseeable future. A detailed account is given of the planned Ural-Siberia power system which is designed to transmit electricity produced on the basis of Siberian fuel resources to the western regions.

The use of distribution coefficients in calculations with equivalent circuits. N.A. Mel'nikov, (pp. 9-13).

A description is given of a simple and accurate method of calculating complex equivalent networks on a network analyser by means of measurements of the distribution coefficients of the master currents. This method is particularly applicable to the operating conditions of electrical systems with non-linear loads if iteration is used.

Statistical Methods of calculating Electrical Loads in Industrial Networks. B.V. Gnedenko et al., (pp. 81-85).

A statistical method is proposed for estimating the future power consumption of factories and groups of factories.

Rotating Machines

The Design of Synchronous Motor Compounding Devices. V.V. Iukhov, (pp. 40-45).

A design method is proposed for current transformers in compounding schemes operating via a rectifier on the excitation winding of the exciter of a synchronous motor.

A small synchronous Motor with a Semiconductor Rectifier in its Field Circuit. Iu.I. Chkhikvadze et al., (pp. 45-48).

A description is given of a compact simplified system of excitation for small synchronous motors using a semiconductor rectifier. Many advantages are claimed for it. The special features are the connexion of the rectifier in the "open neutral" of the motor and the use of a two-winding correcting transformer. A 70 per cent reduction in cost is claimed.

Speed Control of a d.c. Motor with a Semiconductor Switch in its Armature Circuit. T.A. Glazenko et al., (pp. 49-55).

A description is given of a more compact, reliable and efficient system of controlling the speed of a reversible d.c. drive using a semi-conductor triode (transistor) as a switch in the armature circuit. Equations are also produced to determine the mechanical characteristics, the total amplitude of the pulsed current, the speed and the power losses.

Transformers

The Performance of Series-connected Transformers having different Transformation Ratios. P.F. Rybchenko, (pp. 55-61).

A study is made of the performance of series-connected transformers with different transformation ratios. A method of calculation is proposed to assist in the selection of other elements in automatic control systems without resort to time-wasting tests.

THE NEW RUSSIAN POWER STATIONS*

A. R. GERSHTEIN, L. I. DVOSKIN, L. UI. IZRAILEVICH
A. B. KRIKUNCHIK, K. K. LEVITSKII and B. V. ROSS

(Teploelektroproekt)

(Received 13 September 1960)

It is now planned to build 22 new coal-burning power stations in the U.S.S.R. by 1965. These stations, each of 2400 MW output, are to be equipped with 200 and 300 MW units. Each turbine will be connected to a boiler-unit producing steam at a rate of 950 t/hr (pressure 255 atm, steam temperature 585°C with reheat to 570°C).

The generators are to have hydrogen cooling (hydrogen pressure up to 3 atm). The generator voltage is 20 kV. Those produced by the Elektrosila works will have direct hydrogen cooling only for the rotor windings. Those produced by Elektrotiazhmash will have direct hydrogen cooling for both rotor and stator windings.

The Elektrosila generators will be excited direct from high frequency exciters with the current rectified by germanium rectifiers. Provision is made for standby excitation from a motor-generator set incorporating a flywheel.

The plan envisages five types of main building which differ in the position of the coal hoppers and the system of coal pulverization.

Alternative arrangements are also made for totally-enclosed and semi-enclosed turbo-generators, but there is a general specification dispensing with crane-assistance in the erection of the stator, the opening up of the regenerative air heating equipment, and the operation of the ash separators, exhaust fans and blowers in the boiler unit.

Different plans have been proposed for the system of coal pulveriza-

---

* *Elektrichestvo*, No. 3, 1-13, 1961.

tion. A central shop is provided in the fifth scheme [3]. The main building is shown in Fig. 1.

The specific capital cost is 590 to 650 roubles per kW; the specific space factor is 0.49 m^3/kW including the coal pulverization shop and auxiliary building; the specific consumption of conventional fuel is 304 g/kW. hr; the specific consumption of power for auxiliaries is nr; the specific consumption of power for auxiliaries is 3.2 to 3.7% (the feed pumps are steam-driven); the specific employment figure is 0.17 to 0.23 min per 1000 kW; 90% of the building is composed of sectional reinforced concrete components; there are 79 types of such units in the main building.

Output from the first set will commence 26 months after the start of construction. Thereafter new sets will come into operation at intervals of 3.2 months.

The electrical connexions

Provision is made for the electrical connexions to be adjusted to meet local needs and only general plans have therefore been made to supply the 110, 220 and 500 kV networks.

Use is to be made of three-phase 360 MVA booster transformers, 20/110 20/220 and 20/330 kV and similar auto-transformers 20/110/220 and 20/110/330 kV. Single phase transformers 20/500 kV will also be used (120 and 240 MVA in one phase).

Fig. 2 illustrates the connexion of the generators to the 110 and 220 kV distribution gear. Extra reliability is provided by the use of two auto-transformers between the distributing devices. In version 1(a the standby supply for auxiliaries is provided by step-down transformers connected to the compensation windings of the auto-transformers. With 6 kV compensation windings the standby supply is provided by line regulator transformers and reactors connected to the windings of the auto-transformers. In version 1(b) the standby transformers for auxiliaries are connected to the 110 kV feeder bus-bars, but this increases the capital cost and loss of energy. The difference in version 2 is that one of the generators is connected to the L.T. windings of the auto-transformers.

The second version entails no higher capital or running costs, but it is technically more difficult and special requirements have to be met as regards dynamic stability in the use of circuit breakers.

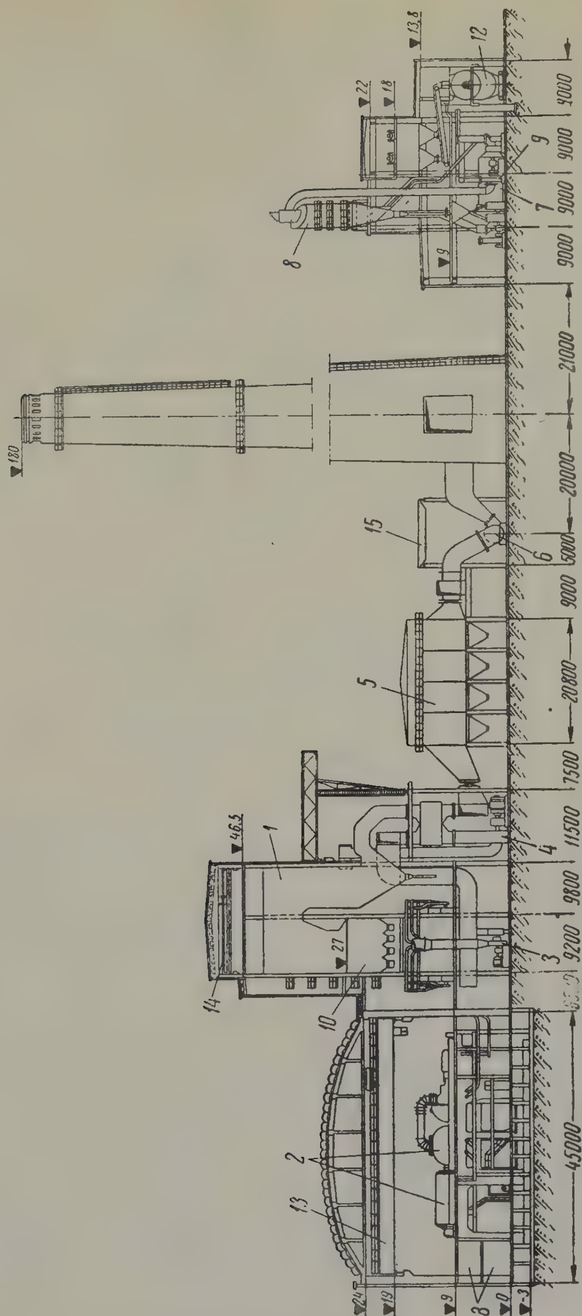

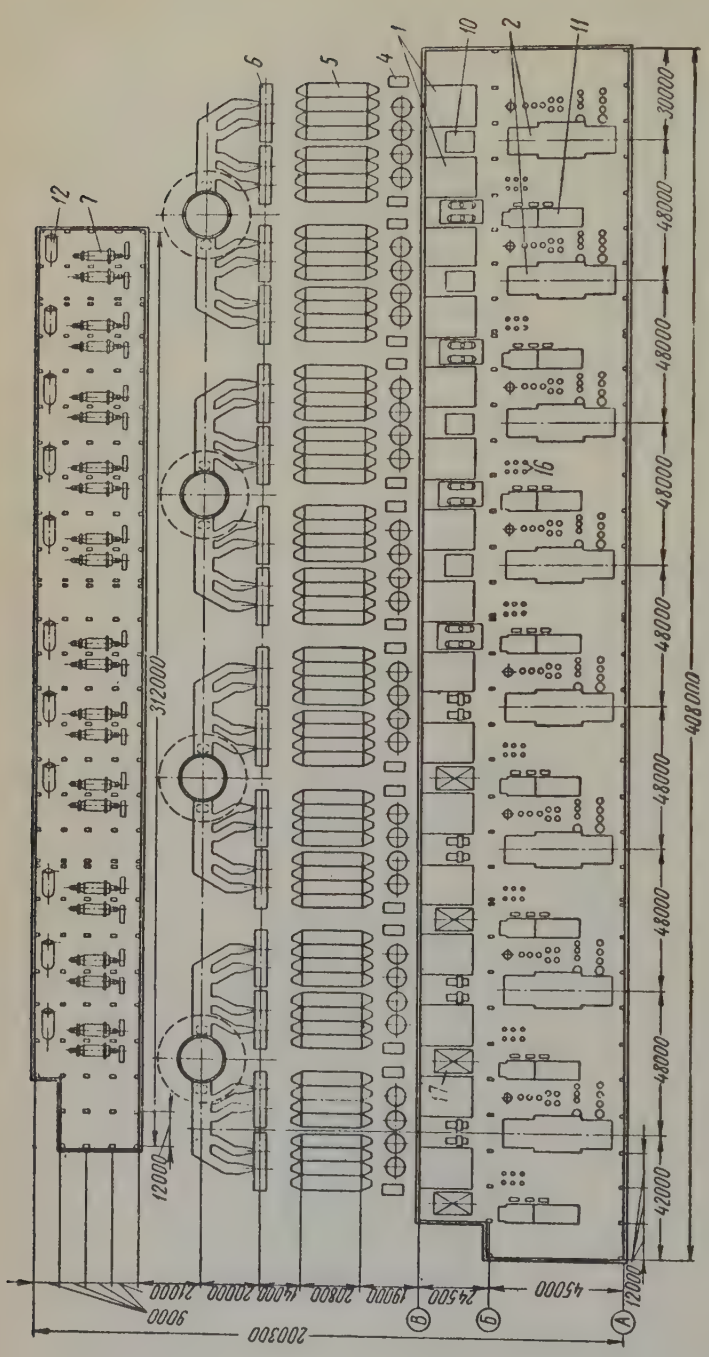

Fig. 1. Section and plan view of the main building of the 2400 MW station (variant No. 5).

1 - boiler 950 t/hr; *2* - 300 MW turbo-unit; *3* - hot blast ventilators; *4* - fans; *5* - electrostatic precipitates; *6* - exhaust fans; *7* - ball mills; *8* - coal-dust cyclones; *9* - mill fans; *10* - coal-dust hoppers; *11* - feed pumps; *12* - steam drier; *13* - 75/20 ton bridge crane; *14* - 10 ton bridge crane; *15* - 30 ton bridge crane; *16* - high pressure steam mains; *17* - control panel for two blocks; *18* - 6 kV distribution gear for internal needs.

The Ministry of Power Stations has recommended version 1(a) with the installation of a circuit breaker at each transformer. Three types of connexion between the generators and transformers have been considered for 500 kV (Fig. 3).

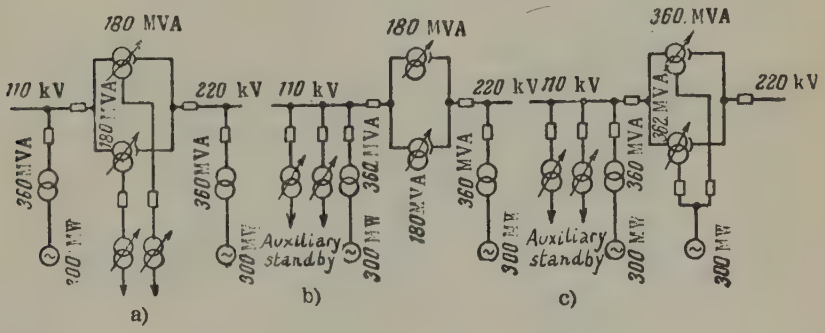

Fig. 2. Alternative systems for connecting the generators to the 110 and 220 kV distribution gear:
a – version 1(a); *b* – version 1(b); *c* – version 2.

Version 1 provides two generators to one group of single phase booster transformers of 3 x 240 MVA with two low voltage windings. The 220 and 500 kV distribution gear is linked by a set of single phase 3 x 135 MVA auto-transformers. The compensation windings of the 220/500 kV auto-transformers can be used as a standby supply for the auxiliaries.

Version 2 provides for the connexion of the generators to the L. T. windings of 220/500 kV auto-transformers. One generator is connected to each set of auto-transformers. Two generators cannot be connected to the same set of auto-transformers owing to the limited power of the available auto-transformers.

In version 3 the number of large 500 kV units is reduced by connecting one generator to a 220/500 kV 3X 240 MVA auto-transformer and the other to a 20/220 kV booster transformer.

Versions 1 and 2 are the cheapest but version 2 incurs the least loss of energy, whilst version 1 is the simplest from the technical point of view.

The main system can only be selected in the light of local conditions, but a typical arrangement has been prepared (Fig. 4). Here two generators are connected to the 110 kV distribution bus, two to the 220 kV bus-bars, and four to the 500 kV bus-bars. Larger units are connected to the 500 kV bus-bars, i.e. two generators per transformer unit, to reduce the amount of expensive 500 kV switchgear. Large modern power systems have an adequate margin for the disconnexion of such units.

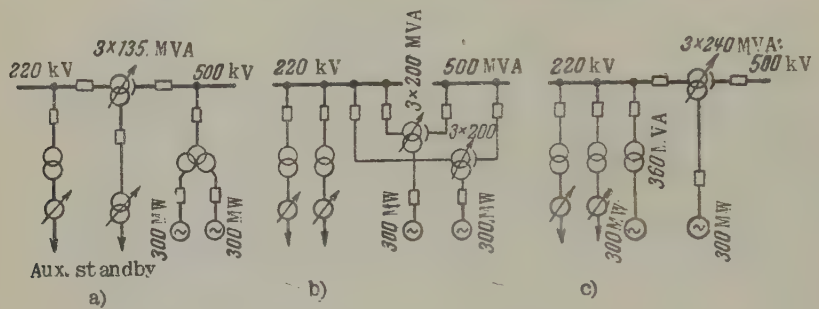

Fig. 3. Alternative systems for connecting the generators to the 220 and 500 kV distribution gear:
a – version 1; *b* – version 2; *c* – version 3.

The number of transmission lines from each station also depends on local conditions. To determine the scale of the distribution gear it was assumed that there would be about ten 110 kV lines, six 220 kV lines and three 500 kV lines.

The distribution gear is supplied by two separate bus-bar systems with a transfer bus. All the line and transformer circuits may be connected to the transfer system. If the number of outgoing lines should be less, simpler arrangements may be used (e.g. generator-transformer-line units, "bridges", "squares" etc).

Works supply

Three phase squirrel cage induction motors are used for most of the internal drives, but synchronous motors are used for the ball mills and compressors. The feed pumps are turbo-driven, except the standby pump which is driven by an induction motor.

A voltage of 6 kV has been adopted for the majority of motors at these large stations.

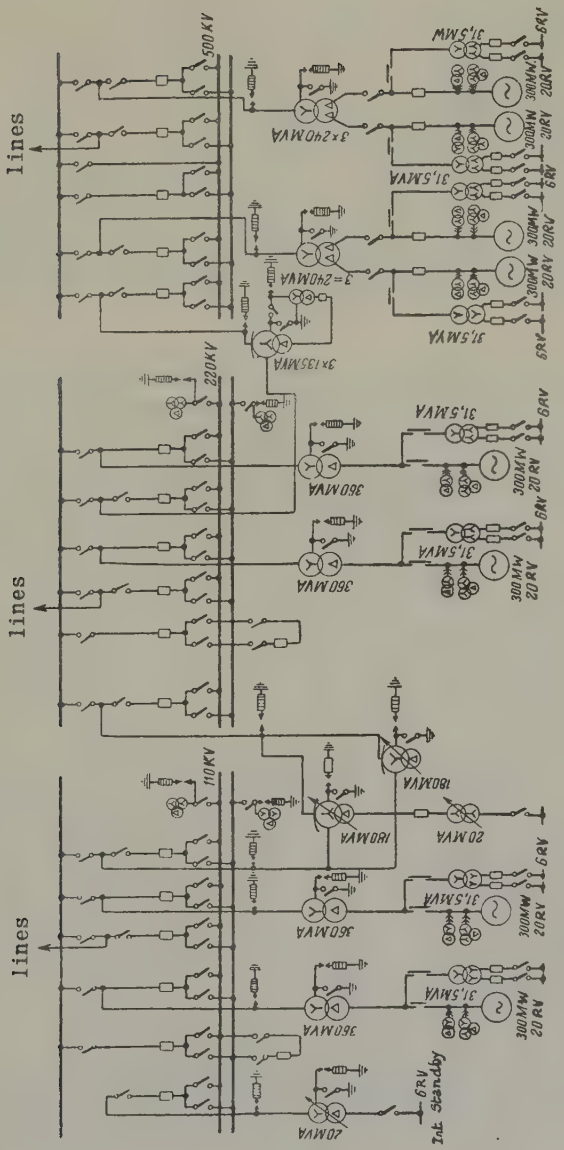

Fig. 4. The main system of electrical connexions.

The ball mills require a 2400 kW motor of 100 rev/min A synchronous motor is better suited to such speeds.

An induction motor was regarded as adequate for the standby feed pump as it is normally shut down and the advantages of a synchronous motor could not be fully used. A synchronous motor would also have led to a more complicated installation and would have increased the short circuit currents in the internal system.

The output and pressure of the standby feed pumps is regulated by hydraulic clutches. The exhaust fans are driven by two motors each of a different speed. The blowers are driven by two-speed motors. These fans and blowers are also regulated by the rotating blades of the turbine control gear.

A voltage of 380 V has been adopted for motors up to 200 kW.

The fuel supply equipment is driven by 220 V d.c. motors to achieve a wide range of speed control. They are fed from a three phase 380 V a.c. network via rectifiers. The standby oil pumps of the turbines and the equipment for the hydrogen cooling of the generators have 220 V d.c. motors so that they can be supplied from batteries in the event of the a.c. supply failing.

A voltage of 380/220 V with earthed neutral is used for the lighting.

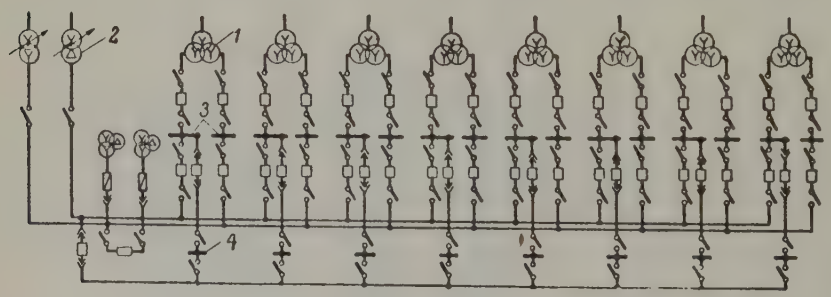

Fig. 5. The main circuit for 6 kV auxiliary power. *1* – Works transformers; *2* – standby works transformers; *3* – *6* kV busbars of the works distribution gear; *4* – the feeders of the coal pulverization shop.

The unit or "block" supply system is used for the works supply (see Figs. 5 and 6).

Each motor unit is supplied via a three phase 31.5 MVA 20/6 kV transformer with a split 6 kV winding. This transformer is connected to a tapping from the generator circuit. Such transformers make it possible to limit the short circuit currents on the 6 kV sections of the bus-bars to suit the VMG - 133 circuit oreakers and to simplify the system as a whole.

The 6 kV bus-bars of each unit are in two sections so as to separate each pair of auxiliaries. In the event of faults, at least half the turbine and boiler auxiliary drives will remain in operation.

The 6 kV motors for the general station plant are supplied from special works transformers. The motors of the standby plant are supplied from different sections in different blocks.

The 380 V works system is built on the same unit principle as the 6 kV system. Each unit has three 6/0.38 kV transformers; each supplies a particular section of the auxiliary feeders. These three sections supply all the general station plant in the main building as well as the plant in the particular blocks. The motors of general station plant outside the main building are supplied from separate transformers.

The type of internal equipment also depends on the type of coal pulverization. In one scheme the works supply is met by one central set of distribution gear and in the other schemes by a central unit with "group feeders" disposed near the motors. The second arrangement is more economical in non-ferrous metals and cable. If the separate coal pulverization shop is adopted, the 6 kV motors in this shop and some of the general station plant are supplied from the 6 kV feeders in the pulverization shop itself. It is considered desirable to have eight such feeders, the same number as there are blocks. Each feeder is supplied by cable from the main 6 kV section.

The standby works supply has two 20 MVA transformers which are either connected to the feeder busbars of the 110 kV distribution gear or to the compensation windings of the auto-transformers. These two transformers can start or stop any two blocks at the same time. A spare un-used 31.5 MVA transformer was suggested but the Ministry preferred a system in which the main works transformer would be replaced automatically and any two blocks started or stopped at the same time.

One battery is provided for each two blocks for emergency supply of the 220 V d.c. motor oil pumps, lighting and the control circuits. A reverse battery is also provided for the central control desk. The batteries are charged from dry rectifiers.

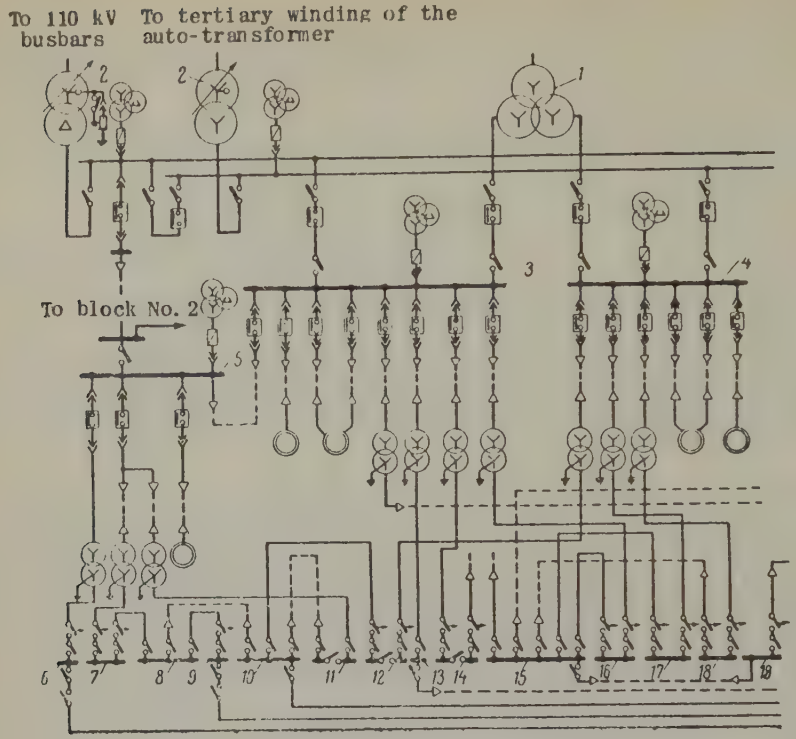

Fig. 6. The internal circuit for the first unit: *1* – No. 1 35.5 MVA works transformer 20 ± 2 x x 2.5%/6.3/6.3 kV; *2* – primary 20 MVA transformers; section 1A of the 6 kV works distribution gear;

4 – section 1B of the 6 kV works distribution gear; *5* – the 6 kV feeder of the coal pulverizing shop; *6* – the 380/220 V feeder of the coal pulverizing shop; *7* – the fuel supply feeder (section No. 1); *8* – standby fuel supply feeder of the auxiliary buildings; *11* – compressor house; *12* – feeder of auxiliary premises; *13* – the lighting in block No. 1; *14* – outdoor distribution gear; *15* – standby feeder of No. 1 block; *16* – engine room (section 1A); *17* – engine room (section 1B); *18* – boiler house (section 1C); *19* – standby feed of No. 3 block.

The electrical installation

The turbo-generators are transverse to the axis of the engine room.

The generators are connected to the booster transformers and supply the works transformers through single phase conductors in aluminium housings to eliminate interphase short circuits (Fig. 7). The conductors between the generators and transformers consist of two box-shape aluminium bus-bars 225 x 105 x 17.5 mm in section. These particular dimensions were chosen from the point of view of heating and current density.

The enclosed conductors are cooled by a closed system ventilation with a water air-cooler. The cooled air is first passed into the middle compartment. It then passes to the extreme compartments and then back to the fan. De-ionizers are fitted at the junctions between the middle compartments. The voltage transformers are connected direct on the conductors by plug (pin) contacts without voltage dividers or fuses. They are single phase with their winding connected between phase and earth.

The Electrosila works has placed the neutral leads of the 300 MW turbo-generator in the upper part of the face section in a special box which contains all the other leads and neutral leads "from two parallel branches of the generator and transformer for transverse (shunt) differential protection". This arrangement simplifies the erection and exploitation of the main leads as well as the neutral leads.

The phase and neutral leads of the 300 MW generators produced by the Electrosila works are provided with built-in TUL-20 type current transformers.

Any circuit breakers in the generator circuits are mounted under the generator.

A 75 ton bridge-crane is provided in the engine room for the erection and repair of the generator and removal of the rotor. The stator, which weighs 225 tons, is erected by a special appliance fixed to the side wall of the engine room (Fig. 8). The stator is delivered on a special transporter by rail straight into the engine room. An electric winch on a mobile "carriage" is used to lift it from the rail transporter. It is rotated 90° and drawn into the "carriage". The "carriage" is then moved through an opening in the outside wall of the engine room to its

foundations.

The best position for the internal distribution gear is on the outside wall of the engine room, but this involves taking a large number of cables through the engine room since must of the plant is near the boiler. Consequently some of the 6 kV motors are fed from the central distribution gear and others from group feeders near the motors.

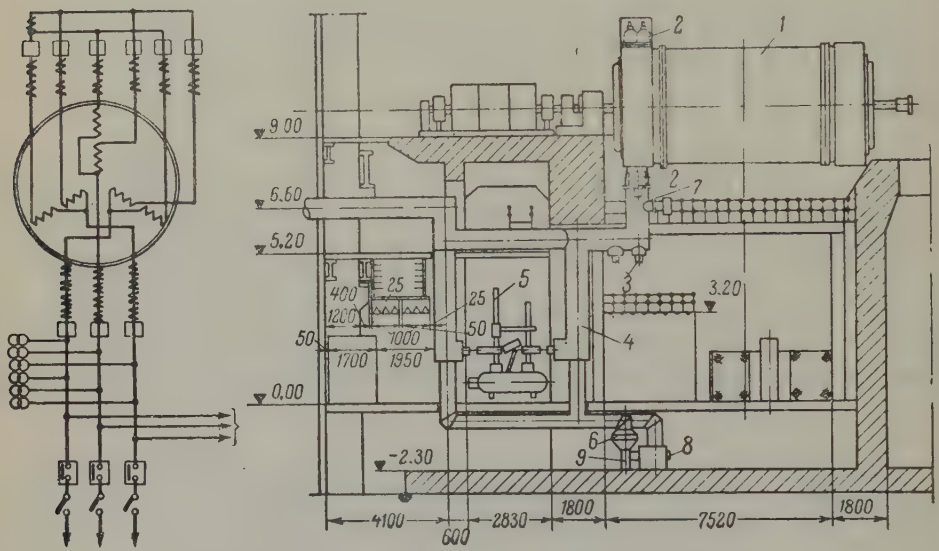

Fig. 7. The stator winding connexion of the generator and the layout of the generator in the engine room (version with a circuit breaker in the main circuit):
1 - generator; *2* - current transformers; *3* - voltage transformers; *4* - enclosed busbar feeder; *5* - air blast circuit breaker; *6* - air cooler; *7* - de-ionizer; *8* - viscous (vision) filter; *9* - centrifugal fan.

Thus the bulk of the internal electrical plant is in two tiers along the wall of the machine building (Fig. 9). This includes the central 6 kV distribution gear for all the blocks (first tier), the 380 V block control panels of the engine room, the 220 V d.c. gear for the whole station and the generator excitation equipment (second tier). There is an intermediate cable run between these two tiers.

The 380 and 220 V distribution gear and 6 kV feeders for the boiler house are either in the boiler house or in the coal store. The arrange-

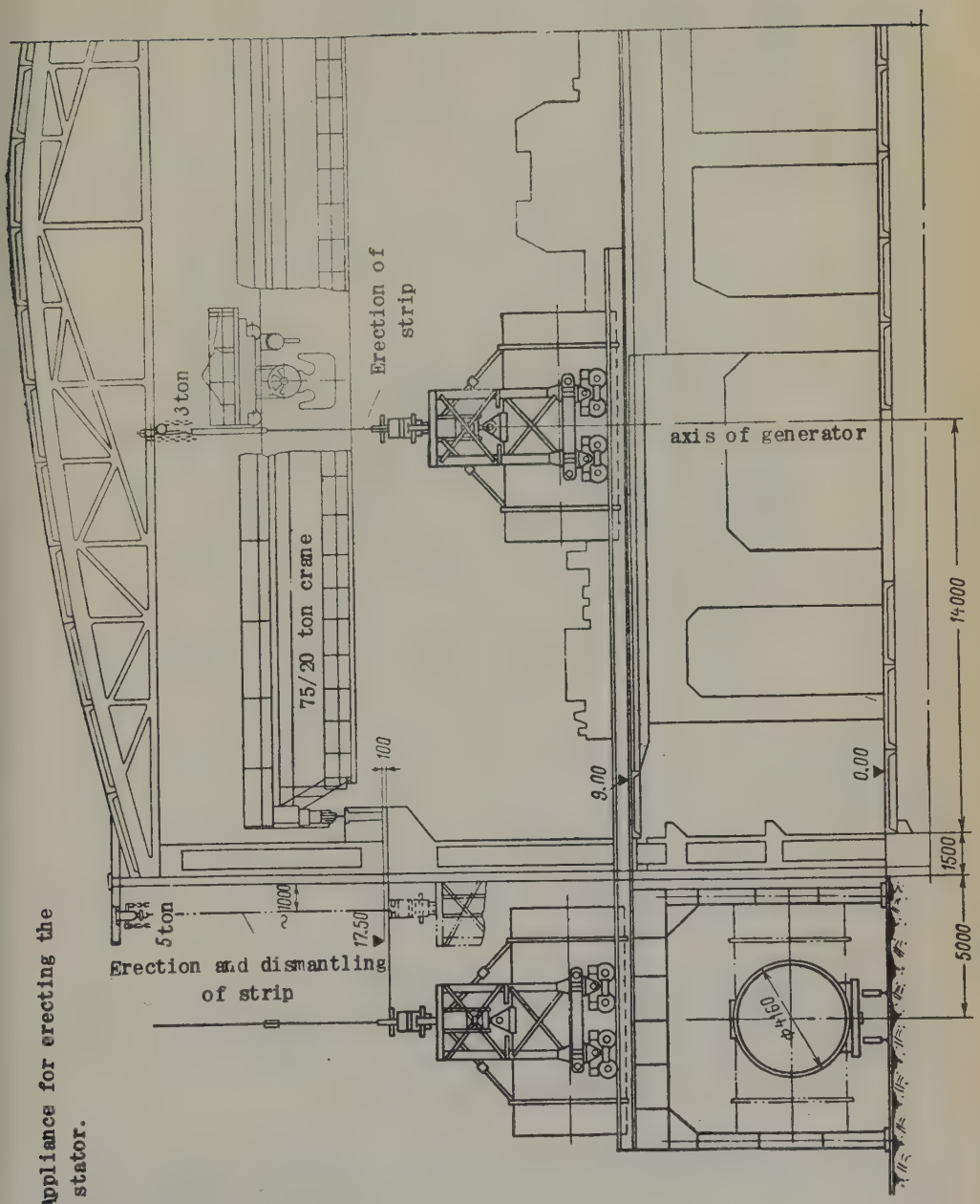

Fig. 8. Appliance for erecting the generator stator.

ment of the other equipment can be seen in Figs. 9 and 10.

The booster transformers are arranged along the railway track outside the machine house. The auto-transformers are mounted near the 110 220 and 500 kV distribution gear.

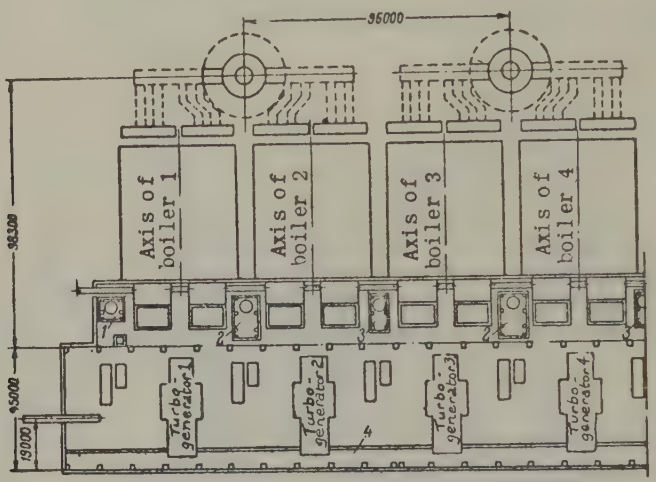

Fig. 9. Part plan of the main building.
1 - central control desk; *2* - unit control panels; *3* - 0.38 kV distribution gear; *4* - 6 kV distribution gear for works supply.

Generator-transformer units are very heavy and there is no special area available in the engine room. It is presupposed that the transformers can be repaired and inspected in situ.

The transformers are made smaller and more accessible by forced oil cooling and radiator-type air-coolers.

The weight of that part of the transformer which is raised during repairs is reduced by making the tank sides and tap detachable from the bottom so that the transformer can be stripped without lifting the core and windings. The part of the tank to be lifted weighs about 55 to 60 tons, whereas the core is about 200 to 250 tons.

On erection the transformers are taken from the transporters and mounted on their foundations by winches and jacks etc. They are delivered ready for inspection and use, only slight adjustments being required.

Fig. 11 illustrates the method of inspecting and repairing the trans-

formers. The π-shaped tower is placed over the transformer in the same plane as the main axis of the transformer. Its width depends on the length of the tank without radiators (9.5 to 10 m). It is fixed at 12 m. The tower must be high enough to lift the tank by longitudinal and transverse braces which greatly reduces the distance between the hooks of the hoist and the ground. This distance is about 15 to 16 m. The tower is dismantled by an ordinary lorry-mounted crane as no part weighs more than 5 tons.

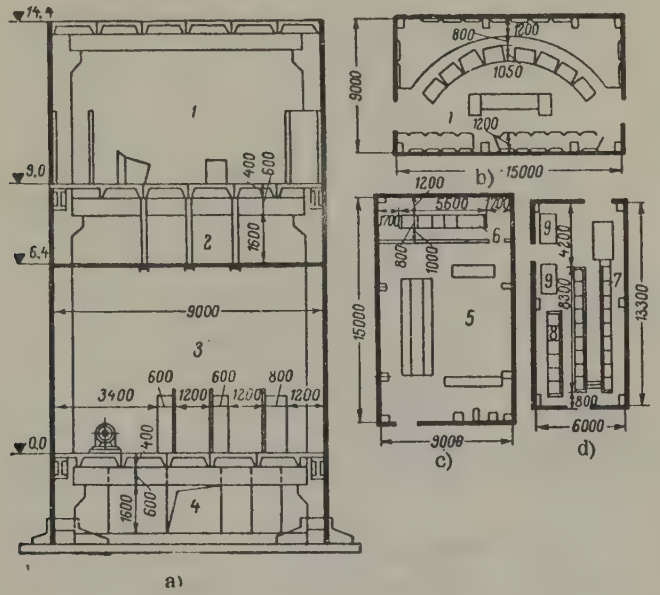

Fig. 10. Layout of the electrical equipment at the unit control panels (*a*, *b*), the central control panel (*c*) and the 0.38 kV distribution gear (*d*):

1 – unit control panel; *2* – intermediate cable run; *3* – the 0.38 kV distribution gear; *4* – cable basement; *5* – central control panel; *6* – d.c. panel; *7* – the 0.38 kV distribution gear; *8* – the d.c. boiler control panel; *9* – converters.

For the outdoor distribution gear of all voltages, use is made of a "centre arrangement" with all line and transformer circuit breakers in one row. The busbar isolators are stepped as in Fig. 12. The "cross-pieces" joining the isolators of the two sets of busbars are now underneath the busbars. This reduces the height of the pylons, simplifies

their construction and allows the use of reinforced concrete sections. The same hollow reinforced concrete pillars are used for the outdoor distribution gear as for the transmission lines. Sectional reinforced concrete structures are also used to support the distribution apparatus.

Owing to corona conditions, the leads of the 500 kV outdoor distribution gear are to be aluminium conductors with steel cores. Each phase at present consists of three such conductors but the new hollow AP-500 type aluminium conductors will make it possible for each phase to consist of two such conductors.

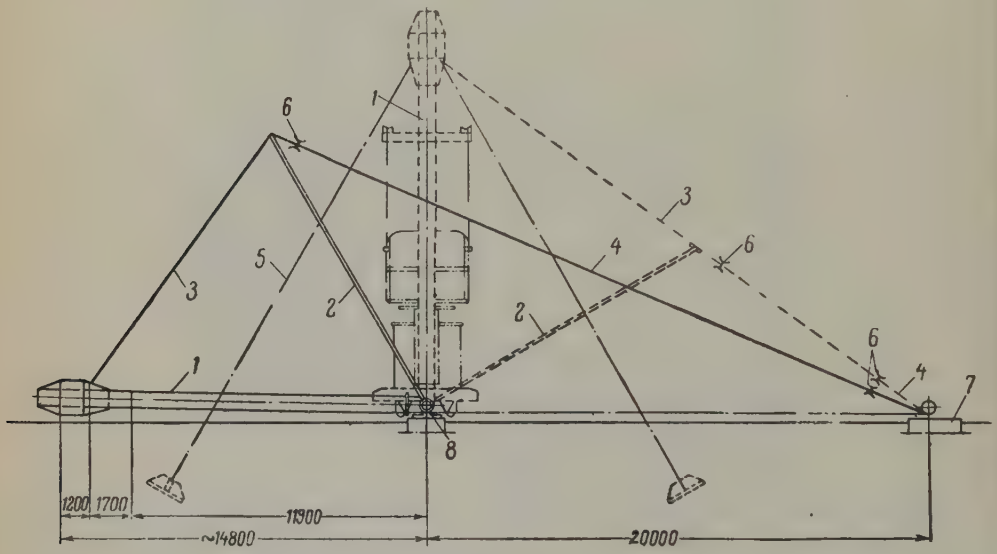

Fig. 11. Appliance for inspecting and repairing the transformers at the outdoor distribution gear: *1* - tower; *2* - A-shaped boom; *3* - rope from support to boom; *4* - rope from boom to winch; *5* - brake cable; *6* - pulley block; *7* - the 5 ton winch for lifting the tower; *8* - tower shoe.

The groups of 110/220 and 220/500 kV auto-transformers are arranged adjacent to the common points of the appropriate distribution gear.

The outdoor distribution gear may be sited in front of the engine room to the side of the engine room which is clear, or behind the coal store (Fig. 13).

In the latter arrangement each 110-330 kV booster transformer and group of single phase 500 kV transformers has a single-circuit steel

1	2	3	4	5	6	7	8
Auto-transformer	Transfer breaker	Booster tfmr 1	Outgoing line 1	Booster tfmr 2	Outgoing line 2	Gross pieces	Outgoing line 3

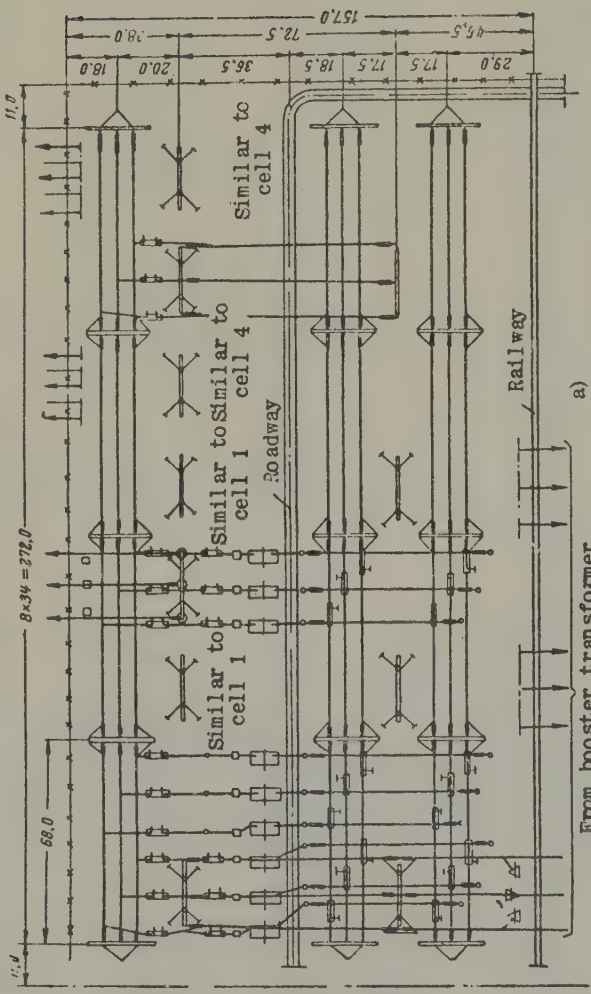

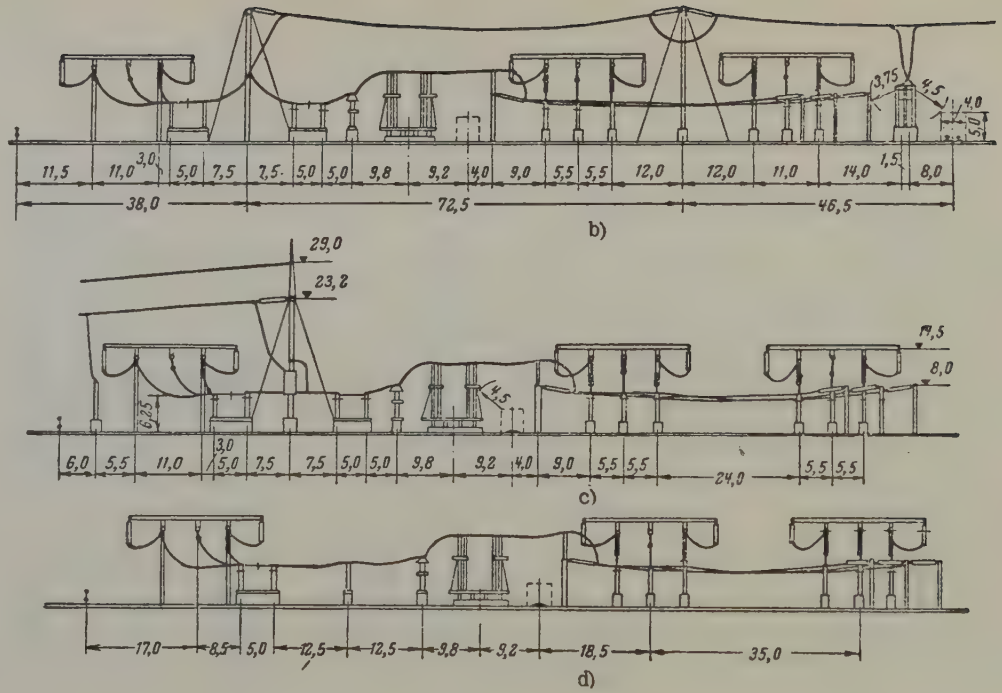

Fig. 12. The 500 kV outdoor distribution gear with sectional reinforced concrete components:

a – plan view; *b* – section across transformer cubicle; *c* – section across transmission line; *d* – section across transfer circuit breaker cubicle.

anchoring support 67 m high with the conductors in the horizontal position.

The height of the support depends on the distance between the conductors and the highest point of the main building (Fig. 15). The chimney stack acts as the next support for two 110-330 kV circuits or one 500 kV circuit. The conductors are secured on the stack at a point along ground level depending on the height of the anchor column and the permissible sag of the conductors (stress of 1.5 kg/mm^2).

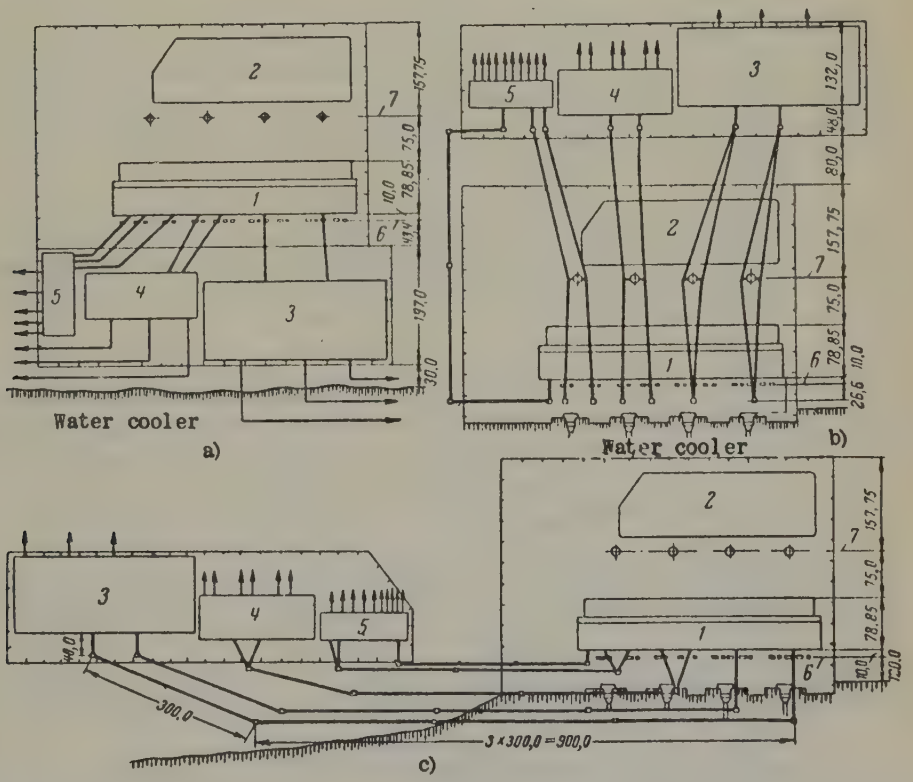

Fig. 13. Layout of the outdoor distribution gear in relation to the main building:
a – version 1, *b* – version 2; *c* – version 3.
1 – main building; *2* – coal store; *3* – the 500 kV outdoor distribution gear; *4* – the same, 220 kV; *5* – the same, 110 kV; *6* – axis of the booster transformers; *7* – axis of the chimney stacks.

No supports are fixed on the roof of the main building as this is constructed of sectional reinforced concrete units. A very large saving in cable has been made.

Control

The various control devices are operated from the various unit control panels. A control panel is installed between each pair of adjacent units.

The unit control panels are coordinated with the 110, 220 and 500 kV general station control devices on a central control desk in the main building. Manual control and visual inspection has been replaced by automatic controls to the maximum possible extent and maximum decentralization has been the aim.

Remote control and inspection devices have only been retained for work which cannot as yet be made fully automatic, for the standby controls of essential automatic devices and for inaccessible or very remote control objects.

To reduce the size of the unit and central control panels, all the relay protection and automatic devices are placed near the apparatus or objects which they protect or control.

Fig. 15 shows the central control panel.

A small despatcher-type panel is used to supervise (watch) and coordinate the station equipment and control panels.

Provision is made for automatic optimization of the distribution of the "active" and "reactive" loads between the units.

A d.c. voltage of 48 to 60 V is used to facilitate the use of soldered connexions and lightweight cheap cables.

It is planned to apply automation to all the boiler operations (combustion, water supply, coal pulverization, draught and air blast etc). and to the protection of the main and auxiliary equipment. Technological "blocking" and automatic connexion of standby equipment is employed. Boiler cleaning will also be done automatically.

The turbine unit is automatically controlled and regulated under normal operating conditions and automatic protection is provided.

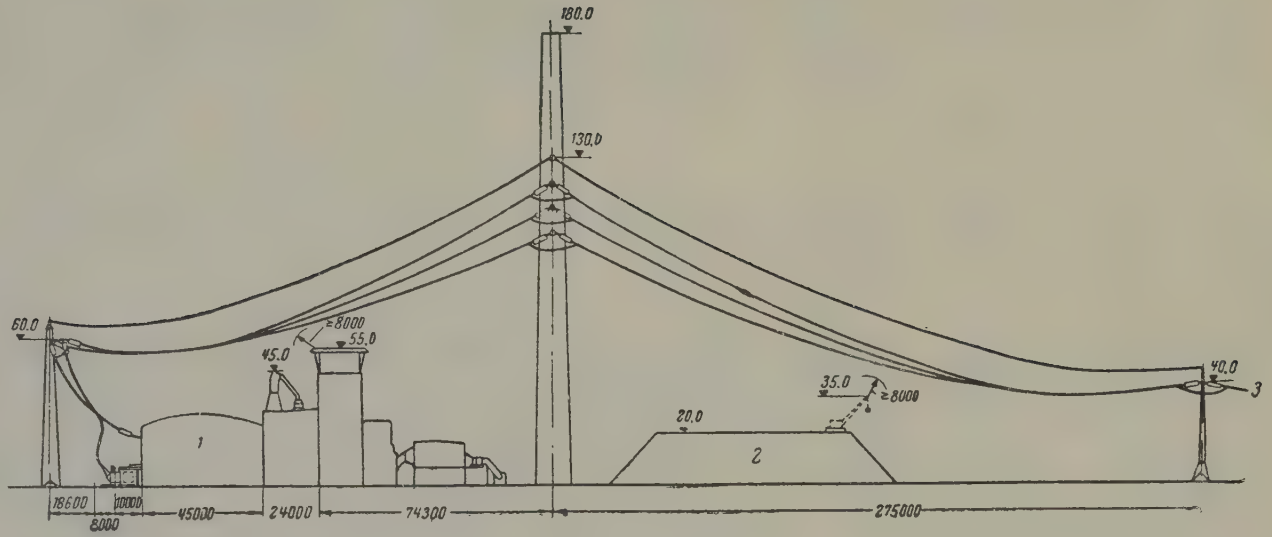

Fig. 14. The overhead transmission from the booster transformers to the outdoor distribution gear:
1 - engine room; 2 - coal store; *3* - to tower of the outdoor distribution gear.

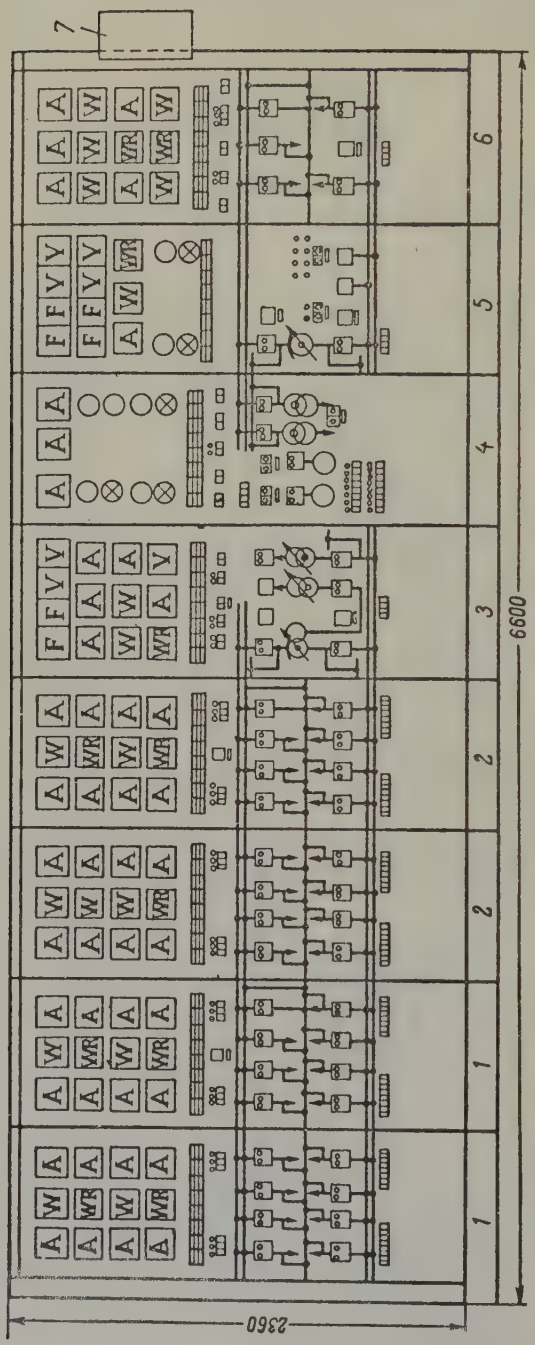

Fig. 15. Front view of central control panel:

1 - 110 kV lines; *2* - 220 kV lines; *3* - 110/220 kV auto-transformer and works transformer, bus-bars of 110 kV equipment; *4* - central indication, circuit breakers of 500 kV blocks, standby exciters, selsyns; *5* - 220-500 kV transformer and bus-bar equipment 220 kV; *6* - 500 kV lines; *7* - synchronizing column.

The fuel supply, water supply, and chemical water purification will be mainly automatic and technological "blocking", automatic protection and automatic connexion of the standby equipment will be provided.

If the equipment or automatic devices cease to function properly there is an alarm system to call the appropriate personnel.

A central communication system is used for inspection purposes to provide printed information, statistical control and inducation of mal-adjustments.

Multiple – camera television equipment is provided to review the decentralized control panels and observe the combustion process and state of the equipment.

Further automatic devices are to be installed as they become available with the ultimate aim of applying complete automation to each entire station.

Conclusion

Such big power stations were not a practical proposition until the large 330 and 500 kV transmission systems had been developed.

Work has been proceeding since 1957 on the production of steam turbines up to 300 MW, turbo-generators up to 300 MW with forced hydrogen cooling and water cooling of the stator windings, 110, 150 and 220 kV three-phase transformers, 220/110 kV auto-transformers of 120, 180 and 240 MVA rating, 330 and 500 kV transformers and auto-transformers, 110 kV and 150 kV air blast circuit breakers with rupturing capacities of 6 GVA, 220 kV breakers with rupturing capacities of 10 GVA, 330 kV breakers with a rupturing capacity of 10 GVA and of 500 kV for 12 GVA, totally enclosed single- and two- speed outdoor motors for the auxiliary equipment of the boilers, hydraulic clutches for controlling the speed of the feed pumps and compact totally enclosed conductors for generators currents of 6, 7.5 and 9 kA.

It cannot however be said that the U.S.S.R. occupies a leading world position in these matters as it does in hydro-electric power and long distance transmission. The rate of production of the large units required for fuel-fired power stations is not keeping pace with demand. About 6000 MW of new power is now being produced annually. This figure is to be increased to 12,000 MW by 1965, 18,000 MW by 1970 and 25,000 MW by 1975. The electrical industry will have to produce still larger

units if this programme is to be fulfilled.

It takes four to five years to design and actually produce a new large set. A start must therefore be made at once on still larger equipment if the requirements are to be satisfied in the period after 1965.

Turbine and generator factories are already engaged on the development of single-shaft 500 MW units and twin-shaft units of 800 and 1000 MW. But long term planning requires that boiler, transformer and switchgear works should be following suit. Research and development should commence on three-phase a.c. transmission of 750 kV and d.c. transmission of $\pm$ 700 kV together from fuel-fired power stations with units of 500, 800 and 1000 MW.

Translated by O.M. Blunn

REFERENCES

1. L.I Dvoskii and A.B. Krikunchuk; *Elektrichestvo*, No.11, (1957).
2. V.G. Zhilin; *Elektr. stants.*, No.8,(1959).
3. V.G. Zhilin and A.M. Nekrasov; *Elektr. stants.*, No.6, (1960).

A STATISTICAL METHOD OF ESTIMATING THE RELIABILITY OF ELECTRIC LOCOMOTIVES*

I.P. ISAEV (Moscow Institute of Railway Engineers) and
V.S. SONIN (Urals department of the TsNII MPS)

(Received 6 April 1960)

Estimates of the reliability of the individual units in the power circuit of electrical locomotive and of the system as a whole are required before better control systems can be devised.

The electrical equipment of an electric locomotive can fail suddenly because of latent defects or gradually wear out in use. Here the important factors are the standards of production and erection and the operating conditions.

On the one hand the utilization of the locomotive can be complicated by faults in design or erection, and on the other, the electrical, mechanical and thermal strength of the locomotive can be upset by incorrect use.

These various factors may be of a regular nature (e.g. non-uniform loading of the motors, amount of cooling air etc) or else random (breakdown of the insulation, rupture of the leads, incorrect operation of the relays etc).

The reliability of an electric locomotive can be reduced by all these factors.

Up to the present time the reliability of an electric locomotive has only been conceived in a purely qualitative sense. But it has been shown by an analysis of operating experience with electrified railways that a quantitative definition is also possible.

The power and control circuits of all electric locomotives consist of

* *Elektrichestvo*, 3, 18-22, 1961.

a large number of separate units, each of which can be regarded as a set of component items. Although certain units may be connected in parallel in operation, the reliability of a locomotive depends nevertheless on the reliability of each component item. Since the operating conditions vary even for the same type of item, it follows that a statistical approach must be followed [1-3].

We will define the *operational reliability of an electrical locomotive* (scheme) as the probability of faultless operation over a given distance for defined tolerances in the production and installation of the units under given operating conditions. Every random fault α_i in a unit is then defined as a function of the distribution density of the probabilities $\lambda_i(L)$ or as the probability of a fault over the given distance $(0, L)$:

$$p(\alpha_i) = \int_0^L \lambda_i(L)\, dL. \tag{1}$$

Conversely, the probability of faultless operation of this unit is:

$$1 - p(\alpha_i).$$

The reliability of the locomotive circuits can therefore be established by the relation between the probability of the individual items being reliable and the probability of the whole circuit being reliable, i.e. by forming the reliability function of the system.

Since the whole system is out of order if any of the m items fail in the locomotive circuits, the general reliability function of the whole system therefore takes the form:

$$P = \prod_1^m [1 - p(\alpha_i)]. \tag{2}$$

An analysis of this expression provides certain relationships which can be verified by operational data and these relationships can be used to solve certain new problems.

Operational faults in the electrical equipment and power circuits. The power circuit of an electric locomotive is composed of k independent units all of which may fail independently of another failure. Consequently, the reliability function on the basis of expression (2) can take the form

$$R = 1 - \prod_1^k [1 - p(\alpha_i)]. \tag{3}$$

Since the system must possess a high degree of reliability, its unreliability can be approximated in the form:

$$R = p(\alpha_1) + p(\alpha_2) + \ldots + p(\alpha_k),$$

where $p(\alpha_i)$ is the probability of the individual units failing.

When considered with (1), we get:

$$R = \int_0^L \lambda_1(L)\,dL + \int_0^L \lambda_2(L)\,dL + \int_0^L \lambda_k(L)\,dL.$$

Suppose we put Λ for the function of the density distribution of the probability of failure in the power circuit as a single whole, then

$$R = \int_0^L \Lambda(L)\,dL, \tag{4}$$

where

$$\Lambda(L) = \sum_1^k \lambda_i(L).$$

Thus, the distribution density of faults in the power circuit equals the sum of the distribution densities of faults in the units. Having the statistical distribution of the faults in the units of the locomotive system as a function of its distance travelled, we can either define the reliability of the system for a given distance, or with the adopted probability of faultless travel, for a given degree of reliability of the locomotive system.

As an example we will consider the available data for faults in the units in the power circuits of d. c. locomotive equipped with DPE-400 type traction motors. An analysis of these data has shown that 36% of electric locomotive breakdowns are attributable to the units in the traction motors, 31% to the electrical apparatus and 3% to the auxiliary machines.

Table 1 lists the particular faults causing the failure of the least unreliable unit in locomotives (the motors) as a percentage of the total number of faults.

Table 1 shows that the most unreliable unit in the traction motor is the armature.

TABLE 1

Motor unit	Faults, %
Armature	53.7
Brush holders and brackets ..	17.3
Cable leads and cross pieces ..	14.3
Bearings	6.2
Main poles and compoles	3.7
Other	4.9

These data have been statistically treated and a bar diagram produced for the distribution of the faults over the units of the DPE-400 type traction motor as a function of distance (Fig. 1). We have also analytically established the functions for the distribution density of the probability of the individual units failing with distance (Table 2).

TABLE 2

Motor unit	Probability density of faults λ_i
Armature	$0.179L^{0.835}e^{-0.407L}$
Brush holders and brackets ..	$0.055L^{-0.755}e^{-0.0337L}$
Cable leads and cross pieces ..	$0.038L^{-0.232}e^{-0.129}$
Bearings	$0.0185L^{-1.456}e^{-0.188L}$
Main poles and compoles	$0.022L^{-0.0979}e^{-0.219L}$

Using these analytical expressions it can be shown, for example, that the reliability of the armature is 0.69, that of the brush holders and brackets 0.968, the cable leads and crosspieces 0.935 and main poles and compoles 0.932 for an average distance travelled before repair (400,000 km).

Consequently, using (2), the reliability function of the locomotive power system is

$$P = \prod_{1}^{4} [1 - p(\lambda_i)] = 0.69 \cdot 0.968 \cdot 0.935 \cdot 0.932 = 0.53.$$

This means that about 53 of every hundred traction motors are free of faults up to the mean repair.

An analysis of armature faults shows that they are mainly due to the breakdown of the winding insulation.

It is therefore of practical value to obtain an estimate of the probability of a failure of the armature winding insulation for the various production standards.

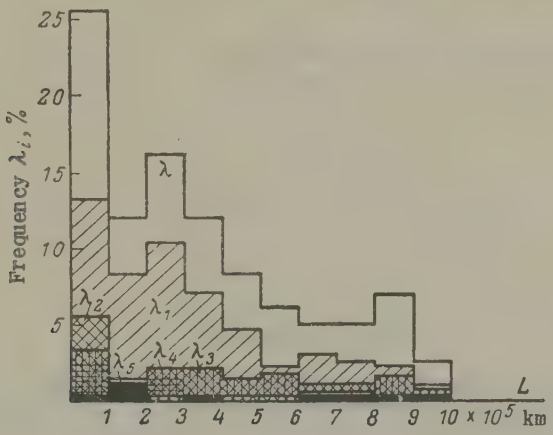

Fig. 1. Histogram of the distribution of faults in the components of DPE-400 type traction motors.

Each conductor and each section of the armature winding is insulated and fitted separately and there is no relationship between variations in binding tension, insulation thickness, or other such technological factor. We can assume that the law governing the distribution of mileage covered prior to breakdown due to the insulation of the armature winding is normally distributed about the mean mileage of the locomotive.

Suppose we put λ_s for the probability of a breakdown in the insulation of an individual section of a winding and $\lambda_b = n\ \lambda_s$ the probability of a breakdown in the insulation of an armature winding with n slots.

We then get:

$$\lambda_b = n\lambda_s = \frac{n}{\sqrt{2\pi}} \int_x^\infty e^{-\frac{x^2}{2}} dx,$$

where $$x = \frac{\bar{L} - L}{\sigma_L}.$$

Consequently,

$$\frac{\lambda_b}{n} = \frac{1}{2} - \Phi(x),$$

where $\Phi(x)$ is a Laplace function.

Since for DPE-400 type traction motors

$$\lambda_b = 0{,}64 \text{ and } n = 57,$$

it follows that

$$\Phi(x) = \frac{1}{2} - \frac{\lambda_b}{n} = 0.489,$$

which corresponds to $x = 2.3$ and, consequently, to $\bar{L} - L = 2.3\sigma_{L1}$.

Now, if we assume for purposes of comparison that the probability of the armature winding remaining intact must be at least 0.9, we then get $x = 3.6$ and $\bar{L} - L = 3{,}6\sigma_{L2}$ in a similar way.

This implies that given the type of insulation material and similar operating conditions, a 90% probability of the winding remaining intact requires an alteration in the method of production which will ensure that the mean square deviation in mileage of the locomotive σ_{L2} does not exceed 0.64 σ_{L1}.

Incidentally, in integrating the analytical relationships in Table 2 for the distribution density of faults in traction motor units with respect to mileage, we can define the faultless mileage for a given degree of reliability as the value of L corresponding to the integral in question.

The effect of tolerances. Definite tolerances are allowed in production and repair for the current I, voltage U and speed n etc.

These allowances cause a change in the function of the density of unreliability of the locomotive system equal to

$$d\Lambda = \sum_{1}^{m} \frac{\partial \Lambda}{\partial \lambda_i} d\lambda_i,$$

where $$d\lambda_i = \sum_1^k \sum_1^p \frac{\partial \lambda_i}{\partial L} \cdot \frac{dL}{dq}\, dq;$$

n – the number of nodes in the system;

k – the number of items in the i-th unit;

p – the number of standardized parameters of the i-th unit, and

q – a particular standardized parameter of the unit

In its general form the distribution density of faults in the i-th unit of the system can be represented in the form (see Table 2):

$$\lambda_i = aL^{\alpha i} e^{-\beta_i L},$$

Therefore,

$$d\lambda_i = \sum_1^k \sum_1^p \lambda_i \left[\frac{\alpha_i}{L} - \beta_i\right] \frac{dL}{dq}\, dq. \qquad (5)$$

Thus, the estimation of tolerances merely involves determining the increment in the functions of unreliability of the system from the given parameters.

As an example, the effect of divergence in the characteristics of DPE-400 type traction motors or the unreliability of their armatures can be estimated from (5) by the increment

$$d\lambda_1 = \frac{\partial}{\partial L} (0.179 \cdot L^{0,835} \cdot e^{-0,407L}) \frac{dL}{dI}\, dI, \qquad (6)$$

in which the function of the unreliability density λ_1 is taken from the first line in Table 2 and the load divergence dI is defined in terms of the standardized divergence dn of the speed characteristics of traction motors in the form:

$$\Delta I = \left| \frac{1}{\frac{\partial n}{dI}} \right| \Delta n.$$

For example, given the mean repair, the maximum divergence of the speed characteristics of DPE-400 type traction motors is + 9.5% (for the appropriate air gap tolerances) corresponds to a maximum load divergence of ± 20% [4].

The term in (6) for the rate of variation in the mileage covered as a function of the load is conventionally defined as the ratio of the mileage between repairs ΔL to the difference in loads ΔI on the traction motors between two consecutive repairs as measured by the divergence in the speed characteristics of traction motors during period overhauls (Fig. 2). This definition is used since no statistics are as yet available about variations in the characteristics of traction motors with operating time or mileage.

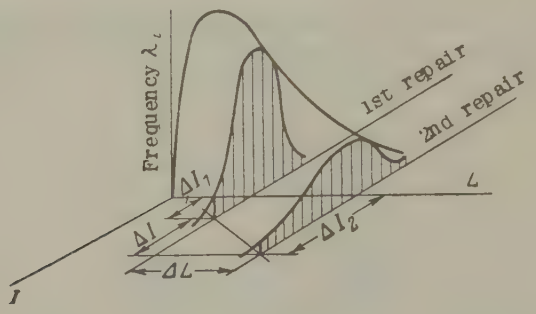

Fig. 2. The effect of tolerances on the reliability function of a locomotive unit.

As an example, for running repairs and periodic overhauls of traction motors

$$\frac{\Delta L}{\Delta I} = 6.7 \times 10^3 \text{ km/A}$$

Using (6) we can find the change in the function of the density of unreliability of the armatures of DPE-400 type traction motors (after an average overhaul):

$$\Delta\lambda_1 = 0.69\left[\frac{0.835}{2\cdot 10^5} - 0.407\right]6.7\times 10^3 = \\ = -1.87\times 10^{-5}\Delta I.$$

It follows from this example that deviations in the parameters of a locomotive scheme may have a substantial effect on operational reliability.

For a fuller estimate of this influence it must be borne in mind that the statistical distribution of the deviations in the parameters between the limits of the field of tolerances is usually governed by a

normal Gaussian law [4]. Therefore, supposing $\frac{\lambda_i - \bar{\lambda}_i}{\sigma_{\lambda i}} = t$, we can establish that the distribution density of the probability of defects in the items of a scheme due to allowances for parameters is governed by a Gaussian law with a mean value λ_i of the probability of defects and a standard deviatioh

$$\sigma_{\lambda i}^2 = \sum_1^k \sum_1^p \left[\bar{\lambda}_i \left(\frac{\bar{\alpha}_i}{\bar{L}} - \bar{\beta}_i \right) \frac{dL}{d\bar{q}} \right]^2 \sigma_q^2,$$

where σ^2_q is the deviation in the distribution of the parameter q of the i-th item of the system.

Similarly, from (4) we can estimate the effect of allowances on the reliability of the whole locomotive system by the parameters of the Gaussian distribution in the form $\bar{\Lambda}$ and

$$\sigma_\Delta^2 = \sum_1^m \left(\frac{\partial \Lambda}{\partial \bar{\lambda}_i} \right)^2 \sigma_{\lambda i}^2,$$

Using these we can determine the reliable travel of an electric locomotive with accepted probability of defects by a Laplace function in the form:

$$L = \bar{L} - t\sigma_\Delta.$$

The technical specifications (TU) and State Standards (GOST) which lay down the allowances for deviations in the parameters of the items and units in the electrical circuits of electric locomotives thus define the probability of reliable operation over a given mileage as well as the operational characteristics and power utilization of the locomotives.

The relationships which are obtained in this way can be used in the development of power and control circuits for new types of locomotive as well as for operational purposes in order to reduce the probability of defects in the individual units.

In addition, this method can be used to estimate the number of standby parts and arrange repair schedules etc.

The solution of such problems must be based on the cost analysis of alternative arrangements.

Translated by O.M. Blunn

REFERENCES

1. V.I. Siforov; *Methods of calculating the reliability of systems containing many items, (O metodakh rascheta nadezhnosti sistem soderzhashchikh bol'shoe kolichestvo elementov).* Akad. Nauk SSSR, OTN, No.6, (1954).
2. Sh.K. Bebiashvili; *Contribution to the theory of the reliability of systems containing many items, (K teorii nadezhnosti raboty sistem soderzhashchikh bol'shoe kolichestvo elementov).* Akad. Nauk SSSR, OTN, No.10, (1955).
3. G.V. Druzhinin; *Avtomet. i telemekh.*, No.12, (1957).
4. I.P. Isaev; *The tolerances on the characteristics of electric locomotives, (Dopuski na kharakteristiki elektricheskikh lokomotivov).* Transzheldorizdat, (1958).
5. A.S. Zingerman; *Zh. tekh. fiz.*, XVIII, No.8, (1948).

THE RELATIONSHIP BETWEEN THE INTERNAL LOSS AND REACTIVE OUTPUT OF SYNCHRONOUS MACHINES*

Professor I. A. SYROMIATNIKOV

(Received 21 October 1960)

To solve the problems connected with the choice of the rated power factor of synchronous machines and the efficient allocation of reactive output between individual sources, we need to know the marginal loss and how the losses in synchronous machines vary with their reactive output.

In synchronous generators and motors where the losses caused by the active output are constant, the internal losses caused by the reactive output depend on the losses in the stator and rotor windings. Here the variable internal losses in the stator vary in proportion to the square of the reactive power. But the losses in the rotor winding are governed by a much more complicated law [1, 2].

We will use the following notation:

$\Delta P_{s.r}$ – stator winding loss, including the additional losses, under rated conditions;

$\Delta P_{e.r}$ – excitation winding loss under rated conditions;

$I_{e.r}$ – the rated excitation current;

I_{el} – the excitation current for an active load $P_1 = \beta P_{11}$ and $\cos \phi = 1$;

β – damping coefficient;

$P_1 = \beta P_{1r}$ – the consumption of active power from the network for a motor or that supplied to the network for a generator;

P_{1r} – the same but on rated load;

---

* *Elektrichestvo*, No. 3, 44-48, 1961.

Q – the reactive power of the machine load;

Q_r – the rated reactive power;

S – total output;

I_e – the excitation for the active load $P_1 = \beta P_{1r}$ or the reactive load Q;

$Q_1 = \alpha Q_r$ – the reactive power for operation on the active load $P_1 = \beta P_{1r}$ with rated excitation current;

I_{ac} and I_{reac} – the active and reactive components of the stator current.

The losses in the stator due to the reactive power are

$$\Delta P_{s.\,reac} = \Delta P_{s.\,r} \frac{Q^2}{Q_r^2} \sin^2 \varphi_r \tag{1}$$

The losses in the rotor in synchronous generators and motors depend on the reactive power of these machines:

$$\Delta P_{e.\,reac} = \Delta P_{e.\,r} \left(\frac{I_e^2}{I_{e1}^2} - \frac{I_{e.\,r}^2}{I_{e.\,r}^2} \right). \tag{2}$$

The rotor current can safely be found from the following formula as a function of the reactive power

$$I_e = I_{e1} + (I_{e.\,r} - I_{e1}) \frac{Q}{Q_1}$$

Substituting the ratio

$$\frac{I_e}{I_{e.\,r}} = \frac{I_{e1}}{I_{e.\,r}} + \left(1 - \frac{I_{e1}}{I_{e.\,r}} \right) \frac{Q}{Q_1} = k_1 + (1 - k_1) \frac{Q}{Q_1}$$

in formula (2), we get:

$$\Delta P_{e.\,reac} = \Delta P_{e.\,r} \left[(1 - k_1)^2 \frac{Q^2}{Q_1^2} + 2k_1 (1 - k_1) \frac{Q}{Q_1} \right],$$

or

$$\Delta P_{e.\,reac} = \Delta P_{e.\,r} \left[(1 - k_1)^2 \frac{Q^2}{\alpha^2 Q_r^2} + 2k_1 (1 - k_1) \frac{Q}{\alpha Q_r} \right], \tag{3}$$

where

$$k_1 = \frac{I_{e1}}{I_{e.\,r}}.$$

The total losses depend on the reactive power

$$\Delta P_{\text{reac}} = \Delta P_{\text{s.r}} \sin^2 \varphi_{\text{r}} \frac{Q^2}{Q_{\text{r}}^2} + \Delta P_{\text{e.r}} \times \left[(1-k_1)^2 \frac{Q^2}{\alpha^2 Q_{\text{r}}^2} + 2k_1 (1-k_1) \frac{Q}{\alpha Q_{\text{r}}} \right]. \quad (4)$$

Suppose we put

$$A = \Delta P_{\text{s.r}} \sin^2 \varphi_{\text{r}} + \frac{\Delta P_{\text{e.r}} (1-k_1)^2}{\alpha^2} \quad (5)$$

and

$$B = \frac{2\Delta P_{\text{e.r}} k_1 (1-k_1)}{\alpha}, \quad (6)$$

We then get:

$$\Delta P_{\text{reac}} = A \frac{Q^2}{Q_{\text{r}}^2} + B \frac{Q}{Q_{\text{r}}}. \quad (7)$$

In synchronous compensators and variable losses in the stator vary in proportion to the square of the reactive power:

$$\Delta P_{\text{s}} = \Delta P_{\text{s.r}} \frac{Q^2}{Q_{\text{r}}^2}.$$

The total losses in the rotor are found by the formula

$$\Delta P_{\text{e}} = \frac{\Delta P_{\text{e.r}}}{I_{\text{e.r}}^2} \left[I_{\text{e.nl}} + (I_{\text{e.r}} - I_{\text{e.nl}}) \frac{Q}{Q_{\text{r}}} \right]^2,$$

where $I_{\text{e.nl}}$ is the excitation current on no load.

Putting $k_{\text{nl}} = \dfrac{I_{\text{e.nl}}}{I_{\text{e.r}}}$, we get:

$$\Delta P_{\text{e}} = \Delta P_{\text{e.r}} \left[k_{\text{nl}}^2 + (1-k_{\text{nl}})^2 \frac{Q^2}{Q_{\text{r}}^2} + 2k_{\text{nl}} (1-k_{\text{nl}}) \frac{Q}{Q_{\text{r}}} \right].$$

The total losses are

$$\Delta P = \Delta P_{\text{c}} + \Delta P_{\text{e.r}} k_{\text{nl}}^2 + [\Delta P_{\text{s.r}} + \Delta P_{\text{e.r}} (1-k_{\text{nl}})^2] \frac{Q^2}{Q_{\text{r}}^2} + \quad (8)$$

$$+ 2\Delta P_{\text{e.r}} k_{\text{nl}} (1-k_{\text{nl}}) \frac{Q}{Q_{\text{r}}},$$

or

$$\Delta P = C + A\frac{Q^2}{Q_r^2} + B\frac{Q}{Q_r}, \tag{9}$$

where

$$C = \Delta P_c + \Delta P_{e.r}\, k_{nl}^2; \tag{10}$$

$$A = \Delta P_{s.r} + \Delta P_{e.r}(1 - k_{nl})^2; \tag{11}$$

$$B = 2\Delta P_{e.r}\, k_{nl}(1 - k_{nl}); \tag{12}$$

and ΔP_c represents the constant losses.

The excitation currents I_{el}, and $I_{e.nl}$ and the reactive power Q_1 have been found by a graphical-analytical method using a vector diagram of the machine. The coefficients k_1 and α are defined by the formulae:

$$k_1 = \sqrt{\frac{1 + \beta^2 x_d^2 \cos^2 \varphi_r}{1 + x_d^2 + 2x_d \sin \varphi_r}}; \tag{13}$$

$$\alpha = \frac{\sqrt{1 + x_d^2(1 - \beta^2 \cos^2 \varphi_r) + 2x_d \sin \varphi_r} - 1}{x_d \sin \varphi_r}. \tag{14}$$

Fig. 1 shows $(1-k_1)^2$ and $2_1(1-k_1)$ as a function of x_d for β = 1, 0.75 and 0.5 and cos ϕ_r = 0.8, 0.9 and 1.

Fig. 2 shows the coefficients α and

$$\alpha_1 = \frac{Q_1}{S_r} = \frac{\sqrt{1 + x_d(1 - \beta^2)} - 1}{x_d} \tag{15}$$

as a function of β for cos ϕ_r = 0.8, 0.9 and 1.

Tests show that this graphical-analytical method gives much better results than Potier diagrams. Corresponding curves obtained by Potier diagrams are plotted in Fig. 1 for β = 1 by way of comparison.

The reactive power should be distributed between its various sources on an equal marginal loss basis. The marginal loss is defined as the first derivative of the internal (active), which depends on the reac-

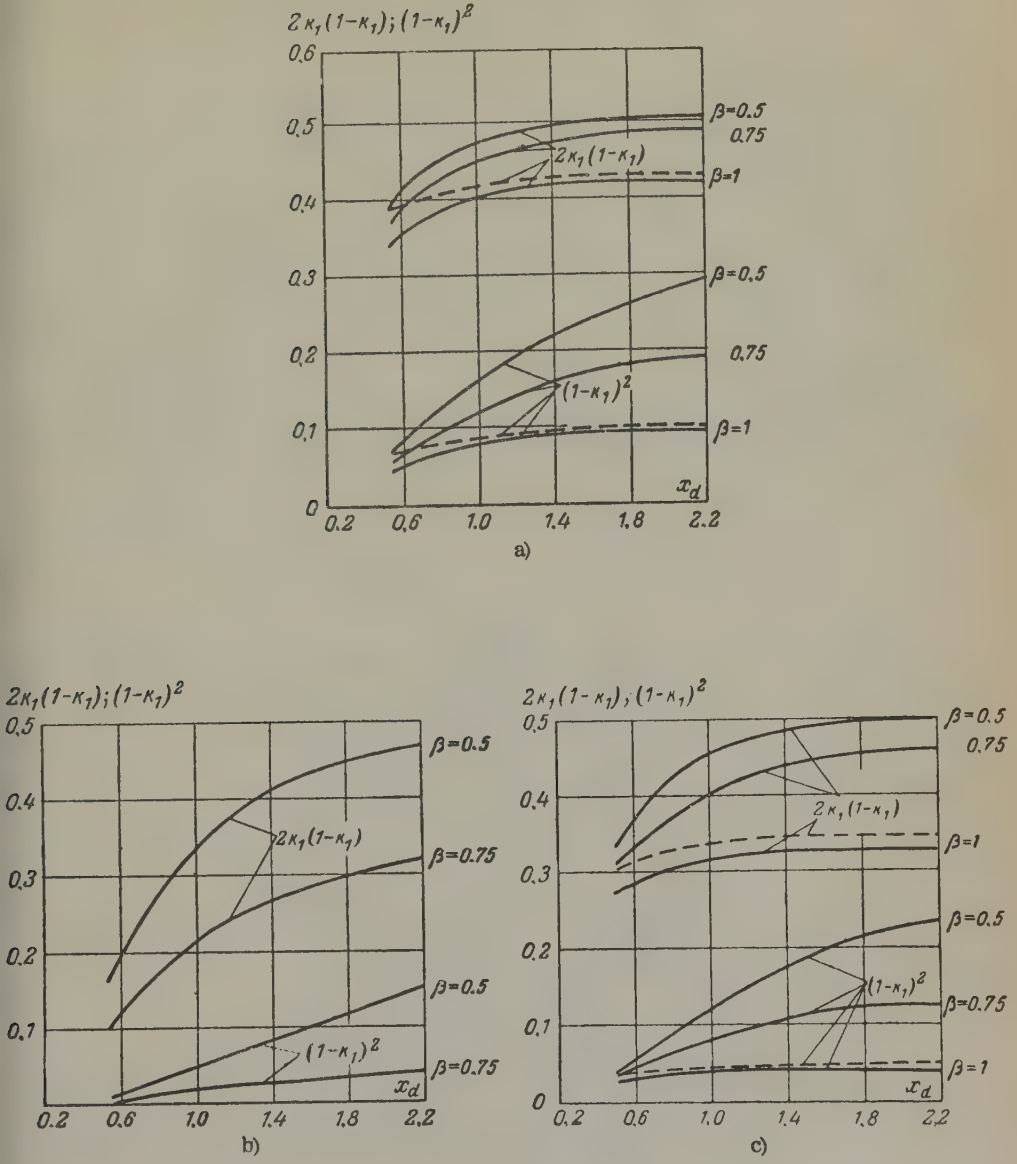

Fig. 1. The variation in $2k_1(1-k)$ and $(1-k_1)^2$ with x_d. *a* – when $\cos\phi_r = 0.8$; *b* – $\cos\phi_r = 0.9$; *c* – $\cos\phi_r = 1$; ---- calculated by a Potier diagram.

tive power, with respect to the reactive power

$$g = \frac{d(\Delta P_{reac})}{dQ} = \frac{2AQ}{Q_r^2} + \frac{B}{Q_r}. \qquad (16)$$

This proposition only refers to the condition when the sources of reactive power are connected in the same electrical circuit. The inclusion of a source of reactive power in a circuit can only be decided if the fixed loss component is considered; if this is neglected, wrong conclusions may be reached. Thus, for example, it was found that a synchronous compensator (or generator used as a compensator) ought to be run with a very small load. But the actual reduction in the internal loss in the synchronous compensator itself (mainly fixed losses in this case). It was therefore only permissible to include the synchronous compensator in the network (or to leave it there) if the other sources of reactive power were fully loaded up to the limit, it therefore being impossible to distribute all the reactive load between them.

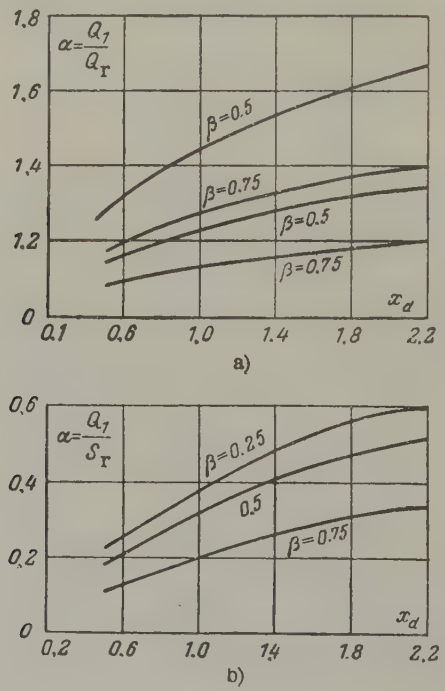

Fig. 2. The coefficient as a function of x_d for $\cos \alpha_r = 0.9$ (two upper curves) and $\cos \phi_r = 0.8$ (two lower curves) (*a*) and the coefficient α_1 as a function of x_d for $\cos \phi_r = 1$ (*b*).

The following Table shows the fixed loss components of synchronous generators (the mechanical and stator iron losses including the additional loss) and compensators.

Type		T-2-6-2	T-2-12-2	T-2-25-2	T-2-50-2	TBC-30	TB-50-2	TB-2-100-2
Generator	Fixed loss component, kW	139	205	391	918	214	368	810
Compensator	Power, MVA	7.5	10	15	30	37.5	75	–
	C, kW	104	105	196	379	188	325	–

It follows from expressions (5) and (6) that the value of A and B as well as the marginal loss all remain practically constant if the active power load varies.

Consider the following example. It is required to find the active losses ΔP_{reac}, which depend on the reactive power, marginal loss or the real load for $\beta = 1$, 0.75 and 0.5 in respect of a DSP-type synchronous motor of 1300 kW, 1520 kVA, 1500 rev/min, $\cos \phi_r = 0.9$, $Q_r = 660$ kVar, $\Delta P_{s.r} = 28.6$ kW, $\Delta P_{e.r} = 8.55$ kW, $\Sigma P = 64.7$ kW and $\eta_r = 0.953$.

Assuming that $x_d = 1.6$ and from Fig. 2 that $2k_1 \cdot (1-k_1) = 0.35$, we then get for $\beta = 1$:

$$A_r = 0.436^2 \cdot 28.6 + 0.05 \cdot 8.55 = 5.86 \text{ kW}$$

$$B_r = 0.35 \cdot 8.55 = 3 \text{ kW}$$

$$\Delta P_{reac.r} = 5{,}86 \frac{Q^2}{Q_r^2} + 3 \frac{Q}{Q_r}$$

and

$$g_r^{\prime} = \frac{2 \cdot 5.86 Q}{660 Q_r} + \frac{3}{660} = 0.0178 \frac{Q}{Q_r} + 0.00455.$$

For $\beta = 0.75$ and $\beta = 0.5$, we respectively get:

$$\Delta P_{reac(0,75)} = 6.1 \frac{Q^2}{Q_r^2} + 2.86 \frac{Q}{Q_r},$$

$$g_{(0,75)} = 0{,}0185 \frac{Q}{Q_r} + 0{,}0043;$$

$$\alpha_{(0,75)} = 1{,}35;$$

$$\frac{\Delta P}{\text{reac}^{(0,5)}} = 6{,}2 \frac{Q^2}{Q_r^2} + 2{,}7 \frac{Q}{Q_r};$$

$$g_{(0,5)} = 0{,}0188 \frac{Q}{Q_r} + 0{,}0041;$$

$$\alpha_{(0,5)} = 1{,}57.$$

The variation in losses and the marginal increase as a function of the reactive power are practically identical for loads of 1, 0.75 and 0.5 rated load. The difference is that the motor can be loaded with a reactive load above the rated load at loads less than the rated load. Thus $\alpha_{(0.75)} = 1.35$ for $\beta = 0.75$ and $\alpha_{(0.5)} = 1.57$ for $\beta = 0.5$.

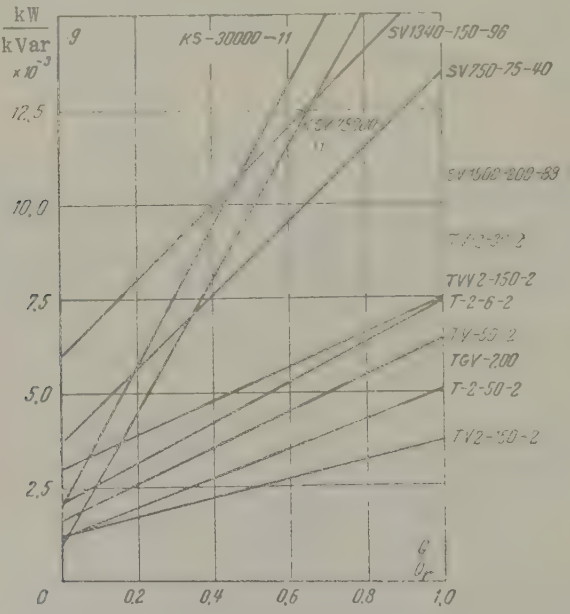

Fig. 3. Marginal loss g as a function of $\frac{Q}{Q_r}$ in synchronous compensators.

Figs. 3 and 4 show the straight line marginal loss curves of various types of synchronous machine.

The tangent of the angle of the marginal loss curve is defined by

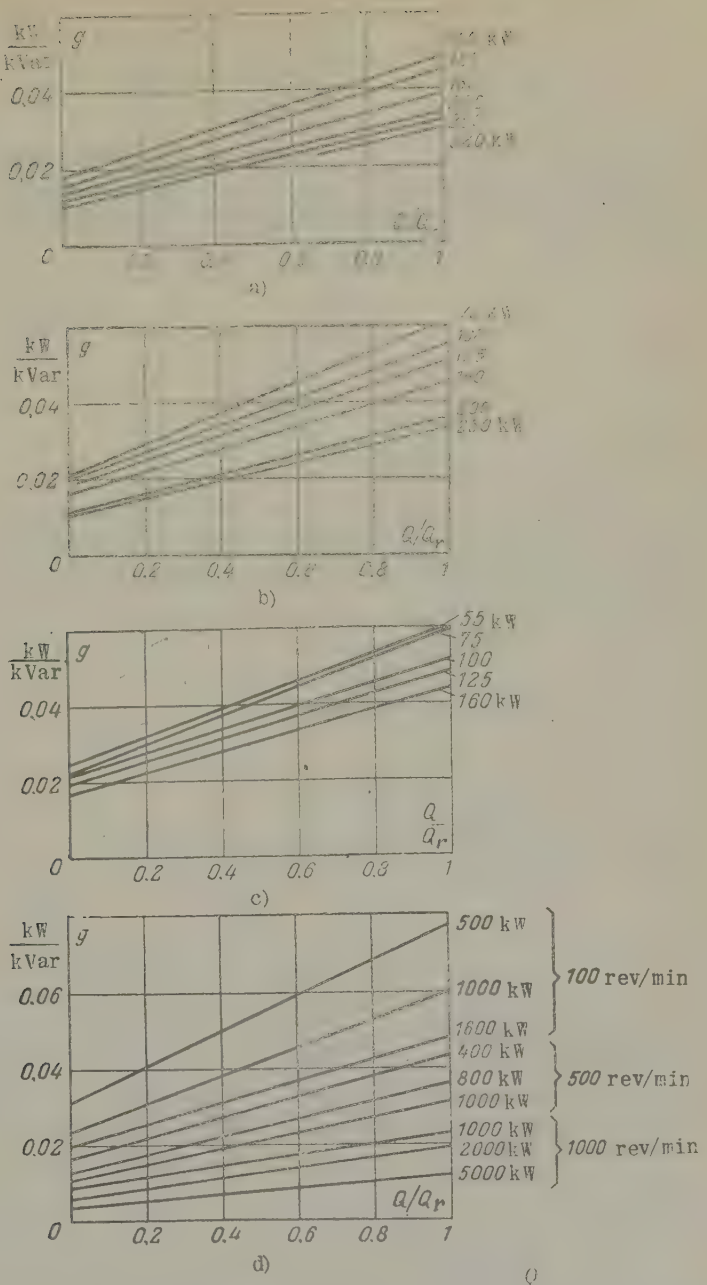

Fig. 4. The marginal loss g as a function of $\frac{Q}{Q_r}$ in synchronous motors:

a – DS type motor of 380 V and 1500 rev/min for cos $\phi_r = 0.9$; *c* – DS type motor of 380 V and 750 rev/min for cos $\phi_r = 0.9$; *d* – SDN type motor of 6 kV for cos $\phi_r = 0.9$.

the expression

$$\tan\psi = \frac{2A}{B}.$$

The value of tan ψ is a minimum for synchronous motors and a maximum for synchronous compensators. Thus, for example, tan ψ = 7.4 to 17 for synchronous compensators, whereas tan ψ = 1.2 to 2.2 for DS-type synchronous motors.

Translated by O.M. Blunn

REFERENCES

1. L.V. Litvak; *Prom. energet.*, No.10, (1956).
2. I.A. Syromiatnikov; *The technical and economic advantages of synchronous motors, Synchronous motors, (Teknikoekonomicheskie preimushchestva sinkhronnykh dvigatelei, Sinkhronnye dvigateli).* Gosenergoizdat, (1959).

A NEW BRUSHLESS SYNCHRONOUS ALTERNATOR FOR USE IN AIRCRAFT*

L. M. PALASTIN

(VNIIEM)

(Received 26 November 1961)

The electrical supply in aircraft has until recently been mainly d.c. However, high altitude flying has considerably increased the brush wear of the electrical machines due to the low humidity of the air at high altitudes and commutation has been adversely effected. The brush assemblies have to be inspected and serviced much more frequently than the other units, whilst the dismantling and replacement of the machine because of brush wear is a time-consuming and costly operation. It has therefore become an urgent matter to eliminate the brush contact from the electrical machine in civil aviation and a number of other cases. In this connexion, there has been a comparatively rapid development of synchronous brushless alternators in the U.S.A. and U.K. for the a.c. supply of aircraft.

Use is currently made of synchronous alternators of 40 to 130 kVA for aircraft purposes [1]. Alternators of such powers are usually provided with separate exciters. The alternator rotor and exciter armature are usually mounted on the same shaft. Unlike general-purpose synchronous machines, use is made of a.c. exciters with a rotating a.c. armature winding which supplies the excitation winding of the alternator via a rotating rectifier.

The following observations can be made about the brushless a.c. alternators which have been used in aircraft [1, 2].

It is inexpedient to use comparatively large asynchronous alternators in aircraft owing to the considerable weight of the capacitors and the

---

* *Elektricheshtvo*, No.3, 51-56, 1961.

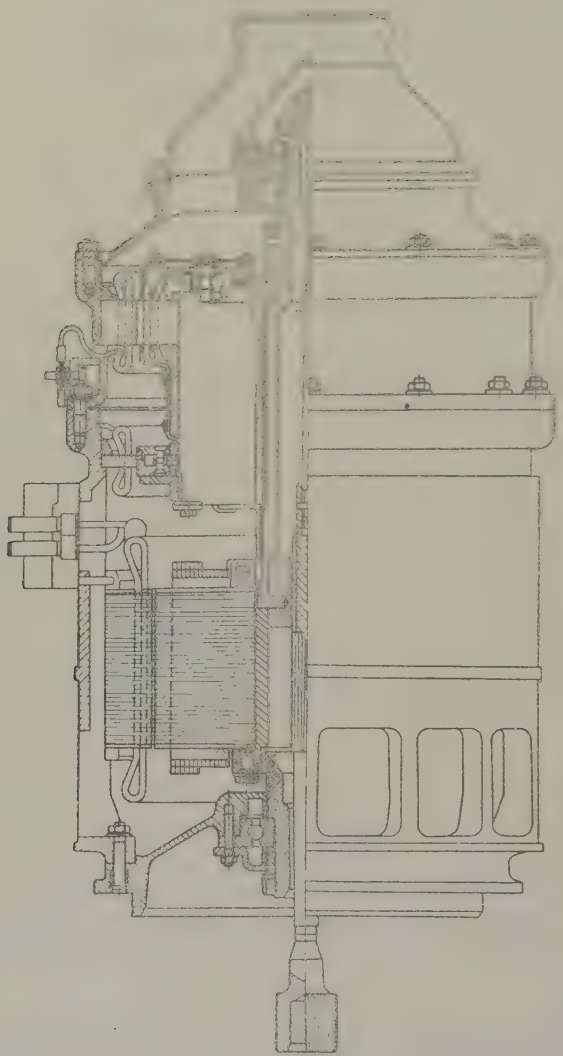

Fig. 1. A British brushless synchronous alternator of 40 kVA.

devices for controlling the capacitance.

Inductor alternators have been widely used in foreign and Russian aircraft for single phase high frequency [illegible] of relatively low power. The normal requirement is now for three phase alternators of 400 c/s with a small number of poles and it is inexpedient to use inductor alternators for this frequency. However, there is justification for using inductor alternators where an a.c. supply of 2000 c/s is required for electronic equipment.

"Rosenberg" alternators are heavy and bulky and there are difficulties in ventilation so that they are only used to a limited extent.

Alternators with excitation from permanent magnets have also been used abroad and in the U.S.S.R. for the supply of single and three-phase low-ohmic loads at low frequencies. Such machines have not until recently been used for outputs of the order of several dozen AVA owing to the difficulties involved in the production of relatively large rotating permanent magnets with the requisite magnetic properties and mechanical strength. Neither is there any simple and economical means of regulating the output voltage of alternators with permanent magnets.

Homopolar alternators have been produced both abroad and in the U.S.S.R. In these machines constructional parts of the machine, i.e. the frame and shields are used in the magnetic circuit. The flux is produced by one or two fixed annular excitation windings; it passes through the stator, which is external to the yoke (or frame) and shields, and then through two additional air gaps into the rotor shaft and from the shaft into the air gap stamping of the machine and the stator. These machines have not been widely used owing to their large weight and size and the difficulties involved in providing adequate excitation and ventilation.

Alternators with a fixed excitation winding have been produced by a number of American firms under the name "Seskin". Their weight has been reduced compared with machines of the foregoing type by arranging the magnetic flux in the constructional parts which enter into the rotating inductor of the alternator. The magnetic circuit has four air gaps so that a comparatively large excitation is required. The design and production of such alternators is quite a complicated matter however and they have not been extensively used owing to the difficulties involved in ventilation. Such machines may be useful for low outputs.

Synchronous brushless alternators are synchronous machines with a rotating field system, the winding of which is supplied by direct current

via rectifiers from the armature of the a.c. exciter. The rotor, excitation armature and rectifiers are all mounted on the same shaft.

Until recently, the production of brushless machines has been limited by the absence of semiconductor rectifiers with the requisite reliability, small dimensions, heat resistance and mechanical strength. Such alternators are free of the cited disadvantages. They are lighter in weight and more compact than the normal synchronous alternators with d.c. exciters.

Brushless synchronous alternators with an a.c. exciter and permanent magnet "sub-exciter" were proposed in 1955 by Bertinov [2]. A similar type of brushless synchronous alternator was produced in Great Britain in 1958.

Fig. 1 illustrates the British 40 kVA alternator on show at Farnborough in September 1958. The silicon rectifiers are mounted in a ring with their axes transverse to the axis of the shaft. The self-excitation of the alternator is provided by an auxiliary exciter in addition to the a.c. exciter. This auxiliary exciter is a synchronous alternator with excitation from permanent magnets.

The main and auxiliary exciters are machines with relatively large diameter armatures and short "active" length. The rotors of the exciters are disposed on a ribbed bush which can be slipped over the shaft. The space between the ribs of the bush allows for ventilation since there is very little aerodynamic resistance to the air entering the whole machine.

Short exciters with a relatively large diameter have a large number of poles and generate voltages of a higher frequency than that in the main alternator. Such exciters have the advantage of a short time constant which leads to a rapid recovery of the alternator voltage in the event of sudden load fluctuations.

The British company followed up with an improved version in which the auxiliary exciter was repositioned at the end of the armature of the main alternator on the drive side. This reduced the total length of the machine without adversely affecting the ventilation.

Brushless synchronous alternators have also been produced by other British and American firms for outputs up to 150 kVA.

Their main disadvantages are as follows:

1. Special measures must be taken to provide self-excitation and

these adversely affect the characteristics of the alternators. The use of a third machine with a similar outside diameter to that of the main generator and exciter considerably increases the weight, size and cost of the unit.

2. The large excitation power of an exciter with electromagnetic excitation is due to the large number of poles.

3. Multi-pole exciters with electromagnetic excitation are very complicated to make.

4. The power of the electromagnetic excitation winding of the main alternator is disproportionately large compared with other generators.

5. The time constants of the electromagnetic excitation windings of the main alternator and exciter are relatively large.

Brushless synchronous alternators with mixed excitation

The weight and size of brushless synchronous alternators can be greatly reduced if the auxiliary exciter is eliminated and self-excitation provided by the main exciter. This also improves the characteristics and reliability of the alternator.

The author has patented [3] a brushless synchronous alternator with mixed excitation (Fig. 2). The main alternator is of conventional construction having a fixed external armature 1 and a rotor with an excitation winding 2. The a.c. exciter has a fixed external controllable field circuit with excitation from permanent magnets and with a rotating armature 4 which supplies the excitation winding of the main alternator via rotating rectifiers 5. The exciter therefore combines two types of excitation, i.e. that from the permanent magnets and electromagnetic excitation. Each pole of the field circuit consists of one or two permanent magnet bars 7 and the magnetic shunt 6 made from soft magnetic steel. The inductor accommodates the coils of the regulator winding 3 which is supplied with direct current.

Under normal operating conditions the excitation of the alternator is produced by the joint effect of the permanent magnets and the control winding of the exciter field. Self-excitation of the alternator is provided by the permanent magnets of the exciter. The flux of the permanent magnets passes through the air gap and the exciter armature and is partially shunted by the magnetic shunts which increase the

leakage fluxes of the permanent magnets. The current in the control winding is in such a direction that the magnetic flux which it produces in the poles of the exciter is in the same direction as the flux produced by the permanent magnets. Hence the flux in the shunt due to the control winding is in the opposite direction to the leakage flux of the permanent magnets which is shunted through this same shunt. If it is necessary to increase the flux in the air gap of the exciter, the magnetic flux of the control winding draws the leakage flux of the magnets from the shunt into the gap.

The main alternator voltage is controlled by varying the flux in the exciter gap. This leads to a change in the flux in the gap of the main alternator.

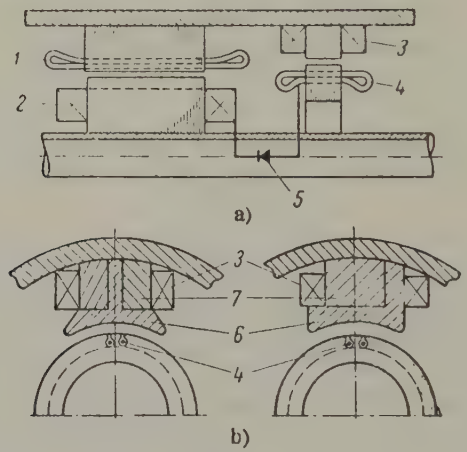

Fig. 2. Longtudinal (*a*) and cross (*b*) sections of a brushless synchronous alternator with mixed electromagnetic and permanent magnet excitation. *1* – armature winding of main alternator; *2* – excitation winding of main alternator; *3* – control winding of exciter; *4* – rotating armature winding of exciter; *5* – rotating rectifiers; *6* – magnetic shunt of soft magnetic steel; *7* – permanent magnets.

To control the alternator voltage, the control winding of the exciter must produce an m.m.f. which compensates the effect of the voltage reactions and drops in the armature circuits of the alternator and exciter. Here the control winding requires much less excitation power than an electromagnetic rotor (inductor) of equal volume since the main part of

the excitation flux of the exciter is provided by the permanent magnets. In the exciter with the electromagnetic field, the control winding must produce an m.m.f. which ensures that all the magnetic flux passes through the magnetic circuit and which will also compensate the effect of voltage drops and reactions in the armature circuit. The control winding in the permanent magnet exciter has to produce a much smaller m.m.f. since it regulates the total flux in the exciter gap by varying only a small part of it (i.e. the leakage fluxes of the permanent magnets in the magnetic shunts). However, the main part of the flux in the exciter gap is provided by the permanent magnets. If we bear in mind that the magnetic energy of a permanent magnet can be greater than that of an electromagnet of the same size, it immediately becomes clear why the excitation is reduced so much.

It is quite expedient to reduce the excitation power or the weight and size of the main alternator to reduce the electromagnetic time constant of the main excitation winding by providing the alternator with combined electromagnetic and permanent magnet excitation.

If the supply frequency must be high, the alternator can be provided with a salient pole rotor with mixed excitation. The advantages of this construction are already well known [4, 5, 6]. For the normal a.c. supply frequency the alternator can be provided with a rotating salient-pole exciter with mixed excitation.

Most of the permanent magnet flux in salient pole rotors with mixed excitation passes into the gap, but a portion is shunted in two side shunts by increasing the leakage flux of the magnet. The coils of the excitation winding around the magnet bars with magnetic shunts regulate the flux in the gap by acting upon the leakage fluxes of the magnets which are shunted in the magnetic shunts. Consequently, if the basic dimensions, electromagnetic loads on the machines, and the parameters and dimensions of the magnets, magnetic shunts and excitation windings are all correctly chosen, variable voltage machines with permanent magnets have a number of real advantages over similar machines with electromagnetic excitation as shown by tests.

We will give the details of tests which have been carried out on two identical machines with two permanent bar magnets per pole made from "magnico" alloy and electromagnetic excitation as used for the exciters of brushless synchronous alternators.

Certain characteristics are expressed in relative units to assist comparison.

No load characteristics

For purposes of comparison, Fig. 3 shows the test no load characteristics (the no load voltage at the terminals of the armature windings of the exciter as a function of the m.m.f. of their excitation windings at rated speed). Fig. 3 also shows the variation in the no load voltage as a function of the power of the excitation windings. It will be seen from a comparison of these curves that the excitation winding m.m.f. is 1.0 and 1.85 respectively for the permanent magnet exciter (curve 1) and that with electromagnetic excitation (curve 2) given a specific no load voltage. This shows that the total excitation winding m.m.f. of permanent magnet exciters is much less, other things being equal, than that of an exciter with electromagnetic excitation. Such a considerable reduction in the excitation ampere-turns causes an even greater reduction in the excitation power since the latter varies in proportion to the square of the ampere-turns for a specific volume of copper.

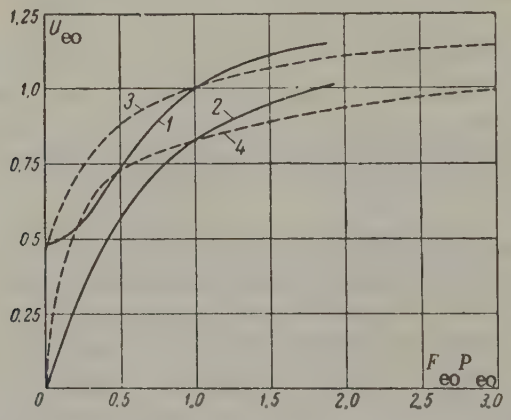

Fig. 3. The no load characteristics (———) and variation in the no load voltage as a function of excitation power (– – – –) for permanent magnet exciters (curve 1 and 3) and electromagnetic exciters (curves 2 and 4).

It will be seen from a comparison of the variation in the no load voltage as a function of the power of the excitation windings that the letter is 1.0 and 3.04 respectively for the permanent magnet exciter (curve 3) and that with electromagnetic excitation (curve 4).

Consequently, the electromagnetic exciter requires three times more excitation power than a corresponding permanent magnet exciter.

Incidentally, the voltage in a permanent magnet exciter can be increased 15 to 20% above its rated value without any significant increase in excitation power, whereas such an increase is impossible in electro-magnetic exciters owing to the saturation of the magnetic circuit.

Self-excitation

The self-excitation of the foregoing alternators without a special "sub-exciter" or other appliance requires quite a large residual flux in the a. c. exciter or the main alternator. It is not an easy matter to produce the large residual flux in electromagnetic exciters as required for reliable self-excitation. But even when this can be successfully arranged, the magnetization characteristic of the exciter has a wide hysteresis loop which adversely affects the conditions for stabilizing the alternator voltage.

This contradiction is eliminated by using a permanent magnet exciter.

It can be seen from the curves in Fig. 3 that the residual no load voltage in a permanent magnet exciter is 50% of rated. This is quite adequate for self-excitation. The magnetization characteristic has the same narrow hysteresis loop as an electromagnetic exciter having very little residual voltage at which self-excitation is not assured. The dimensions of the permanent magnets were chosen to ensure the minimum excitation power. If the excitation power is increased by 15 to 20 per cent above its minimum value, the volume of the permanent magnets can be fixed so that the residual voltage of the exciter is close to the rated value.

The time constants of the excitation windings of the exciters

The electromagnetic time constants of the excitation windings of the permanent magnet and electromagnetic exciters. Fig. 4 shows the experimentally-determined variation in the time constant as a function of the excitation winding m.m.f.'s. It will be seen from Fig. 4 that the time constants of the permanent magnet exciter are 1.3 to 2.0 times less than in the electromagnetic exciter over the operating range. These data agree with those published by A.I. Kantor, T.G. Soroker and others who showed that transients take place more quickly in machines with permanent magnet excitation than in machines with electromagnetic excitation. Permanent magnet exciters can therefore considerably reduce

the duration of transient phenomena in the control system compared with electromagnetic excitation.

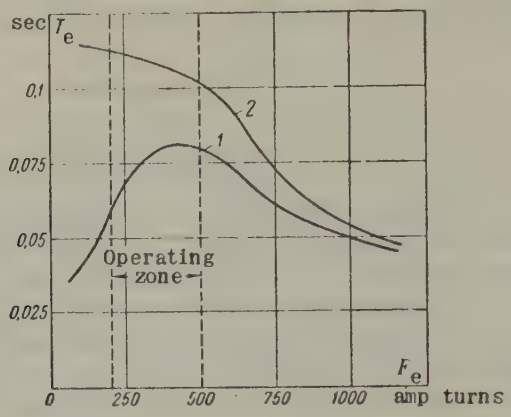

Fig. 4. The time constants of the excitation windings as a function of their m.m.f.
1 - for permanent magnetic exciters; *2* - for electromagnetic exciter.

The magnetization of permanent magnets

The permanent magnets of electrical machines are usually magnetized by special magnetizing plant. In practice it is not possible to achieve complete magnetization of the magnets in the assembled state owing to the negative effect of the air gap, the leakage permeance of the magnetic circuit and the fact that an adequate m.m.f. cannot be produced in the armature windings.

In the proposed permanent magnet exciters the excitation winding directly embraces the permanent magnets and the total flux passes through the magnets along their magnetic axis. The permanent magnets can therefore be magnetized in the assembled exciter by the excitation windings by passing a high direct current along it for a short period of time. (This current is 3 to 5 times higher than the rated value). This is a very important point in the production and utilization of machines with permanent magnets.

The effect of short circuit currents on permanent magnets

In conventional synchronous alternators the permanent magnets are

demagnetized by short circuit currents so that their efficiency is significantly reduced.

In the exciter in question and machines with mixed excitations the permanent magnets are protected from de-magnetization by the magnetic shunts. The total flux of the magnet is practically constant and the flux in the gap and leakage flux in the magnetic shunt are redistributed as a function of the magnitude of the de-magnetizing m.m.f. affecting the magnet. Machines with mixed excitation therefore require no stabilization of the permanent magnets in air to compensate for either short circuit currents or the effect of the air. The energy of the permanent magnets is used to better effect than in other known types of permanent magnet machines.

The following Table gives the main characteristics of the machines which can be used as a.c. exciters for brushless synchronous alternators.

Characteristics	With permanent magnets	With electromagnetic excitation
Diameter of armature, mm	85	85
Length of armature, mm	40	40
Length of pole, mm	38	38
Height of pole, mm	16.6	16.5
Width of pole core (magnetic shunt), mm	7	20
Width of permanent bar magnet, mm	10.5	–
Length of permanent bar magnet, mm	38	–
Load, %	100	100
Induction in gap, %	100	100
Maximum excitation power, %	100	304

From test results, the controllable permanent exciter has the following advantages over exciters with electromagnetic excitation:

1. Reliable self-excitation of the synchronous brushless alternator.

2. A considerable reduction in the weight and size of the alternator and an increase in reliability.

3. A considerable reduction in the excitation power of the exciter or its weight and size, other things being equal.

4. Shorter electromagnetic time constant of the excitation winding.

5. The cooling of the alternator is improved by eliminating the "sub-exciter" and accomodating the mixed exciter under the end parts of the armature winding of the alternator.

6. Increased utilization of the energy of the permanent magnets due to the elimination of de-magnetizing factors.

7. The permanent magnets can be magnetized in the assembled exciter without special equipment.

8. There is a substantial reduction in size and weight due to the use of new alloys for the permanent magnets and their high specific magnetic energy.

Translated by O.M. Blunn

REFERENCES

1. A.W. Ford; *El. rev.*, 711, 17 April (1959).
2. A.I. Bertinov; *Electrical alternators for use in aircraft, (Aviatsionnye elektrichekie generatory).* Gos. iz. oboron., prom., (1959).
3. L.M. Palastin; Auth. Cert. No. 131397, (1960).
4. L.M. Palastin and A.I. Chesnokov; *Vest. elektroprom.*, No. 12, (1958).
5. L.M. Palastin and A.I. Chesnokov; *The voltage regulation of synchronous high frequency alternators with permanent magnets, (Regulirovanie napriazheniia sinkhronnykh generatorov povyshennoi chastoty s postoannymi magnitami).* Trud. N.I.I.E.P., vol. 5, (1959).
6. L.M. Palastin; *Vest. elektroprom.*, No. 11, (1959).
7. V.D. Mazhuga; *Elektrichestvo*, No. 3, (1936).

ABSTRACTS FROM PAPERS PUBLISHED IN ELEKTRICHESTVO No. 3, 1961

Apparatus and Switchgear

A Novel Graphical and Analytical Method of calculating the Magnetic Permeance of Electrical Apparatus. B.K. BOOL, (28-35)

A simple and accurate method is proposed for calculating the magnetic fields of electrical apparatus and switchgear, for which the "potential grid", relaxation and Leman-Richter methods are unsuitable. The magnetic permeance (admittances) near the air gaps in the separate parts of the magnetic circuit and the magnetizing coils is taken into account so that the zones of the working and leakage fluxes are easily defined. The design of a particular magnetic circuit can then be estimated graphically.

Automatic control

Determination of the Phase-Amplitude Characteristics of Linear Systems and Elements from their Transient Behaviour S.Ia. Berezin, (pp. 64-69).

Newly compiled tables are given to simplify the determination of amplitude-phase characteristics from the transient phenomena in linear control systems.

Distribution

A Study of the Electrical Loads in the Machine Shops at a Tractor Plant. G.M. Kaialov et al., (pp. 22-27).

An account is given of the disposal diagrams (distribution curves as used by the Soviet Commission on load distribution in industrial undertakings in 1957-1960 to publish regulations governing the load distribution in industrial undertakings. The method was elaborated at the Gipro tractor and agricultural machinery works in 1958-1959.

Insulation

Highly Heat-Resistant Winding Conductors. V.A. Privezentsev, (pp. 76-82).

The author reviews world experience in the insulation of windings (enamelling, inorganic coatings, glass fibre, oxide coatings and fluoroplast insulation such as "flexsolon"), the protection of copper conductors from oxidation and the use of bi- and tri-metal conductors. Cu-Al and Ni-Cu conductors are recommended for 300°C (1500 to 2000 hr), and oxidized Al or Cu-Al-Ag (or Ni) conductors with glass fibre insulation can be used at 450-500° for limited periods.

Power Systems

Some Problems concerning the Utilization of the Stalingrad-Donbas d.c. Transmission System. N.M. Mel'gunov et al., (pp. 14-18).

The proposed 750 MW ± 400 kV d.c. transmission system linking the Stalingrad hydro-electric station and the large industrial Donbas region in the Ukraine will join the Southern and European grids of the U.S.S.R. A study is made of the way to take the most advantage of this possibility.

Rotating machines

The Voltage of Self-Excited Synchronous Generators with Damping Circuits when Switching on a Lagging (RL) Load. G.F. Suprun, (pp. 48-51).

The author shows how to calculate the variation in the voltage of a self-excited synchronous generator with damping windings on various loads (e.g. an RL load) and on no load.

Braking a Motor by simultaneously forcing its Flux and reducing the Generator Voltage. N.P. Kunitskii, (pp. 57-63).

After a mathematical analysis of optimum motor braking time, a detailed account is given of the modifications made to the ionic system of excitation for the generators and motors of a certain reversible rolling mill in the U.S.S.R. which are claimed to achieve the optimum braking time of 0.623 sec under various flux forcing conditions at maximum braking current 2.046 A.

Measurement Techniques

A Device for Measuring d.c. Currents up to 40 kA. D.N. Nasledov et al., (pp. 70-73).

This Russian device is similar to that developed in Western Germany. The intensity of the magnetic field is measured by means of Hall generators using indium arsenide. Measurements are correct to within 0.7%. This paper is said to be the first dealing with the parameters of such devices and their performance.

A Constant Temperature Method of Measuring Power. V.S. Popov, (pp. 73-76).

An accurate means of measuring power is proposed in which the characteristics of each pair of heat converters can have characteristics of quite arbitrary shape. The result is produced either in the form of a direct voltage or a small proportional increase in impedance. The method consists in artificially maintaining the temperature or electrical power constant during the process of measurement in the heater of one of the heat converters of the thermo-electric wattmeter. The device is said to be 10 times more accurate and of wide application.

Null Measurement of the Dielectric Loss Angle. M.S. Mikitinskii, (pp. 87-88).

A novel method is proposed for measuring the dielectric loss angle in capacitors and insulation which is more convenient than the "KEK" or $(\frac{C}{C})(\frac{r}{r})$ bridge method. The measuring device consists of cathode followers with a transfer constant of about 0.9. These followers are connected to separate screens with individual anode supply. Sensitivity as regards capacitance and impedance is of the order of 0.1%.

Transformers

The Dielectric Properties and Stability of Transformer Oils

Research has been undertaken into the production of transformer oil to ensure the right electrical characteristics and their immunity to oxidation in use. The adsorption method of production is recommended instead of acid-alkali purification.

Transistors

Means of controlling triode switches. O. A. Kossov, (pp. 35-44).

A comparison is made between the various ways of controlling junction type transistors operating as switches in power amplifiers with a d.c. output. The dissipated power is considered for various loads and then switching time, the angle of connexion and the mark-space ratio.

ELEKTRICHESTVO

Editor-in-Chief: N. G. DROZDOV

EDITORIAL BOARD

ELECTRIC TECHNOLOGY, U.S.S.R.

1961 VOLUME 1

CONTENTS

Printed in Great Britain by Pergamon Printing & Art Services Ltd., London